The role of lens-derived signals in the development of the corneal endothelium

By

Zenzele Silla

Submitted in fulfilment of the academic requirements for the degree of

Master of Science

School of Life Sciences
College of Agriculture, Engineering and Science
University of KwaZulu-Natal
Westville Campus
Durban

February 2013

As the candidate's supervisor I have/have not approved this thesis/dissertation for submission.

Signed:_____ **Name:** *Dr. Paula Sommer* **Date:**_____

ABSTRACT

Corneal endothelial development is an intricate process driven by finely tuned gene expression. Its formation is necessary for the continued normal development of the anterior segment of the eye. The presence of an inductive lens able to secrete factors such as TGFβ2 as well as the expression of *Foxc1* and *Pitx2* is essential to corneal endothelial development, as in the absence of any of these; the corneal endothelium fails to form. Corneal endothelial development begins as peri-ocular mesenchyme (POM) cells migrate into the space between the lens and surface ectoderm at E11.5. From E12.5, these cells begin to transition from a mesenchymal to an epithelial/endothelial (MET) phenotype, differentiating into a monolayered endothelium by E15 characterised by inter-cellular junctions. To study the initial process of development, immortalised POM cell lines from E12.5 and E13.5 embryos were used. Expression of the key genes, the transcription factors, *Foxc1* and *Pitx2* and two genes involved in EMT/MET, *Slug* and *Tsc22*, were analysed at these stages to establish the developmental norm. The effect of the lens on these expression levels was then determined. To establish whether TGFβ2 is the lens secreted signal responsible for gene expression changes, cells were subjected to TGFβ2 treatment. In all these experiments, the role of *Foxc1* in regulating gene expression was determined by *Foxc1* overexpression and knockdown. The effect of the lens on cellular proliferation and on the expression and cellular arrangement of *N-cadherin*, a junction protein was also determined.

The results showed that, at E12.5, the lens downregulates *Foxc1* and *Pitx2* expression, is a potent inducer of *Tsc22* expression and is required for maintaining *Slug* levels. TGFβ2 was shown to play a role in *Foxc1* and *Pitx2* downregulation. Analysis suggests that *Tsc22* expression is responsive to lens signals, but that TGFβ2 is not the signal responsible for its downregulation between E12.5 and E13.5. The lens has no effect on *Slug* expression in the presence of *Foxc1*, but when *Foxc1* is silenced, *Slug* is induced. Thus, *Foxc1* plays a crucial regulatory role in *Slug* expression. At E13.5, as differentiation is initiated, *Foxc1* expression remains responsive to the lens and to TGFβ2. *Pitx2* expression is still induced by the lens but, at this stage, TGFβ2 does not play a part in *Pitx2* regulation suggesting involvement of other unknown lens secreted signals. Other lens secreted signal/s were also shown to downregulate *Tsc22* and *Slug* at this stage. The lens was implicated in MET as it was shown to have an effect on *N-cadherin* localisation in 3-dimensional culture. E12.5 Spheroids exposed to E6 lenses formed a distinct lattice arrangement of *N-cadherin* compared to the

uniform distribution in control cells. Although the 13.5 control cell aggregates also showed a lattice framework, it was more pronounced in the lens treated cells. The transcriptional role of Foxc1 was determined by overexpression and knockdown experiments where *Foxc1* overexpression and knockdown upregulated *Tsc22* and downregulated *Pitx2* and *Slug* at E12.5. At E13.5, *Pitx2* was downregulated and *Slug* was upregulated in response to aberrant expression of *Foxc1*. This was illustrative of the sensitivity these genes have to *Foxc1* expression during development.

It is known that the presence of a functioning lens and Foxc1 are essential for proper development of the corneal endothelium, which in turn is necessary for normal eye development. The understanding of the precise molecular mechanisms required for corneal endothelial development and the processes requisite for cell proliferation and differentiation has important consequences for providing further insight into the pathophysiology of anterior segment dysgenesis and glaucoma. Previous studies suggest that stem-cell like qualities are conferred in cells undergoing EMT. Such an investigation may lead to application in regenerative medicine such as the bioengineering of corneal tissue.

PREFACE

The experimental work described in this dissertation was carried out in the School of Life Sciences, University of KwaZulu-Natal, Durban, from January 2011 to December 2012, under the supervision of Dr. Paula Sommer.

These studies represent original work by the author and have not otherwise been submitted in any form for any degree or diploma to any tertiary institution. Where use has been made of the work of others it is duly acknowledged in the text.

PLAGIARISM DECLARATION

I, Zenzele Silla, declare that

1. The research reported in this thesis, except where otherwise indicated, is my original research.

2. This thesis has not been submitted for any degree or examination at any other university.

3. This thesis does not contain other persons' data, pictures, graphs or other information, unless specifically acknowledged as being sourced from other persons.

4. This thesis does not contain other persons' writing, unless specifically acknowledged as being sourced from other researchers. Where other written sources have been quoted, then:
   a. Their words have been re-written but the general information attributed to them has been referenced
   b. Where their exact words have been used, then their writing has been placed in italics and inside quotation marks, and referenced.

5. This thesis does not contain text, graphics or tables copied and pasted from the Internet, unless specifically acknowledged, and the source being detailed in the thesis and in the References sections.

Signed: ……..... Date:.....

CONTENTS

Abstract....i
Preface....iv
Plagiarism declaration....v
Table of contents....vi
List of Figures and Tables....x
Acknowledgements....xv
1. Introduction and Literature review....1
1.1. The Eye....1
1.1.1. Eye development: An overview....2
1.1.2. Prenatal development of the anterior segment of the eye....4
1.1.3. The cornea and the lens....5
1.2. Pathologies of eye development....8
1.2.1. Glaucoma....9
1.2.2. Peters' anomaly....10
1.2.3. Axenfeld-Rieger Syndrome....11
1.3. Key factors involved in eye development....12
1.3.1. Paired box protein, *PAX6*....13
1.3.2. Paired-like homeodomain transcription factor 2, *PITX2*....14
1.3.3. Forkhead box c 1, *FOXC1*....15
1.4. Lens derived signals associated with *Foxc1* in development of the corneal endothelium....17
1.4.1. Transforming growth factor *Beta* 2, TGFβ2....17
1.5. Transforming growth factor Beta stimulated clone 22, *TSC22*....18
1.6. Epithelial-mesenchymal transitions (EMT) and mesenchymal-epithelial transitions (MET)....19
1.6.1. Factors associated with EMT/MET in corneal endothelium development....20
1.6.2. The *Cadherins*....20
1.6.3. Neural cadherin, *N-cadherins*....21
1.6.3. Zinc finger protein, *SLUG*....21
1.7. Aims and Objectives....22
2. Materials and methods....24

2.1. Immortalisation of cells using Simian vacuolating virus 40 large T-antigen (SV40 T-ag)....24
2.1.1. Maintenance....24
2.1.2. Cell Treatments....25
2.2. Cell proliferation....25
2.2.1. MTS assay....25
2.2.2. Cell Counts....26
2.3. *Foxc1* knockdown....26
2.3.1. Overview....26
2.3.2. *Foxc1*-shRNA sequence....27
2.3.3. Generation of *Foxc1*-pshRNA....28
2.3.3.1. PCR amplification of shRNA....28
2.3.3.2. Agarose Gel Electrophoresis....28
2.3.3.3. Gel extraction....28
2.3.3.4. Plasmid ligation and transformation....29
2.3.3.5. Plasmid Miniprep....29
2.3.3.6. Restriction enzyme digest....29
2.3.3.7. Sequencing....30
2.3.3.8. Plasmid Midiprep....30
2.4. Transfections....30
2.5. Lens treatments....31
2.5.1. Animal handling....31
2.5.2. Lens dissections....31
2.5.3. Assessing the effect of the lens on proliferation....32
2.5.4. Real time quantitative polymerase chain reaction (qPCR) analysis....32
2.6. TGFβ2 treatments....32
2.7. RNA isolation....33
2.7.1. RNeasy Mini kit protocol....33
2.7.2. RNA gel electrophoresis....33
2.8. cDNA synthesis....34
2.8.1. SuperScript®III First-strand cDNA Synthesis....34
2.8.2 SuperScript®VILO™ cDNA MasterMix....34
2.9. Real time quantitative polymerase chain reaction (qPCR)....35
2.9.1. qPCR using 5X HOT FIREPol® EvaGreen® qPCR Mix Plus....37
2.9.2. qPCR using SYBR® Green JumpStart *Taq* ReadyMix™....37

2.10. Confocal Microscopy....37
2.10.1. Monolayer Culture....37
2.10.2 Hanging drop Culture....37
2.10.3. Immunocytochemistry....38
2.10.3.1. Sample preparation....38
2.10.3.2. *N-cadherin* staining....38
2.10.4. Visualisation....38
3. Results....40
3.1. POM Cell morphology....40
3.2. SV40 large T-antigen....40
3.3. Real time quantitative PCR analyses....43
3.3.1. Compliance with MIQE guidelines....43
3.3.2. Validation of RNA purity and integrity....43
3.3.3. The use of *Hprt* and *Rps12* as reference genes and validation of the $2^{-\Delta\Delta C_T}$ method of data analysis....45
3.4. Comparison of *Foxc1, Pitx2, Tsc22* and *Slug* expression levels of E12.5$^{+/+}$ and E13.5$^{+/+}$ POM cells....47
3.5. Confirmation of transfection and functional efficiency of plasmids....48
3.6. The effect of overexpression and knockdown of *Foxc1* on *Pitx2, Tsc22* and *Slug* expression in POM cells at E12.5 and E13.5....50
3.7. Real time quantitative qPCR of the effect of the lens on *Foxc1*, *Pitx2, Tsc22* and *Slug* expression at E12.5....52
3.8. Real time quantitative analysis of the effect of recombinant TGFβ2 on *Foxc1, Pitx2, Tsc22* and *Slug* expression of POM cells at E12.5....55
3.9. The effect of the lens and TGFβ2 on *Foxc1, Pitx2, Tsc22* and *Slug* expression at E13.5....59
3.10. The effect of the lens on POM cell proliferation....63
3.11. Assessing mesenchymal-epithelial transition in POM cells at E12.5 and E13.5 using *N-cadherin* as a marker of cell differentiation....65
3.11.1 Real time qPCR analysis of *N-cadherin* expression at E12.5 and E13.5....66
3.11.2. Confocal Microscopy....66
3.11.2.1. Monolayer culture....67
3.11.2.2. Hanging drop culture....69
4. Discussion....72

4.1. Overview of events preceeding normal anterior segment development.....72
4.2. SV40 Large T-antigen persists in POM cells, but is no longer temperature sensitive.....73
4.3. E12.5$^{+/+}$ and E13.5$^{+/+}$ POM cell lines are appropriate models to study corneal endothelial differentiation.....74
4.4. Successful *Foxc1* silencing (psh*Foxc1*) using RNA interference.....75
4.5. *Foxc1* overexpression and knockdown affects *Pitx2*, *Tsc22* and *Slug* Expression.....76
4.6. The lens has an effect on *Foxc1*, *Pitx2*, *Tsc22* and *Slug* expression at E12.5.....79
4.7. The lens-derived signal TGFβ2 has an effect on *Foxc1*, *Pitx2*, *Tsc22* and *Slug* expression at E12.5.....81
4.8. The lens and lens-derived signal TGFβ2 has an effect on *Foxc1*, *Pitx2*, *Tsc22* and *Slug* at E13.5.....82
4.9. The lens regulates proliferation of E12.5 POM cells.....84
4.10. The lens can induce an epithelial-like phenotype from mesenchyme cells in 3D culture.....86
4.11. Conclusion.....88
4.12. Future directions.....89
Appendices.....91
References.....127

LIST OF FIGURES AND TABLES

Figure 1.1: The anatomy of a mature human eye. Image adapted from http:www.biographixmedia.com/humaneye-anatomy.html....1
Figure 1.2: An illustration of eye development....4
Figure 1.3: The anterior segment of the vertebrate eye with an insert showing the anatomy of the cornea. Image adapted from http://www.empowher.com/media/reference/corneal-abrasion....6
Figure 1.4: The anterior segment of the eye showing anatomy of the lens. Image adapted from http://marineyes.com/anterior-segment....7
Figure 1.5: A histological comparison of stages in normal eye development of a wild type mouse = W, and mutant showing the characteristic phenotype associated with Peters' Anomaly = W....11
Figure 1.6: A comparison between the characteristics of normal eye development = W and mutant associated with ASD = M, in the mouse....12
Figure 1.7: The expression of *PITX2* and *FOXC1* in anterior segment development....13

Figure 2.1: Schematic diagram of an shRNA molecule....26
Figure 3.1: POM cell morphology....40
Figure 3.2: G418 antibiotic pressure study of E12.5$^{+/+}$ and E13.5$^{+/+}$ POM cells transformed with the temperature sensitive SV40 large T-antigen....41
Figure 3.3: The effect of temperature on SV40-Tag transformed E12.5$^{+/+}$ and E13.5$^{+/+}$ POM cells....42
Figure 3.4: MTS assay of the effect of temperature on cell proliferation of E12.5$^{+/+}$ and E13.5$^{+/+}$ POM cells transformed with the temperature-sensitive SV40-Tag....42
Figure 3.5: *In silico* screen of Nanodrop assessment of RNA quality showing $A_{260/280}$ ratio and corresponding plots....44
Figure 3.6: Denaturing formaldehyde agarose gel analysis of experimental RNA samples, taken from POM cells at E12.5 and E13.5....45
Figure 3.7: The mean change (ΔC_q) between *Hprt* and *Rps12* C_q values plotted against a dilution series of E12.5$^{+/+}$ cDNA. (error bars = SEM)....46
Figure 3.8: Plots of mean C_q of: A) *Hprt* and B) *Rps12* used to calculate amplification efficiency of the qPCR reaction. (error bars = SEM)....47
Figure 3.9: Real time qPCR analysis of *Foxc1, Pitx2, Tsc22* and *Slug* expression in POM cells at E13.5$^{+/+}$ relative to E12.5$^{+/+}$POM cells. (*=p<0.05, n=3; error bars = SEM)....48
Figure 3.10: *Foxc1* overexpression efficiency analysis. Real time qPCR of p*Foxc1*-EGFP transfected E12.5$^{+/+}$ and E13.5$^{+/+}$ POM cells relative to control (untreated) POM cells. (*=p<0.05, n=3; error bars = SEM)....49
Figure 3.11: *Foxc1* knockdown efficiency analysis. Real time qPCR of the effect of psh*Foxc1* on *Foxc1* expression in E12.5$^{+/+}$ and E13.5$^{+/+}$ POM cell lines. (*=p<0.05, n=3; error bars = SEM)....49

Figure 3.12: Real time qPCR analysis of *Pitx2, Tsc22* and *Slug* expression in response to *Foxc1* overexpression on at E12.5, relative to untreated $12.5^{+/+}$ POM cells. (*=p<0.05, n=3; error bars = SEM)....50
Figure 3.13: Real time qPCR analysis of *Pitx2, Tsc22* and *Slug* expression in response to *Foxc1* overexpression on at E13.5, relative to untreated $13.5^{+/+}$ POM cells. (*=p<0.05, n=3; error bars = SEM)....50
Figure 3.14: Real time qPCR analysis of the effect of *Foxc1* knockdown on *Pitx2, Tsc22* and *Slug* expression at E12.5, relative to untreated $E12.5^{+/+}$ POM cells. *Foxc1* knockdown is repeated for comparison. (*=p<0.05, n=3; error bars = SEM)....51
Figure 3.15: Real time qPCR analysis of the effect of *Foxc1* knockdown on *Pitx2, Tsc22* and *Slug* expression at E13.5, relative to untreated $E13.5^{+/+}$ POM cells. *Foxc1* knockdown is repeated for comparison. (*=p<0.05, n=3; error bars = SEM)....51
Figure 3.16: The expression of *Foxc1* in E12.5 POM cells in response to treatment with E6 lenses in normal cells relative to the control. (*=p<0.05, n=3; error bars = SEM)....52
Figure 3.17: The expression of *Pitx2* in E12.5 POM cells in response to treatment with E6 lenses in normal cells and cells in which *Foxc1* expression has been silenced relative to the control....53
Figure 3.18: The expression of *Tsc22* in E12.5 POM cells in response to treatment with E6 lenses in normal cells and cells in which *Foxc1* expression has been silenced relative to the control....54
Figure 3.19: The expression of *Slug* in E12.5 POM cells in response to treatment with E6 relative to the control....55
Figure 3.20: The effect of 30ng/mL TGFβ2 on *Foxc1* expression in normal cells relative to untreated (control) cells at E12.5....56
Figure 3.21: The effect of 30ng/mL TGFβ2 on *Pitx2* expression in normal cells and cells in which *Foxc1* has been silenced (psh*Foxc1*+TGFβ2), relative to untreated (control) cells at E12.5....57
Figure 3.22: The effect of 30ng/mL TGFβ2 on *Tsc22* expression in normal cells and cells in which *Foxc1* has been silenced (psh*Foxc1*+ TGFβ2), relative to untreated (control) cells at E12.5....58
Figure 3.23: The effect of 30ng/mL TGFβ2 on *Slug* expression in normal cells and cells in which *Foxc1* has been silenced (shRNA+ TGFβ2), relative to untreated (control) cells at E12.5....59
Figure 3.24: The expression of *Foxc1* in E13.5 POM cells in response to treatment with E8 lenses and TGFβ2 relative to the control....60
Figure 3.25: The expression of *Pitx2* in E13.5 POM cells in response to treatment with E8 lenses in normal cells and cells in which *Foxc1* expression has been silenced, and cells treated with TGFβ2 relative to the control....61
Figure 3.26: The expression of *Tsc22* in E13.5 POM cells in response to treatment with E8 lenses in normal cells and cells in which *Foxc1* expression has been silenced, and TGFβ2 relative to the control....62

Figure 3.27: The expression of *Slug* in E13.5 POM cells in response to treatment with E8 lenses in normal cells, cells in which *Foxc1* expression has been silenced, and TGFβ2 treated cells relative to the control....63
Figure 3.28: Cell proliferation at E12.5 quantified by MTS assay at 490nm. E12.5$^{+/+}$ POM cells were exposed to E6 whole chick lenses and proliferation compared to unexposed E12.5$^{+/+}$ POM cells.....64
Figure 3.29: Cell proliferation at E13.5 quantified by MTS assay at 490nm. E13.5$^{+/+}$ POM cells were exposed to E8 whole chick lenses and proliferation compared to untreated E13.5$^{+/+}$ POM cells.....65
Figure 3.30: Real time quantitative analysis of *N-cadherin* expression in POM cells at E12.5 and E13.5. (*=p<0.05, n=3; error bars = SEM)....66
Figure 3.31: 63x confocal image of A) DAPI stained cells B) *N-cadherin* stained cells C) Merged DAPI and *N-cadherin* images....68
Figure 3.32: 25x confocal image of fixed and mounted E12.5 (left) and E13.5 (right) POM cells spheroids. A) DAPI image B) *N-cadherin* image C) DIC image D) Image merge. Scale bar is 20µm....69
Figure 3.33: 63x confocal image of E12.5, E12.5 + lens treated and E13.5 and E13.5 + lens treated hanging drops. 70
Figure 4.1: Schematic diagram of the events occurring during normal eye development in chronological order. The main objectives of this investigation are also shown....73
Figure 4.2: The effect of aberrant *Foxc1* expression on *Pitx2*, *Tsc22* and *Slug* expression at E12.5 and E13.5....78
Figure 4.3: A summary of the lens and TGFβ2 effects on *Foxc1*, *Tsc22*, *Pitx2* and *Slug* expression at E12.5....81
Figure 4.4: A summary of the lens and TGFβ2 effects on *Foxc1*, *Tsc22*, *Pitx2* and *Slug* expression at E13.5....84
Figure 4.5: An illustration of the lens effects on development at E12.5 and E13.5 as demonstrated in the hanging drop investigation....87
Figure 4.6: The summary of findings....89
Figure 5.1: shRNA primers targeting *Foxc1*, designed by Dr Marco Weinberg, University of Witwatersrand....99
Figure 5.2: *In silico* screen of *Foxc1* shRNA-2 target sequence....100
Figure 5.3: pGEM®-T Easy Vector map (Promega, USA)....100
Figure 5.4: 1.5% agarose gel electrophoresis of *EcoRI* restriction digest on pGEM®-T Easy plasmid....101
Figure 5.5: *In silico* screen of BLAST search result of a p*Foxc1*-shRNA 2 clone....102
Figure 5.6: qPCR analysis of E12.5+/+ POM cells transfected with a control plasmid encoding a scrambled shRNA sequence that does not target any known mRNA....103
Figure 5.7: peGFP-N1 vector map....103

Figure 5.8: qpCR analysis of *Foxc1*, *Tsc22*, *Pitx2* and *Slug* expression in E12.5 POM cells after 24 hour exposure to boiled E6 lens, relative to the control (untreated POM cells). ($p<0.05$; error bars =SEM)....105
Figure 5.9: *In silico* screen of results for No-RT experiments....107
Figure 5.10: *In silico* screen of of *Hprt* primer BLAST against *Mus musculus* genome....108
Figure 5.11: *In silico* screen of *Foxc1* primer BLAST against *Mus musculus* genome....108
Figure 5.12: *In silico* screen of *Pitx2* primer BLAST against *Mus musculus* genome....109
Figure 5.13: *In silico* screen of *Tsc22* primer BLAST against *Mus musculus* genome....109
Figure 5.14: *In silico* screen of *Slug/Snai2* primer BLAST against *Mus musculus* genome....110
Figure 5.15: *In silico* screen of *N-cadherin* primer BLAST against *Mus musculus* genome....110
Figure 5.16: *In silico* screen of *Rps12* primer BLAST against *Mus musculus* genome....111
Figure 5.17: qPCR protocol for use with 5x HOT FIREPol®EvaGreen®qPCR Mix Plus....112
Figure 5.18: qPCR protocol for use with SYBR®Green JumpStart™ Taq ReadyMix™....113
Figure 5.19: Melt curves, amplification curves and gel electrophoresis of qPCR product for *Hprt* primer set....114
Figure 5.20: Melt curves, amplification curves and gel electrophoresis of qPCR product for *Foxc1* primer set....115
Figure 5.21: Melt curves, amplification curves and gel electrophoresis of qPCR product for *Pitx2* primer set....116
Figure 5.22: Melt curves, amplification curves and gel electrophoresis of qPCR product for *Tsc22* primer set....117
Figure 5.23: Melt curves, amplification curves and gel electrophoresis of qPCR product for *Slug/Snai2* primer set....118
Figure 5.24: Melt curves, amplification curves and gel electrophoresis of qPCR product for *Rps12* primer set....119
Figure 5.25: Melt curves and amplification curves for *N-cadherin* primer set....120
Figure 5.26: Amplification curves for the serial dilution of E12.5 cDNA and plot used to determine qPCR amplification efficiency for the *Hprt* primer set....121
Figure 5.27: Amplification curves for the serial dilution of E12.5 cDNA and plot used to determine qPCR amplification efficiency for the *Foxc1* primer set....121
Figure 5.28: Amplification curves for the serial dilution of E12.5 cDNA and plot used to determine qPCR amplification efficiency for the *Pitx2* primer set....122
Figure 5.29: Amplification curves for the serial dilution of E12.5 cDNA and plot used to determine qPCR amplification efficiency for the *Tsc22* primer set....122
Figure 5.30: Amplification curves for the serial dilution of E12.5 cDNA and plot used to determine qPCR amplification efficiency for the *Slug* primer set....123

Figure 5.31: Amplification curves for the serial dilution of E12.5 cDNA and plot used to determine qPCR amplification efficiency for the *Rps12* primer set.....123
Figure 5.32: No-template control quantitation for *Hprt*, *Pitx2*, *Foxc1*, *Tsc22* and *Slug*. Analysis of the products by agarose gel electrophoresis showed that the peaks corresponded to primer dimer.....125
Figure 5.33: 63x confocal image of E12.5$^{+/+}$ no-primary antibody control. Scale bar is 20μm.....126
Figure 5.34: 63x confocal image of E12.5$^{+/+}$ monolayer no-secondary antibody control. Scale bar is 20μm.....126

Table 1.1: Common ASD disorders and their causative agents. As seen in Sowden (2007).....9
Table 2.1: Primer sequences for reference genes *Hprt* and *Rps12*; and genes of interest, *Foxc1*, *Pitx2*, *Tsc22*, *Slug* and *N-cadherin*.....36

ACKNOWLEDGEMENTS

I would firstly like to thank my supervisor, Dr. Paula Sommer whose guidance, and encouragement have developed me as a student and a scientist. Your faith and patience have developed me as an individual, my sincerest thanks.

To Drs. Dalène and Andrè Vosloo, my gratitude for your instruction and use of laboratory equipment.

My thanks to James Wesley-Smith, Celia Snyman and Shirley Mackellar for their invaluable help with techniques.

I would also like to thank the staff of the BRU at Westville Campus especially Dennis, David and Linda.

My appreciation goes to the College of Agricultural and Engineering Science and Medical Research Council for funding the research.

Thank you to Baatseba Mafoko whose confidence motivated this journey.

To my colleagues and friends, Nimisha Singh, Kerryn Houston, Roxanne Harris-Wheeler, Lilli Holst, Theshnie Naidoo, Maggie Reddy, Cassandra Naidoo, Charlotte Ramdhani, Joy Mongwe, Taona Chadliwa and Ushler Manganyi: Thank you all for the assistance, time and encouragement you invested in me.

Special thanks are extended to Lionel Lesoma for his help, counsel and humour. You have made everything easier.

My deepest gratitude and appreciation go to my Mother and Brother, Dr. Edna Kunjeku and Kuda Sila, whose unlimited support and motivation has made all opportunities possible. Thank you. There are not words enough to express my appreciation. Finally, to Mel Jr. whose youthful wisdom and energy have been an inspiration.

CHAPTER 1: LITERATURE REVIEW

1.1. The Eye

The vertebrate eye is a complex structure of different cells and tissues in constant communication to facilitate normal visual function (Gilbert, 2006; Ittner *et al.*, 2005; Kidson *et al.*, 1999). It is an asymmetrical sphere comprising two distinct portions, the anterior segment and the posterior segment. The opaque posterior segment is made up of the choroid, sclera, and retina; the sensory apparatus of the eye. While the shape of the eye is restricted by the dense connective tissue of the sclera, the internal pressure of the posterior segment is maintained by the viscous vitreous humour (Tortora and Grabowski, 2003; Cvekl and Tamm, 2004). The smaller, transparent anterior segment is made up of the cornea, conjunctiva, iris, pupil, anterior and posterior chamber filled with aqueous humour, ciliary body and lens (Gould *et al.*, 2004; Gilbert, 2006). The structure of the eye is shown below in Figure 1.1.

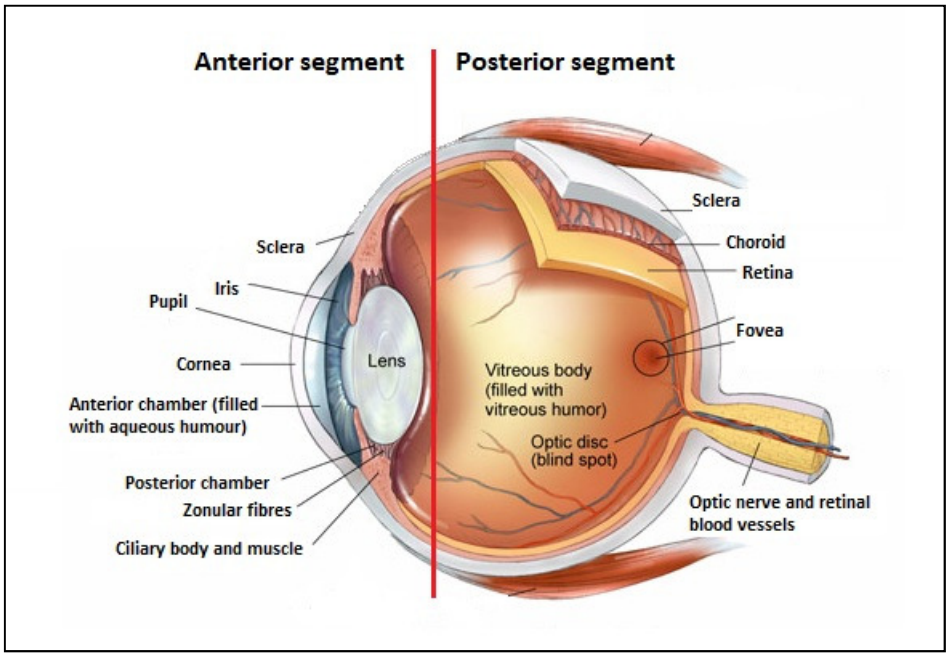

Figure 1.1: The anatomy of a mature human eye showing the anterior and posterior segments. Image adapted from http://www.biographixmedia.com/humaneye-anatomy.html.

The cornea is continuous with the sclera by means of a limbus and together, they form the fibrous tunic, the external layer of the eye (Gould *et al.*, 2004; Tortora and Grabowski, 2003). The vascular tunic is made up of the choroid, extending throughout the inside of the posterior segment and terminating in the ciliary body and iris. The role of the vascular

tunic is to provide nutrition to the posterior retinal surface (Tortora and Grabowski, 2003; Cvekl and Tamm, 2004). The aperture through which light enters the posterior chamber is called the iris. It is controlled by musculature capable of contracting and relaxing thereby dilating or reducing the pupil (Napier and Kidson, 2007). Suspended behind the pupil is the lens. This structure is connected to the ciliary body by ligaments known as the zonular fibres (Tortora and Grabowski, 2003). The neural tunic consists of the retina, a double epithelium carrying the photoreceptors of the eye. This tissue extends throughout the internal surface of the eye to the ciliary processes and inner surface of the iris (Tortora and Grabowski, 2003).

Normal vision is achieved when these structures respond to light efficiently and in concert. The curved cornea allows the passage of light, while focussing and refracting the incident rays (Cvekl and Tamm, 2004; Davis *et al.*, 2003). By tension and relaxation, the iris regulates the amount of light entering the eye. The light path is further refracted as it passes through the lens (Cvekl and Tamm, 2004) and is projected onto the retina. The extent to which light refracts is determined by the diameter of the lens which, in turn, is controlled by the ciliary body to which it is attached. Light is perceived by the photoreceptors of the retina, converted to signals that are subsequently transported via the optic nerve and interpreted into a visual image by the brain (Cvekl and Tamm, 2004). Without the proper development of the structures and tissues of the anterior segment, normal vision would be impeded, if not impossible.

1.1.1. Eye development: An overview

Gastrulation is the process in early development during which the three germ layers giving rise to all the tissues in the body are formed (Tortora and Grabowski, 2003). Vertebrate eye components develop as follows: the ciliary/iris epithelium, retina and optic nerves are derived from the diencephalon neuroectoderm (Reneker *et al.*, 2000) while surface ectoderm subsequently gives rise to the lens and corneal epithelium (Davis *et al.*, 2003). The neural crest/mesoderm gives rise to the sclera, choroid, blood vessels, corneal endothelium and stroma, ciliary body and iris, and surrounding mesenchyme (Gilbert, 2006; Graw 2010; Gage *et al.*, 2005).

Constant communication between adjacent cell groups and tissues facilitate the complex process of eye development. These cell groups permit behavioural changes in response to each other. This interaction, called induction, is when the inducing cells produce a signal

that acts on another group of cells known as the responder (Gilbert, 2006; Gage and Zacharias, 2009). The collaboration of transcription factors and inductive signals in a series of sequential and reciprocal inductions are crucial to proper development, especially as vertebrate eye tissues originate from all three germ layers (Mann, 1964; Gilbert 2006).

Mouse eye development is initiated when an eye field is specified on the anterior forebrain at embryonic day 8.5 (E8.5) (Pei and Rhodin, 1970; Gage and Zacharias, 2009). Development begins as protuberances of the lateral aspects of the diencephalon (developing forebrain), known as the optic vesicles, bulge outwards through a layer of mesenchyme towards the neural ectoderm (Cvekl and Tamm, 2004; Gould *et al.*, 2004; www.theodora.com/anatomy/the_organ_of_sight.html). In the mouse, this occurs at approximately E9.5 corresponding to E28 in humans (Pei and Rhodin 1970, Cvekl and Tamm, 2004) (Figure 1.2). The proximity of the optic vesicle with the surface ectoderm induces a few cells in close spatial arrangement to the neural ectoderm to form a local thickening of the cells in that area due to increased proliferation (Pei and Rhodin, 1970; Lovicu and McAvoy, 2005). This thickening of cells, known as the lens placode (Gilbert, 2006; Pei & Rhodin, 1970; Cvekl and Tamm, 2004) is fated to become the lens (Reneker *et al.*, 2000) by receiving and responding to inductive signals (Gilbert 2006). The thickened ectoderm (the lens forming portion) invaginates at E10.5, inducing the underlying optic vesicles of neural ectoderm (Gould *et al.*, 2004) to fold inwards forming bi-layered optic cups (Mann, 1964; Gilbert 2006; Gould *et al.*, 2004; Gage and Zacharias, 2009). The inner layer is the prospective retina characterised by rapid proliferation, and the outer layer is the prospective pigmented epithelium (Cvekl and Tamm, 2004). The lens placode continues to grow and eventually forms the lens pit and subsequently the lens vesicle (Graw, 1999; Cvekl and Tamm, 2004). At this point, the lens vesicle is still attached to the surface ectoderm (Pei and Rhodin, 1970). Detachment of the lens vesicle and sinking into the optic cup at E11 (E44 of human development) approximately marks the beginning of anterior segment development in mice (Reneker *et al.*, 2000; Sowden, 2007).

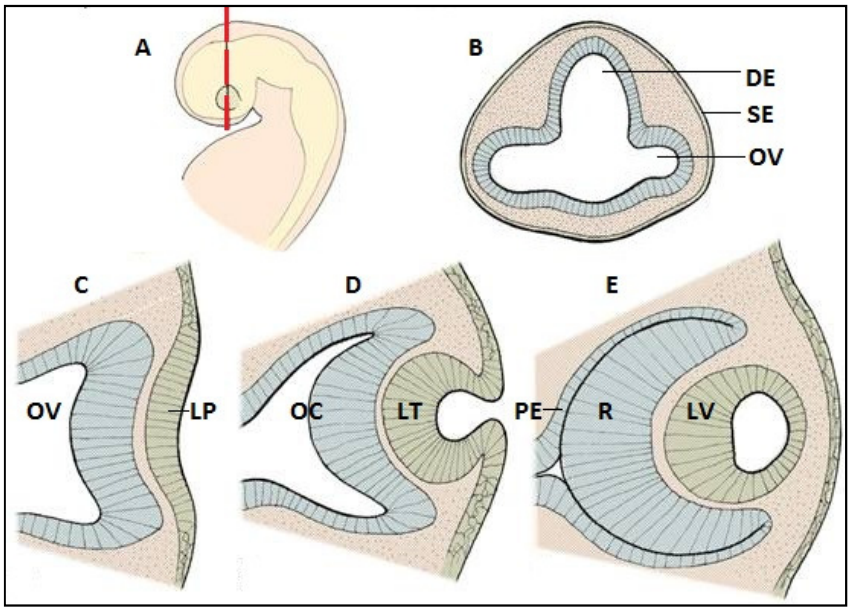

Figure 1.2: An illustration of eye development. A) A developing embryo showing the plane of the section in red. B) ~E9.5 in the mouse, the optic vesicles = OV are bulging outward from the diencephalon = DE toward the surface ectoderm = SE. C) ~E10, the lens placode = LP is induced by the optic vesicle D) ~E10.5, Lens pit invaginates inducing the optic cup = OC E) ~E11, prospective pigmented epithelium = PE is distinct from the prospective retina = R, lens vesicle = LV detaches from surface ectoderm. Image adapted from http://www.bionalogy.com/eye_and_ear.htm.

1.1.2. Prenatal development of the anterior segment of the eye

Between E11.5 and E12.5, the newly developed space between the lens vesicle and restored surface ectoderm becomes filled by a wave of migrating periocular mesenchyme (POM) cells of predominantly cranial neural crest origin (Ittner *et al.*, 2005; Cvekl and Tamm, 2004; Gilbert, 2006; Reneker *et al.*, 2000). These POM cells will differentiate into the corneal endothelium and stroma, iris, ciliary body and trabecular meshwork (Mann, 1964; Reneker *et al.,* 2000). E12.5 is marked by high POM cell proliferation till the cells begin to condense at E13.5 as the differentiation of the mesenchyme is initiated. This change in morphology involves weakening of cell-lens adhesions and changes in adjacent cell-cell interaction to form junctions. Between E6 and E9 in the chick (approximately E13.5 and E15 in the mouse), the POM cells respond to signals from the lens (Beebe and Coats, 2000), encouraging differentiation into the corneal endothelium by mesenchyme to epithelial transition. From E14.5, the presumptive corneal endothelium appears as a continuous monolayer (Gage and Zacharias, 2009; Pei and Rhodin, 1970). These cells continue to differentiate, changing morphology from stellate to elongate. The corneal endothelium must be established as it is essential to the formation of an anterior chamber

as well as the development of the other structures of the eye (Gilbert, 2006; Cvekl & Tamm 2004; Kidson *et al.* 1999; Reneker *et al.*, 2000). The space created by the detachment is fated to become the anterior chamber filled with aqueous humour (Gage and Zacharias, 2009). By E16.5, the mouse anterior chamber is fully formed. Keratocytes of the corneal stroma proliferate and the number of cells peaks at E17 as they begin to assume lamellar arrangement (Gould *et al.*, 2004; Sowden, 2007). From E17, the neuroectoderm differentiates to become the ciliary body (Cvekl and Tamm, 2004; Gould *et al.*, 2004). In tandem, the iris extends into the cavity between the cornea and lens (Reneker *et al.*, 2000). The last tissues to develop in the anterior segment are the trabecular meshwork and Schlemm's canal, which are both involved in drainage of the aqueous humour (Cvekl and Tamm, 2004).

Undoubtedly, the most necessary structure relevant to proper development of the anterior segment is the lens (Beebe and Coats, 2000; Gould, 2002) and its role in a carefully timed 'conversation' with the corneal precursors across a permissive extracellular matrix. Lens ablation and transplantation studies have shown that the cornea degenerates or does not form (depending on developmental stage) in the absence of a lens (Kidson *et al.*, 1999).

1.1.3. The cornea and the lens

The cornea is the outermost structure of the eye covering the tissues of the anterior segment. It is transparent, therefore non-vascularised, and obtains its nutrition from the aqueous humour and tear fluids. The cornea is innervated and has a curvature which contributes to the total refractive power of the eye, specifically focussing light onto the lens.

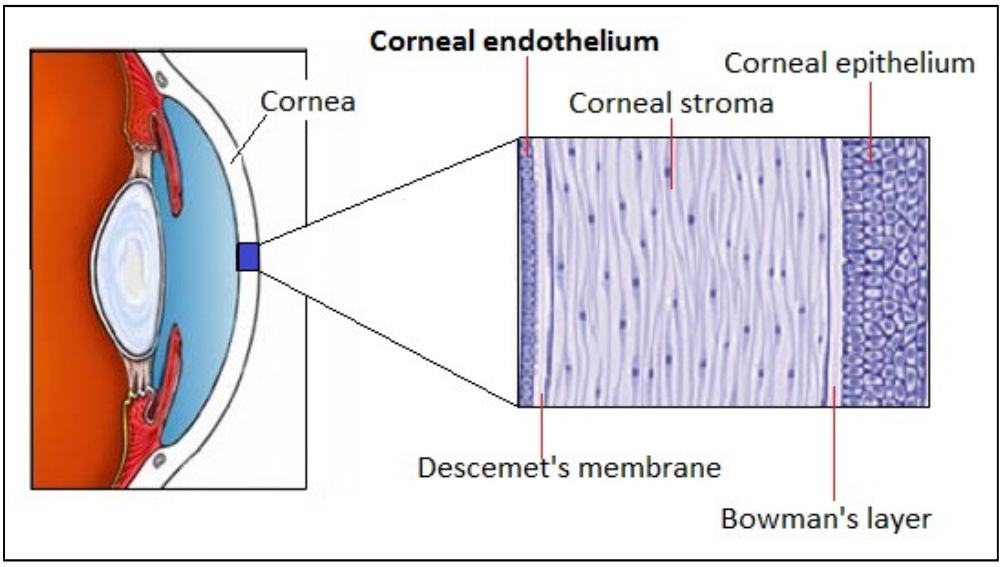

Figure 1.3: The anterior segment of the vertebrate eye with an insert showing the anatomy of the cornea. Image adapted from http://www.empowher.com/media/reference/corneal-abrasion and http:www.aafp.org/afp/2004/0701/p123.html.

The corneal tissue in humans is comprised of five layers: The outermost corneal epithelium, Bowman's layer, corneal stroma, Descemet's membrane and the innermost corneal endothelium (Figure 1.3). The corneal epithelium is a multi-cell stratum of squamous epithelial cells that are proliferative and regenerative. The anterior most layer of cells is responsible for oxygen diffusion from the air via tear moisture and is constantly shed as new tissue is regenerated in the base. Bowman's layer is a tough collagenous layer of fibrils that protects the stroma beneath. The corneal stroma is a thick layer of approximately 200 layers of collagen fibres arranged in parallel and on top of one another. Keratocytes are interspersed amongst the fibrils, helping to maintain the layer by functioning as connectors. Descemet's membrane is below and it is an acellular layer of a more flexible collagen. Lastly and most significantly, the corneal endothelium is a squamous monolayer that controls the fluid and solute exchange between the aqueous humour and stroma. Cells of the corneal endothelium are incapable of regeneration. When cells of the endothelium die, the remaining cells compensate by spreading out thereby affecting efficiency of fluid regulation (Kivelä and Uusitalo, 1998; Scheef *et al.*, 2007; Tortora and Grabowski, 2003). This results in edema which can significantly damage the tissue leading to visual impairment. When the cornea is distressed, by mechanical damage or viral infection, an irregularly arranged patch of collagen will be deposited (by the stroma) causing opacity (Cubitt *et al.*, 1993). This is a leukoma.

The lens is a non-vascularised, non-innervated, transparent structure lying behind the cornea and iris. It is biconvex and alters its shape in order to manipulate the focus effect of the light entering the eye. This is achieved by the tension and relaxation of the zonular fibres, ligaments suspending the lens between the muscles of the ciliary body. The lens consists of a lens capsule, lens epithelium and a cortex of lens fibres (Figure 1.4) (Tholozan and Quinlan, 2007; Tortora and Grabowski 2003; Wormstone *et al.*, 2006). The lens fibres contribute the most, by bulk, to the constitution of the lens. They are transparent densely packed cells. The capsule is a supple, collagenous membrane that, as implied by its name, encapsulates the whole structure. The lens epithelium is a layer of cuboidal epithelia that lies between the capsule and lens fibres on the anterior portion of the lens. Osmolarity, volume and current are maintained by the lens epithelium. Both the capsule and lens fibres are generated by the epithelium (Lovicu and McAvoy, 2005; McAvoy and Chamberlain 1989).

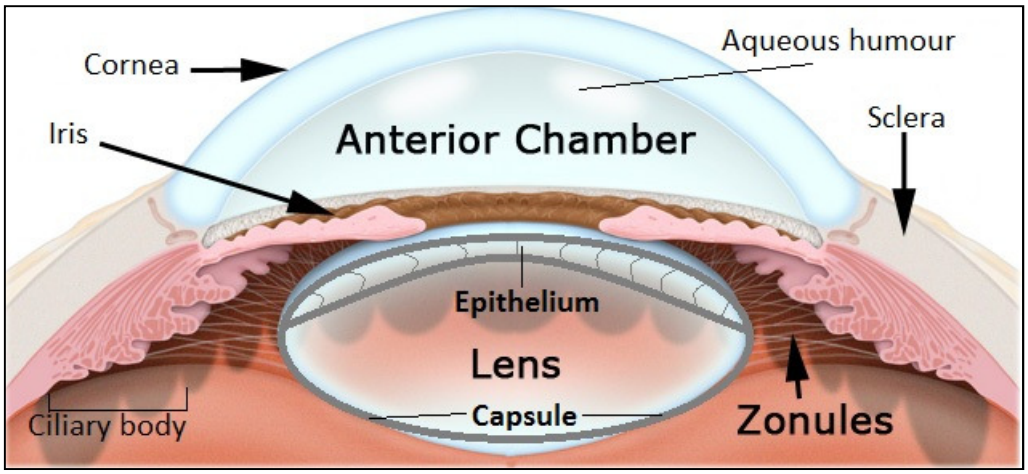

Figure 1.4: The anterior segment of the eye showing anatomy of the lens. Image adapted from http://www.marineyes.com/anterior-segment.

In summary, the lens develops from the surface ectoderm while POM cells of neural crest origin develop into the corneal endothelium (Tripathi *et al.* 1991; Pei and Rhodin, 1970). The most significant contributors to the function of the cornea and lens are the lens epithelium and the corneal endothelium respectively (Genis-Galvez, 1966). Both layers serve as the homeostatic preservers of their corresponding tissues (Tholozan and Quinlan, 2007; Lovicu and McAvoy, 2005). Furthermore, the lens epithelium is essential for the formation of the corneal epithelium. Beebe and Coats (2000) showed that corneal endothelial cell development could be induced by the lens in the avian eye between E4 and

E15 and that orientation of the lens was central to this process. Corneal endothelial cells were only stimulated in proximity to the anterior surface of the lens implicating secreted signals from the lens epithelium in an interaction with the migrating corneal endothelium precursors (POM cells). Correct development therefore is facilitated by the action of transcription factors in conjunction with secreted signals. Although the timing of these events is well understood, the molecular mechanisms underlying the processes remains relatively unknown (Graw, 2010; Gould *et al.*, 2004). Any primary defect in these two structures or their development would result in disintegration of the processes dictating normal anterior segment development.

1.2. Pathologies of eye development

The structures of the anterior segment of the eye are formed in a series of carefully synchronised, highly regulated series of interactions between the neural crest and ectoderm. Any defect in these complex structures or loss of function of regulators will lead to anterior segment dysgenesis (ASD) (Gage *et al.*, 2005; Sowden, 2007; Nishimura *et al.,* 2001) and visual dysfunction. ASD disorders are complex and genetic causative factors are not specific to a particular disorder phenotype. Conversely, the same phenotype can be linked to different genetic factors as seen in Table 1.1 (Gould *et al.*, 2004; Sowden, 2007). ASD leads to a wide range of developmental ocular disorders the most common and notable of which are congenital glaucoma, Peter's Anomaly and Axenfeld-Rieger Syndrome.

Table 1.1: Common ASD disorders showing the associated mutant genes. Adapted from Sowden (2007).

	Axenfeld-Rieger syndrome	**Peter's anomaly**	**Primary congenital glaucoma**
ASD clinical features			
Corneal opacity		■	
Corneal opacity with lens/iris adhesions		■	
Pupil-polycoria corectopia	■	■	
Abnormal angle iris strands to trabecular meshwork/ cornea-peripheral anterior synechiae	■	■	■
ASD genes			
PITX2 4q25	■	■	
FOXC1 6p25	■		
PAX6 11p13	■	■	
FOXE3 1p23		■	
CYP1B1 2p22		■	■

1.2.1. Congenital Glaucoma

Glaucoma is a leading cause of blindness worldwide characterised by visual field defects as a result of damage to the optic nerve and degeneration of retinal ganglion cells. It is treatable with early detection and is most commonly associated with or is the direct result of increased intraocular pressure (IOP) (Nishimura *et al.*, 2001; Mears *et al.*, 1998; Tamimi *et al.*, 2006; Evans and Gage, 2005; Gould *et al.*, 2004; Smith *et al.*, 2000; Baulmann *et al.*, 2002; Kume *et al.*, 1998). Aqueous humour, produced by the ciliary body, fills the space between the cornea and lens which is further divided into two chambers by the iris, nourishing the avascular cornea and draining out via the trabecular meshwork into Schlemm's canal (the irido-corneal angle)(Smith *et al.* 2000; Sowden, 2007; Tortora and Grabowski, 2003). IOP is maintained when the aqueous humour production and drainage is properly regulated (Sowden, 2007). Congenital glaucoma is thought to involve malformation of the irido-corneal angle which contains the drainage system for the aqueous humour (Smith *et al.*, 2000; Kidson *et al.*, 1999). This malformation can be caused

by any process leading up to the development of the irido-corneal angle such as defective migration or differentiation of mesenchymal cells necessary for development of these structures (Smith *et al.*, 2000; Kume *et al.* 1998; Saleem *et al.*, 2001). IOP increases as aqueous humour fails to drain into the venous system thereby exerting pressure on the optic nerve and fovea leading to symptoms associated with glaucoma (Kidson *et al.*, 1999; Baulmann *et al.*, 2002).

Congenital glaucoma may also be the direct consequence of Peters' anomaly and Axenfeld-Rieger Syndrome.

1.2.2. Peters' anomaly

Peters' anomaly is predominantly characterised by leukoma, corectopia (displaced or distorted pupils) and the adhesions of the iris to the lens, the lens to the cornea and the cornea to the iris (Sowden, 2007; Cvekl and Tamm, 2004) (Figure 1.5). Polycoria (ectopic pupils) have also been reported (Sowden 2007). Cataract will result when the lens adheres to the cornea. Cases of Peters' anomaly are isolated and increased IOP is implicated in 50-70% of these (Cvekl and Tamm, 2004). The basis of Peters' Anomaly is a principal defect in Descemet's membrane, corneal stroma or corneal endothelium during development (Reneker *et al.*, 2000; Cvekl and Tamm, 2004).

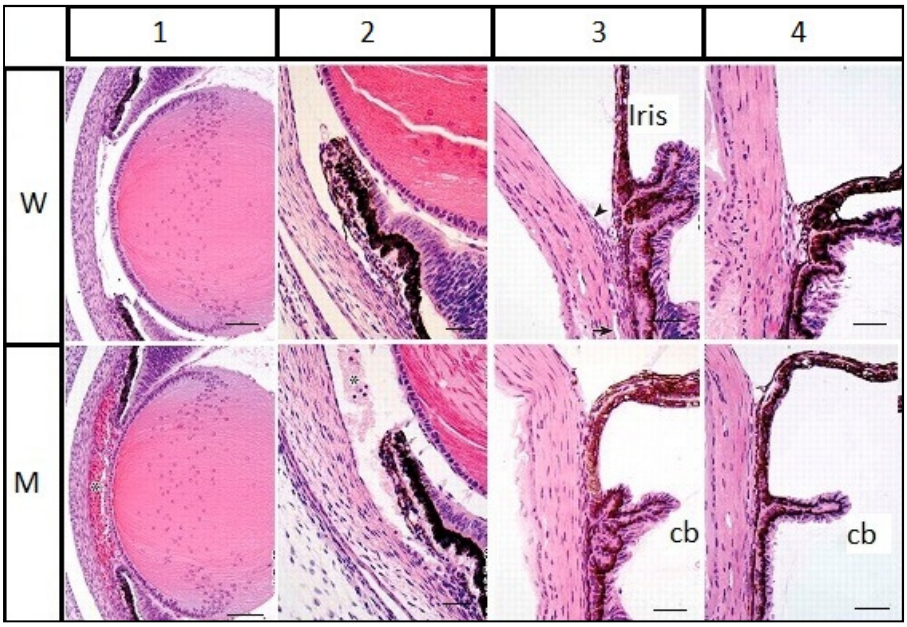

Figure 1.5: A histological comparison of stages in normal eye development of a wild type mouse = W, and mutant showing the characteristic phenotype associated with Peters' Anomaly = W. The stages shown are arbitrary. Stage 1 in the wild type shows the normal development of an anterior chamber. In the mutant, this chamber does not develop and the lens may remain adhered to the developing cornea. Stage 2 shows a developing iris-lens adhesion in the mutant. A developed Trabecular meshwork (arrowhead) and Schlemm's canal (arrow) can be seen during normal development in Stage 3 whereas in the mutant these are absent. Stage 4 shows a foliated ciliary body = cb, in the wild type. The mutant classically shows no development of the zonular fibres and the irido-corneal angle is adhered to the lens. Scale bar is 50μm. Image adapted from http://www.hmg.oxfordjournals.org/content/16/7/798/F2. expansion.

1.2.3. Axenfeld-Rieger Syndrome (ARS)

ARS is a developmental disorder characterised by dysgenesis of the anterior segment of the eye, dental dysgenesis, craniofacial abnormalities and skeletal dysgenesis. The Rieger anomalies are related to the dental or facial abnormalities while the Axenfeld anomalies are linked to the adhesion abnormalities (Cvekl and Tamm, 2004). Other manifestations include redundant periumbilical skin and congenital cardiac conditions (Huang *et al.*, 2008). Hearing impairment has also been linked to ARS (Sowden, 2007). When inherited in an autosomal recessive fashion, ARS is associated with mental retardation, hydrocephalus, and meningeal calcification (Tamimi *et al.*, 2006; Sowden, 2007; Reneker *et al.*, 2000). Autosomal dominant ARS presents with polycoria, iris hypoplasia, corectopia and aniridia. 50% of cases develop early onset glaucoma (Cvekl and Tamm, 2004; Tamimi *et al.*, 2006; Huang *et al.*, 2008).

The diversity of symptoms/phenotypes associated with ARS point to a malfunctioning developmental foundation. Under the control of various transcription factors and signals, the mesenchymal progenitor cells differentiate into the many structures of the eye. Correct development is dependent on the proper function of these genes and their expression in their relative doses (Sowden, 2007; Gould and John, 2002). Figure 1.6 shows a typical ASD progression compared to normal development. Gene mutations have been identified and associated with the ASD spectrum, validating the importance of these factors in proper eye development.

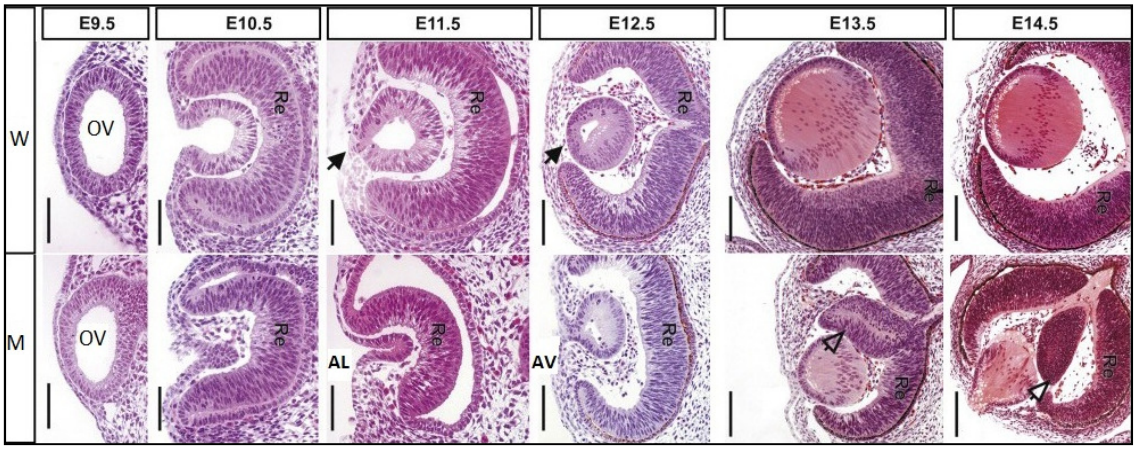

Figure 1.6: A comparison between the characteristics of normal eye development = W and mutant associated with ASD = M, in the mouse. At E9.5 the wild type and mutant phenotypes are indistinguishable as the optic vesicle = OV, is still in contact with the surface ectoderm. At E10.5 the lens vesicles show a difference in size. Re = the developing retina. By E11.5 the lens vesicle should be closed as in the wild type (arrow) but the mutant it remains part of the surface ectoderm = AL. The lens should be separate from the surface ectoderm by 12.5 (arrow) but as observed in the mutant, it is still continuous = AV. The corneal endothelium begins to form at E13.5 and become separated from the lens epithelium by E14.5, creating the anterior chamber. In the mutant, the corneal endothelium does not develop and an optic fissure may develop as shown by the open arrows (E13.5 and E14.5). By E14.5, the anterior segment has not formed as the lens is still continuous with the tissue of the presumptive cornea. Scale bar from E9.5 – E 11.5 is 50μm and 100μm from E12.5 – E14.5. Image adapted from Wurm *et al.* (2008).

1.3. Key factors involved in eye development

Studies have shown that five loci are directly linked to eye development disorders. These are mutations of *PITX2* on 4p25, *FOXC1* on 6p25, *PAX6* on 11p13, *FOXE3* on 1p23, and*CYP1B1* on 2p22 (Sowden, 2007; Kidson *et al.*, 1999). Of these, *PAX6*, *PITX2* and *FOXC1* play key roles in the developing anterior segment by directing the proper differentiation

of ocular mesenchyme (Baulmann *et al.*, 2002; Ittner *et al.*, 2005; Kidson *et al.*, 1999). The expression of *PITX2* and *FOXC1* in different tissues of the anterior segment is shown at different stages of development in Figure 1.7.

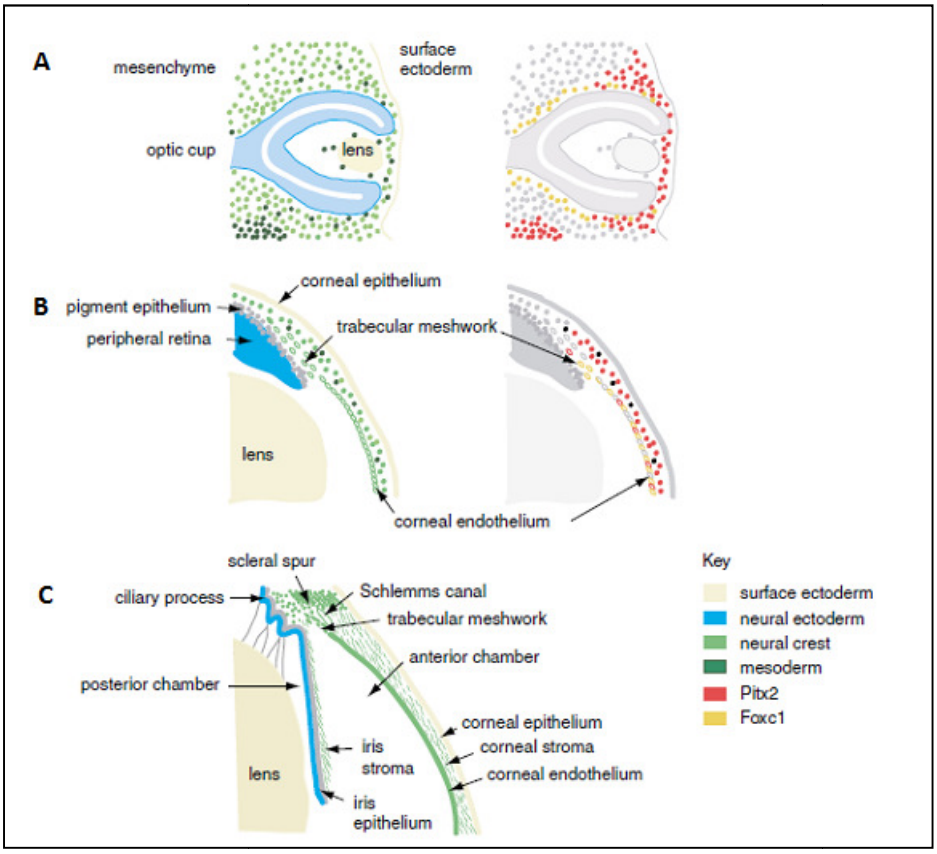

Figure 1.7: The expression of *PITX2* and *FOXC1* in anterior segment development. A) E10.5 in mouse ~ 5th week in human gestation, formation of the optic cup. B) E15.5 ~ 5th month in human gestation, formation of the anterior chamber and corneal endothelium. C) Mature anterior segment showing cornea and irido-corneal angle. Image adapted from Sowden (2007).

1.3.1. Paired box protein, *PAX6*

PAX6, mapped to 11p13 of the human genome, codes for a paired domain transcription factor which has an important regulatory function in the development of vertebrates and invertebrates. It also coordinates the interactions between neural epithelium and mesenchyme cells of the neural crest (Grindley *et al.*, 1995; Cvekl and Tamm, 2004; Baulmann *et al.*, 2002; Quinn *et al.*, 1996). The significance of *Pax6*, the murine homologue, in formation of the anterior segment of the eye has been shown in studies of small eye (*Sey*) mice which carry the *Pax6* mutation (Matsuo, 1993). Homozygous mutations for *Pax6* result in lack of eyes and nasal cavities, and, typically, death soon after birth

(Baulmann *et al.*, 2002; Grindley *et al.*, 1995; Davis *et al.*, 2003). *Pax6* mutations also give rise to iris hypoplasia and leukoma as well as malformation of the irido-corneal angle as a result of defective differentiation of the trabecular meshwork (Baulmann *et al.*, 2002). In a dose-related study, heterozygous mutations of *Pax6* were characterised by failed lens induction or a breakdown of the separation of the lens vesicle from the surface ectoderm (Gould *et al.*, 2004; Cvekl and Tamm, 2004). These experiments highlight the importance of gene dosage as the functional single copy of *Pax6* does not have a sufficient transcriptional activity to overcome this haplo-insufficiency (Cvekl and Tamm, 2004). In humans, *PAX6* mutations are linked to aniridia, foveal hypoplasia and keratitis (Quinn *et al.*, 1996; Davis *et al.*, 2003; Cvekl and Tamm, 2004; Baulmann *et al.*, 2002) indicating a link with Peter's anomaly (Sowden, 2007).

Grindley *et al.* (1995) showed that *Pax6* expression was necessary for lens placode formation hence its expression in the ectoderm, lens placode, lens vesicle and optic vesicle (Baulmann *et al.*, 2002; Quinn *et al.*, 1996; Grindley *et al.*, 1995) during early mouse development. (Davis *et al.,* 2003). In later development, up to E15, *Pax6* expression is most stringent in the epithelia of conjunctiva, ciliary body, neural retina and lens (Quinn *et al.*, 1996; Grindley *et al.*, 1995). *Pax6* has been shown to function as a master gene activating the genes encoding cytoskeletal proteins, structural proteins and membrane proteins with a speculated role in cell adhesion (Graw, 2010; Davis *et al.*, 2003).

1.3.2. Paired-like homeodomain transcription factor 2, *PITX2*

PITX2 is a gene mapped onto 4p25 of the human genome (Sowden, 2007) whose transcription factor, has many functions in cell proliferation, neuronal differentiation and organogenesis (Martin *et al.*, 2004; Hjalt *et al.*, 2000; Huang *et al.*, 2009). Lethality is associated with homozygous mutations of *Pitx2* in mice embryos by E15.5. These mice lack corneal stroma (Evans and Gage, 2005), corneal endothelium and anterior chambers (Zacharias *et al.*, 2011; Sowden, 2007; Martin *et al.* 2004). Hypomorphic gene mutations result in lack of extra ocular muscles, showing that development is dosage sensitive (Gould *et al.* 2004). Interestingly, ARS phenotypes are also demonstrated in *PITX2* overexpression (Sowden, 2007; Gage and Zacharias, 2009). In humans, heterozygous mutations of *PITX2* are responsible for Axenfeld-Rieger malformation phenotypes (Evans *et al.*, 2005; Tamimi *et al.*, 2006; Hjalt *et al.*, 2000; Cvekl and Tamm, 2004) and underlie eye conditions leading to increased intraocular pressure and glaucoma (Evans and Gage, 2005). Learning

difficulties linked to *PITX2* mutations have been described in rare cases (Martin *et al.*, 2004).

PITX2 is expressed in the precursors of the POM and is required for specification of presumptive cornea (Evans and Gage, 2005). Expression is noted beginning at E8.5-E9.5 during normal development as a response to local signals. This is a significant time as the lens vesicle is forming and the anterior segment is about to develop. Expression is then noted in the optic cup and stalk (Gould *et al.*, 2004; Zacharias *et al.*, 2011; Berry *et al.*, 2006) but by E10.5, *PITX2* is localised in the anterior most cells (Sowden, 2007) (Figure 1.3). *PITX2* is strongly expressed in mesenchyme and presumptive corneal stroma, in cells that develop into collagen forming keratocytes, from E13.5 to E15 (Gould *et al.*, 2004; Ittner *et al.*, 2005; Sowden, 2007). By E18, *PITX2* is found predominantly in the tissues that will become the irido-corneal angle (Gould *et al.*, 2004).

As mentioned above, *PITX2* is activated by local signals. Ittner *et al.* (2005) showed that Transforming growth factor beta (TGFβ), a lens derived signal, stimulates *Pitx2* expression in eye tissues and that *Pitx2* expression is negligible in Transforming growth factor beta receptor 2 (*Tgfβ*r2) mutant cells at E15. Neural crest cells and their derivatives require *Pitx2* in order to be competent to receive lens signals without which corneal differentiation will not take place (Evans and Gage, 2005). Gould *et al.* (2004) report that this pattern of expression is similar to that of *FOXC1*.

1.3.3. Forkhead box c 1, *FOXC1*

FOXC1 (Formerly FREAC3/FKHL7/MFH1) is a gene with a forkhead binding domain located at 6p25 of the human genome (Davies *et al.*, 1999; Smith *et al.* 2000). Members of this superfamily have notable functions in embryogenesis (Saleem *et al.*, 2001; Mattiske *et al.*, 2006(b)), angiogenesis (Hayashi and Kume, 2008), organogenesis (Kume *et al.*, 2000) and tumorigenesis (Saleem *et al.*, 2001; Mears *et al.*, 1998). It is apparent that the transcription factor plays a role in cell fate determination and maintenance of cell states, proliferation and differentiation (Mattiske *et al.*, 2006(a); Zhou *et al.*, 2002; Tamimi *et al.*, 2006). *Foxc1* (formerly *Mf1*), the murine homologue, is located on chromosome 13 and shares 98% similarity to human *FOXC1*, making the mouse model an ideal candidate for research (Mears *et al.*, 1998). The extent of *Foxc1* influence is clearly observed in *Foxc1* knockout mice. They present with skeletal, cardiac, renal, meningeal and ocular

abnormalities with homozygous null mutants dying of haemorrhagic hydrocephalus perinatally (Mattiske *et al.*, 2006(b); Lehmann *et al.*, 2003; Smith *et al.* 2000).

FOXC1 is integral in anterior segment formation (Zhou *et al.*, 2002; Zarbalis *et al.*, 2007) and mutations of the gene are a direct cause of ASD (Berry *et al.*, 2006), conditions leading to glaucoma (Davies *et al.*, 1999; Lehmann *et al.*, 2003) and characteristics associated with ARS and PA (Ittner *et al.*, 2005; Kidson *et al.*, 1999; Saika *et al.*, 2001). The role of *FOXC1* in anterior segment development is dose specific as shown in *Foxc1*$^{+/-}$ mice. Adhesions and leukomas are observed in these mice as a result of malformation (Lehmann *et al.*, 2003; Gould *et al.*, 2004). Kidson *et al.* (1999) showed that a functional gene is required for anterior segment specification as mutants did not form the anterior chamber nor did they develop a corneal endothelium.

In normal development, at E10.5, the cells of the optic stalk, express *Foxc1* (Sowden, 2007). *Foxc1* is also expressed in epithelia (of the lacrimal gland) and mesenchyme (Mattiske *et al.*, 2006(b)), but predominantly in the periocular mesenchyme filling the space between the lens vesicle and surface ectoderm at E11.5 (Kidson *et al.*, 1999; Gould *et al.* 2004; Kume *et al.*, 1998). Figure 1.7 shows the migration prior to this stage. *Foxc1* is expressed in the POM cells up to E15 (the same time as complete formation of the cornea). In general, there appears to be a downregulation of *Foxc1* as corneal endothelium differentiation progresses (Kidson *et al.*, 1999). By 16.5, expression is confined to the prospective trabecular meshwork (Tamimi *et al.*, 2006; Gould *et al.*, 2004; Ittner *et al.*, 2005).

FOXC1 is known to regulate other factors such as bone morphogenic protein, BMP (Mattiske *et al.*, 2006(b)) and to activate similar genes to *PITX2* (Smith *et al.*, 2000). In fact, *FOXC1* and *PITX2* are implicated in a common pathway (Berry *et al.*, 2006). *Foxc1* may also regulate its own expression as suggested by Kidson *et al.* (1999). In the presumptive corneal mesenchyme, *Foxc1* is responsive to lens secreted factors and may regulate factors involved in cell-cell adhesion (Kidson *et al.*, 1999; Mattiske *et al.*, 2006(b)) although the specific mechanisms have not been elucidated. As *FOXC1* plays such a significant role in development, the interaction it has with other factors during development is of interest. Lack of *FOXC1* expression has been speculated to initiate, or in the least, play a role in apoptotic induction (Kidson *et al.,* 1999) and very high levels of *FOXC1* in mammary tissue are associated with the high proliferative states typical of cancer (Ray *et al.,* 2010).

1.4. Lens-derived signals associated with the development of the corneal endothelium

Factors controlling the formation of the anterior segment of the eye coordinate their signals through interaction with secreted signals (Cvekl and Tamm, 2004). Wnt, fibroblast growth factors (FGF), bone morphogenic proteins (BMP) and TGFβ are some secreted signals that regulate eye development (Adler & Canto-Soler, 2007; Cvekl & Duncan, 2007). *Wnt* signalling relevance in anterior segment development has also been established by expression of the *Wnts* and corresponding receptors in the lens epithelium (Lovicu & McAvoy, 2005; Donner *et al.,* 2006). FGFs and BMPs are necessary in the development of lens from ectoderm and there is evidence suggesting that a concentration gradient (between anterior and posterior lens) of these factors, plays a role in differentiation in mammals (Lovicu & McAvoy, 2005). Bone morphogenic proteins belong to a super group of ligands under the family name Transforming growth factor *Beta* (Gould *et al.*, 2004) and Donner *et al.* (2006) has explicitly stated that BMP and FGF signals are required for lens specification. Tgfβ2, through its interaction with Foxc1, is speculated to be a significant regulator of corneal endothelium development (Saika *et al.*, 2001; Iwao *et al.*, 2009; Ittner *et al.*, 2005).

1.4.1. Transforming growth factor *Beta* 2, TGFβ2

TGFβ2 is a lens-derived signal belonging to the highly conserved TGFβ and BMP family, that has a role in cell adhesion (including wound repair), growth (and inhibition), differentiation and death (Choi *et al.*, 2005; Gould *et al.*, 2004; Zhou *et al.*, 2002). TGFβ effects are dependent on the cell state and type (Zhou *et al.*, 2002; Choi *et al.*, 2005). Thiery (2003) states that TGFβ induces epithelial-mesenchyme transition, a process that plays a major role in differentiation. TGFβ2 is produced by the lens and ciliary epithelia, and is a major cytokine component of the aqueous humour amongst other cytokines and growth factors (Saika, 2006). Synthesis and degradation of extracellular matrix in the trabecular meshwork is attributed to TGFβ2 activity (Tamm, 2009). Although it is a moderator of cellular events as outlined above, TGFβ is capable of inducing itself (Saika, 2006).

Evidence of the role of Tgfβ2, the murine homologue of human TGFβ2, in eye development is observed in Tgfβ2 knockout mice which die at birth (Saika, 2006). Cells originating from the neural crest are the most affected by the lack of Tgfβ2 (Reneker *et al.*, 2000). These mice have no anterior chamber in the eye, no corneal endothelium nor do they develop an

anterior chamber angle. This phenotype mirrors that observed in *Foxc1* and *Pitx2* mutants. Leukomas and adhesions of the eye anterior structures are common when Tgfβ2 is overexpressed (Gould *et al.*, 2004). Therefore, it is vital that a specific dose is sustained for normal development to occur. Ittner *et al.* (2005) reports abnormal ocular development in Tgfβr$^{+/-}$ mice as above including underdeveloped retina however the anomalous development can be rescued by overexpression of TGFβ1 (Saika, 2006).

Tgfβ2 expression peaks at E13.5 in the developing lens and steadily decreases thereafter (Ittner *et al.*, 2005). It is noted in ciliary epithelia, iris epithelia and chamber angle tissues, showing its influence in corneal morphogenesis (Reneker *et al.*, 2000). The lack of *Foxc1* and *Pitx2* at E13.5 and E15 in Tgfβr2 mutant mice suggests that Tgfb2 can regulate *Foxc1* and *Pitx2* expression in the POM (Ittner *et al.*, 2005). This study went on to show that Tgfβ treatment of embryonic eye cultures dissected at E11 upregulated *Foxc1* and *Pitx2* expression. Subsequently, TGFβr2 mutant cells at E15, became apoptotic when they failed to express *FOXC1* (Ittner *et al.*, 2005). In ovarian and cervical cancer lines, *FOXC1* is shown to be upregulated by TGFβ1 (Mattiske *et al.*, 2006(a); Zhou *et al.*, 2002; Cvekl and Tamm, 2004; Gould *et al.*, 2004). Iwao *et al.* (2009) outlines *Pitx2* and *Foxc1* as downstream molecules of Tgfβ2 in a Smad associated pathway.

1.5. Transforming growth factor *Beta* stimulated clone 22, *TSC22*

TSC22 formerly known as transforming growth factor-*Beta* 1 induced transcript 4 (*TGFβ1i4)* was first identified as a target gene of TGFβ1 but was subsequently found to be upregulated by many factors. Its regulatory activity has now been demonstrated to range from activation to repression (Choi *et al.*, 2005; Kester *et al.*, 2000) and is required in the coordination of transcription factors with extracellular signals (Shibanuma *et al.*, 1992; Hashiguchi *et al.*, 2004; Dohrmann *et al.*, 1999). *TSC22* is highly conserved with mouse (*Tsc22*) and human proteins sharing 98.5% similarity (Kester *et al.*, 2000; Hashiguchi *et al.*, 2004). The factor has a role in epithelial-mesenchymal transitions where it is upregulated (Hashiguchi *et al.*, 2004; Dohrmann *et al.*, 1999). *TSC22* is a reported potential tumour suppressor (Gupta *et al.,* 2003; Kester *et al.*, 2000; Huser *et al.*, 2010) but Portt *et al.* (2011) describe its transcriptional activity as both pro and anti apoptotic.

Tsc22 is localised in many adult tissues but is most extensively expressed in the developing embryo from E6.5 in the mouse (Choi *et al.*, 2005; Sommer *et al.*, 2006). During eye development, *Tsc22* is noted in the optic vesicle in the contact zone of the

vesicle and surface ectoderm. In the ectoderm *Tsc22* is restricted to the area of contact with the optic vesicle compared to the rest of the ectoderm at E9.5 (Dohrmann *et al.*, 1999). Electron microscope investigation suggests that a mesenchymal to endothelial conversion occurs in the cells bordering the lens epithelium, causing a change in cell morphology resulting in the anterior chamber (Kidson *et al.*, 1999). This transition may take place in response to *Tsc22* and may possibly be mediated by lens-derived signals. Sommer *et al.* (2006) suggested that *Tsc22* is downregulated by *Foxc1* in POM cells. The studies showed that there was no significant difference in *Tsc22* expression at E12.5 between wild type and *Foxc1* mutants. However at E13.5, *Tsc22* was significantly downregulated. The specific interaction of T*sc22* and *Foxc1* with respect to anterior eye segment development is unknown and was of interest in this MSc. investigation. A possible explanation of this relationship may be indicated by the communication of *TSC22* with SMAD proteins to promote differentiation, as shown in erythroid cells (Choi *et al.*, 2005). *Foxc1* has also been implicated in the Smad pathway of neural crest cells (Iwao *et al.*, 2009).

1.6. Epithelial-mesenchymal transitions (EMT) and mesenchymal-epithelial transitions (MET)

Epithelial-mesenchyme transition describes the change in cell state from an ordered cohesive structure to a particularised, motile phenotype. It is characterised by the loss of cell junctions and repression of the factors that promote cell-cell adhesion. Mesenchyme-epithelial transition describes the converse. In general, suppression of the genes that direct one transition involves the expression of the genes that promote the other albeit in different pathways. Genes that are highly expressed for EMT must be downregulated for MET to occur, and the reverse is true. Both transitions are reversible. Epithelial and mesenchymal cells are functionally different but can participate in the same processes (Acloque *et al.*, 2009; Thiery *et al.*, 2009; Thiery, 2003; Baum *et al.*, 2008). For example, both EMT and MET are necessary for normal development and tissue repair. Adversely, both are involved in oncogenic pathways (Mani *et al.*, 2008; Baum *et al.*, 2008). Some genes associated with EMT and MET are *SNAIL1*, *SLUG* (also known as *SNAI2*), *FOXC1*, *TWIST*, *NODAL* (a member of *TGFβ* superfamily) and *DORSAL* (Acloque *et al.*, 2009; Baum *et al.*, 2008). Tsc22 is particularly important as it has been shown to be upregulated at sites of EMT (Hashiguchi *et al.*, 2004). Ultimately, it is the effect these genes have on the adhesive interactions between cells that determines the course of EMT and MET.

1.6.1. The Calcium dependant adhesions, *Cadherins*

There are two forms of cell-cell adhesions that are necessary for tissue formation and function. These are the adherens junctions which maintain cell-cell contact and tight junctions which facilitate transport of ions and solutes between cells (Hartsock and Nelson, 2008). Both are associated with different *cadherin* proteins. As their name suggests, the *cadherins* are calcium ion (Ca^{2+}) dependant proteins responsible for cell-cell adhesion, recognition, cell fate determination and tissue morphogenesis. Homophilic interactions maintain the bonds between adjacent cells, for which the Ca^{2+} ion is speculated to be a stabiliser in the interaction. There are three main sub families are *P-*, *E-* and *N-cadherins* all named for the tissues in which they are localised. *P-cadherin* is mostly expressed in placental tissue, *E-cadherin* in epithelial tissue and *N-cadherin* in neural tissues (Van Roy and Berx, 2008; Braga 1999; Reneker *et al.*, 2000). Cellular signals of migrating populations and developmental cues maintain control of *cadherin* expression and specific expression patterns can be an indicator of processes such as EMT as seen when *N-cadherin* is upregulated (Baum *et al.*, 2008).

1.6.2. Neural *cadherin*, *N-cadherin*

N-cadherin is first expressed during gastrulation and has varied functions from mediating hormone secretion, regulating cell motility and differentiation of mesenchyme cells, to roles in the central nervous system (Garcia-Castro, 2000; Suyama *et al.*, 2002; Rubinek *et al.*, 2003; Doherty and Walsh, 1996). Its function is tissue specific. *N-cadherin* has often been associated with a mesenchyme phenotype and identified as a marker of EMT as it is upregulated during this process, but is also involved in MET (Baum *et al.,* 2008; Mani *et al.*, 2008; Thiery, 2003). Studies on cancer cell lines have shown abnormal expression of *N-cadherin* to result in more invasive and motile phenotypes (Hazan *et al.*, 2000; Nieman *et al.* 1999). Tran *et al.* (1999) showed that overexpression of *N-cadherin* in epithelial cells will induce EMT.

The role of *N-cadherin* in eye development has been demonstrated in the formation of the lens vesicle in which a difference in expression was observed between wild type and *Pax6*$^{+/-}$ mice (Cvekl and Tamm 2004) demonstrating a direct relationship between *Pax6* and *N-cadherin* expression. Given the critical role of *Pax6* in development, and the function of *N-cadherin* as a junction protein, the significance of *N-cadherin* in development is implied. Although *N-cadherin* is frequently linked to a mesenchyme phenotype, Reneker

et al. (2000) found that *N-cadherin* is highly expressed in the corneal endothelium cells of mice from E11 but was absent in the corneal epithelium and corneal stroma. Between E12.5 and E15, *N-cadherin* expression serves to differentiate POM cells into corneal endothelium in response lens signals (Kidson *et al.*, 1999; Kidson *et al.*, 2007). The formation of tight junctions through *N-cadherin* upregulation and its continued expression past E15 (development of the whole corneal structure) to adulthood, prepares the corneal endothelium for its role in fluid regulation and permeability (Reneker *et al.*, 2000; Vassilev *et al.*, 2012). Kidson *et al.* (1999) hypothesised that *Foxc1* may regulate expression of *N-cadherin* in early development.

1.6.3. Zinc-finger protein, *SLUG*

SLUG or *SNAI2* is a zinc-finger protein that plays a role in development, the most conserved of which is in development of the mesoderm, neural crest cell migration, carcinogenesis and apoptosis (Hemavathy *et al.*, 2000; del Barrio and Nieto, 2002). These transcription factors are involved in formation of the neural crest and neural differentiation. *SNAIL* members are very closely related in function and often *SLUG* is transcribed along with a related SNAIL protein. In the neural crest, *Slug*, the murine homologue, is expressed in migratory and pre-migratory cells whereas *Snail* is localised to a small group of migratory cells in the mouse head (del Barrio and Nieto, 2002; Acloque *et al.* 2009). *Slug* has been identified to have similar function in the neural crest of *Xenopus*, zebrafish and chick embryos (Jiang *et al.*, 1998). Normally, *Slug*/*Snail* bind target genes to effect transcriptional repression (Hemavathy *et al.*, 2000). Inhibition of the epithelial state by *Slug* is effected through the loss of *E-cadherin* and upregulation of *N-cadherin* (Baum *et al.*, 2008; Thiery 2003). Bolós *et al.* (2002) stated that EMT was induced when *Slug* repressed *E-cadherin* expression in canine kidney epithelial cells. The *Snail* family of transcription factors are potent inducers and regulators of EMT (Thiery 2003; Mani *et al.*, 2008; del Barrio and Nieto, 2002), particulary as targets of TGFβ signalling (Thiery, 2003). These pathways largely involve BMPs and regulation by FGF (Acloque *et al.*, 2009; Thiery *et al.*, 2009). *Slug* is downregulated by retinoic acid (Buxton *et al.*, 1997).

Loss of function (*Slug*$^{-/-}$) experiments in Drosophila embryos have demonstrated a withdrawal of the germ band (Hemavathy *et al.*, 2000). Jiang *et al.* (1998) showed that *Slug* mutants are viable but suggested that their function may have been compensated for by other members of the *Snail* family. *Snail1* mutants show prominent mesoderm markers but lack the mesenchyme morphology (Nakamura and Tokura, 2011).

POM cells themselves are the result of an EMT process wherein cells of the neural crest individualise and migrate to various embryonic tissues (Le Douarin *et al.*, 2000; Acloque *et al.*, 2009). Delamination from the neural crest is induced by TGFβ-BMP-Smad pathway, characterised by the of *E-cadherin* junction complexes and regulated by Wnt signalling and FGF (Nakamura and Tokura 2011).

1.7. Aims and Objectives

Eye development is a complex coordination of transcription factors, cell signals and tissue interactions. It is achieved by a series of sequential inductions. The specification of the corneal endothelium is imperative to the continued and proper development of the anterior segment of the eye. *FOXC1* is a key gene encoding a transcription factor that is equally important in eye development and early development in general. The role of *FOXC1* in anterior segment development has been well established and normal development, as directed by *FOXC1* is dose dependant. Homozygous null mutations of the gene are linked to hydrocephalus and perinatal death in mice while haplo-insufficiency has been directly linked to anterior segment dysgenesis and Axenfeld-Rieger Syndrome. *FOXC1* is an inducer of EMT and its overexpression is associated with tumour metastasis and is currently being considered as a potential prognostic biomarker of basal like breast cancer. Lack of *FOXC1* expression is speculated to initiate apoptosis through a SMAD interaction (the Smad pathway also implicates *Pitx2*, and *Tsc22*). Although very significant, *FOXC1* requires the action of other factors during anterior segment development. While ablation studies on mice have shown that the lens plays a pivotal role in this development, very little data is available to support the relationship between the lens and tissue morphogenesis. TGFβ2 is a lens secreted factor that may be necessary for POM cells to interpret *FOXC1* transcription during corneal endothelium specification.

Two stages of POM cell development were chosen for the investigation, one indicating a proliferative state and the other a differentiated condition. The major objectives of this investigation were firstly, to establish whether lens-derived signals are necessary for *Foxc1* expression; and secondly, to assess the role of the lens-derived signal in MET.

The objectives were:

i) To assess the impact of *Foxc1* overexpression on *Pitx2*, an equally important gene involved in corneal endothelial development as well as two genes involved in mesenchyme to epithelial transition, *Slug* and the *Foxc1* target, *Tsc22*;

ii) To generate an efficient means to study the effect of *Foxc1* silencing on *Pitx2*, *Slug* and *Tsc22*;

iii) To assess the effect of the lens on the expression of *Foxc1*, *Pitx2*, *Tsc22* and *Slug*;

iv) To determine the effect of the lens-derived signal, TGFβ2, on *Foxc1*, *Pitx2*, *Tsc22* and *Slug* expression;

v) To determine whether the lens plays a role in cell proliferation at E12.5 and E13.5;

vi) To determine whether the lens can induce an epithelial/endothelial phenotype from mesenchyme cells.

CHAPTER 2: MATERIALS AND METHODS

2.1. Immortalisation of cells using Simian vacuolating virus 40 large T-antigen (SV40 T-ag)

Immortalised cell lines derived of murine periocular mesenchyme (POM) cells at E12.5 and E13.5 stages of development were generated by another member of the laboratory as previously described (Sommer *et al.,* 2006) (Appendix A). Sommer *et al.* (2006) describe a method of immortalising POM cells at E12.5 and E13.5 by infection with temperature sensitive SV40 large T-antigen (SV40-T-ag) with Geneticin (G418) resistance. These were prepared by another member of the laboratory. Celltiter96® AQueous One Solution was used to test for the presence of the SV40 T-ag in E12.5$^{+/+}$ and E13.5$^{+/+}$ cell lines (Section 2.2.1.) by culture at 33°C and 37°C for 96 hours. Cell counts (Section 2.2.2.) were done concurrently. E12.5$^{+/+}$ and E13.5$^{+/+}$ cells were also subjected to a 13 day G418 pressure study to confirm whether the SV40 T-ag was still encoded within the cell lines. Cells were seeded in culture medium containing 400µg/mL G418, trypsinised out and counted under a compound light microscope.

2.1.1. Maintenance

Cells were cultured in a UV sterilised laminar flow cabinet (Logic Labconco©) using 70% ethanol swabbed equipment (Appendix B.1). The cultures were maintained in DMEM (PAA, Austria) containing 10% FBS (PAA, Austria) and 0.5µg/mL Penicillin-Streptomycin (Invitrogen, USA) (Appendix B.2) at 37°C and 5% CO_2 in a humidified, water-jacketed incubator (Forma Scientific, USA). Cell stocks were grown in T75 canted neck culture flasks (Corning, USA), 10cm and 6cm dishes (Corning, USA) containing 10mL, 10mL and 3mL culture medium respectively. Passage was carried out at 75-90% confluency using 1mL of trypsin-EDTA (PAA, Austria) (Appendix B.3) placed directly on the cells for a maximum of three minutes and subsequently deactivated by a double volume of culture medium. Growth was observed using a Nikon TMS-F inverted light microscope (Nikon, Japan). Treatments were performed on cells of lower passage $6 \leq p \geq 8$ and higher passage $24 \leq p \geq 27$. Cell stocks were stored at -80°C in a 5%v/v DMSO in culture medium (Appendix B.4) in cryotubes (Corning, USA).

2.1.2. Cell Treatments

For this study, the POM cell lines were treated as follows:

1. To establish baselines for proliferation, cells were i) counted and ii) subjected to MTS assay;
2. To establish baselines for *Foxc1*, *Pitx2*, *Tsc22* and *Slug* expression in wild type E12.5 and E13.5 cells and qPCR analysis was performed on untreated cells.
3. To determine the effect of *Foxc1* overexpression on *Pitx2*, *Tsc22* and *Slug* expression, cells were transfected with p*Foxc1*-eGFP. Gene expression was assessed by qPCR;
4. To determine the effect of *Foxc1* knockdown on *Pitx2*, *Tsc22* and *Slug* expression, an shRNA was designed to target and degrade *Foxc1* transcripts. Gene expression analysis was done using qPCR;
5. To determine the effects of the lens on *Foxc1*, *Pitx2*, *Tsc22* and *Slug* expression, E12.5 and E13.5 POM cells were exposed to E6 and E8 whole chick lenses. qPCR analysis was performed to assess gene expression;
6. To determine the effect of recombinant TGFβ2 on *Foxc1*, *Pitx2*, *Tsc22* and *Slug* expression at E12.5, cells were treated with 30ng/mL TGFβ2. Gene expression was analysed by qPCR.
7. To assess the localisation of N-cadherin in cells at E12.5 and E13.5, POM cells were stained with a Cy3-conjugated N-cadherin antibody. Fluorescence was visualised by confocal microscopy.

2.2. Cell proliferation

2.2.1. MTS assay

A calorimetric assay was used to assess the difference in growth rates between cell lines and between treatments. The reagent, [3-(4,5-dimethylthiazol-2-yl)-5-carboxymethoxyphenyl)-2-(4-sulfophenyl)-2H- tetrazolium] (MTS) (Promega, USA) measures cell viability, and inferred proliferation, by the reduction of MTS, a yellow tetrazole, to a purple formazan. All proliferation assays were performed in 96 well plates (Corning, USA), seeded with 100µL culture medium (Appendix B.2) containing $1x10^3$ cells, in triplicate. 20µL of Celltiter96® AQueous One Solution Cell Proliferation Assay (Promega, USA) was added to each of the wells and reaction mixture incubated for 3 hours at 37°C. The absorbance of each reaction was measured at 490nm and recorded using a

PowerWave XS 96 micro-well plate reader (Bio-Tek, USA) using KC4 V3.2 software. Data was corrected by reading wells at 700nm (to account for cell debris) and subtracting the mean absorbance of these from the absorbances at 490nm. The resulting data plotted as a line graph with errors bars indicating the standard error of the mean (SEM).

2.2.2. Cell Counts

Proliferation was also investigated by cell counts using a haemocytometer and Nova compound light microscope (Novatech, USA). Duplicate wells were seeded with $1x10^3$ cells contained in 100µL culture medium. Cells were trypsinised out of the wells and counted every 24 hours for a total period of 96 hours. Collected data was plotted on a line graph.

2.3. *Foxc1* knockdown

2.3.1. Overview

To investigate the effects of *Foxc1* knockdown, a looped RNA sequence that can be used to silence a gene through RNA interference (RNAi) targeting murine *Foxc1* was generated. The small hairpin or short hairpin RNA (shRNA) was composed of a Human U6 promoter, shRNA-sense, loop, shRNA-antisense and termination sequences as shown in Figure 2.1. Primers for the shRNA were designed by Dr Marco Weinberg of the University of the Witwatersrand, and Human Embryonic Kidney 293 (HEK) DNA was as a template for the human U6 promoter. Of the 5 primers designed (Appendix C.1.1, Figure 5.1), shRNA-2 was chosen for this investigation.

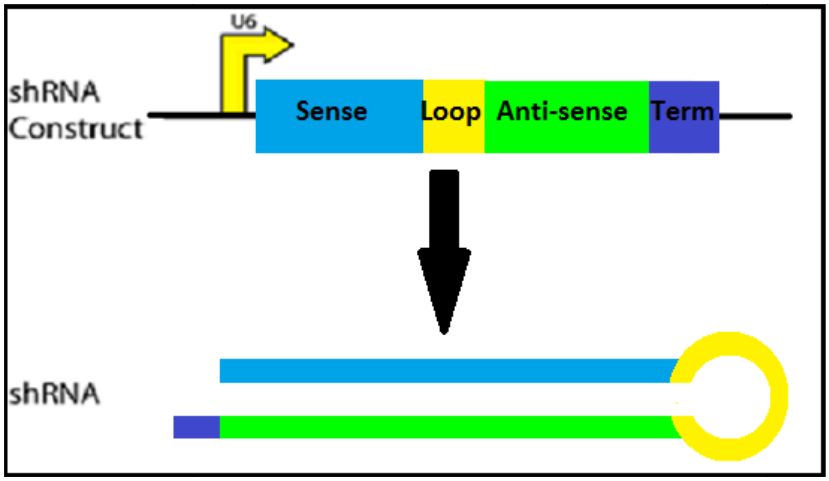

Figure 2.1: Schematic diagram of an shRNA molecule.

2.3.2. *Foxc1*-shRNA sequence

The reverse oligo primer sequence

5'AAAAAATGGGAATAGTAGCTGTCAGATTGGGTCAGGATCTGACAGCTACTATTCCCACGGTG TTTCGTCCTTTCCACAA3'

and the forward U6 promoter primer

5'GATCTCGAGAAGGTCGGGCAGGAAGAGGGCC3'

were ordered from IDT (USA).

The desired 5'→3' shRNA sequence and its components are given below:

GATCTCGAGAAGGTCGGGCAGGAAGAGGGCCTATTTCCCATGATTCCTTCATATTTGCATATAC GATACAAGGCTGTTAGAGAGATAATTAGAATTAATTTGACTGTAAACACAAAGATATTAGTAC AAAATACGTGACGTAGAAAGTAATAATTTCTTGGGTAGTTTGCAGTTTTAAAATTATGTTTTA AAATGGACTATCATATGCTTACCGTAACTTGAAAGTATTTCGATTTCTTGGCTTTATATATCTT GTGGAAAGGACGAAACACCGTGGGAATAGTAGCTGTCAGATCCTGACCCAATCTGACAGCTACT ATTCCCATTTTTT

a) 31bp U6 forward primer: GATCTCGAGAAGGTCGGGCAGGAAGAGGGCC
b) A 221bp U6 promoter sequence: TATTTCCCATGATTCCTTCATATTTGCATATACGATACAAGGCTGTTAGAGAGATAATT AGAATTAATTTGACTGTAAACACAAAGATATTAGTACAAAATACGTGACGTAGAAAGT AATAATTTCTTGGGTAGTTTGCAGTTTTAAAATTATGTTTTAAAATGGACTATCATAT GCTTACCGTAACTTGAAAGTATTTCGATTTCTTGGCTTTATATATC
c) A 21bp sequence corresponding to the 5' end of the human U6 promoter: TTGTGGAAAGGACGAAACACC
d) A 22bp sense sequence containing the target sequence (Appendix C.1.2): GTGGGAATAGTAGCTGTCAGAT
e) A 9bp loop sequence: CCTGACCCA
f) A 21bp anti-sense sequence: ATCTGACAGCTACTATTCCCA
g) A 6bp termination sequence: TTTTTT

2.3.3. Generation of *Foxc1*-pshRNA

2.3.3.1. PCR amplification of the shRNA

DNA was extracted from HEK 293 cells using a QIAGEN DNeasy Blood and Tissue Kit (QIAGEN, USA). The human U6 promoter was amplified in 20µL PCR reactions as follows: 11.7µL nuclease free water (GIBCO, USA), 2.5µL 2mM dNTPs (Fermentas, Canada), 2.5µL 10x KCl_2 buffer containing 15mM $MgCl_2$, 1µL DNA, 1µL 10mM forward primer, 1µL 10mM reverse primer and 0.3µL *Taq* polymerase (Fermentas, Canada). PCR was carried out in a Bio-Rad MyCycler™ Thermal Cycler (Bio-Rad, USA) using a protocol with an initial denaturing cycle at 94°C for 4 minutes followed by 35 cycles of 94°C at 30 seconds, 55°C for 1 minute, 72°C for 1 minute and a final elongation step at 72°C for 7 minutes.

2.3.3.2. Agarose Gel Electrophoresis

The amplified PCR products were separated on a 1.5% TopVision agarose (Fermentas, Canada) gel (Appendix B.5) prepared with 1X Tris-base EDTA buffer (TBE) (Appendix B.6) containing 5µg/mL ethidium bromide, for 45 minutes at 85V in a Bio-Rad Mini-PROTEAN system (Bio-Rad, USA). A 50bp GeneRuler molecular weight marker (Fermentas, Canada) was used to identify product at 331bp. Bands were detected under UV light in a Bio-Rad Chemidoc XRS+ imager (Bio-Rad, USA). The product was quantified using a NanoDrop ND-1000 and accompanying software ND V3.5.2.

2.3.3.3. Gel extraction

The bands containing amplified shRNA were excised using a scalpel and purified using a QIAquick gel extraction kit (QIAGEN, USA). Three volumes of buffer QX1 were then added and the mixture incubated at 52°C for 10 minutes to dissolve the agarose, vortexing as needed. One volume of isopropanol (Merck, USA) was mixed into the solution which was then decanted into a spin-column collection tube assembly, and centrufuged at maximum speed for 1 minute. The flow through was discarded and the membrane washed with 750µL buffer PE. The wash was centrifuged out at 13000 x g for one minute followed by a membrane drying spin at 13000 x g for 1 minute. DNA was eluted out with 50µL Tris-EDTA buffer (Appendix B.7) at 13000 x g for 1 minute.

2.3.3.4. Plasmid ligation and transformation

Purified shRNA product was ligated into pGEM®T-Easy cloning vector (Promega, USA) (Appendix C.1.3., Figure 5.3) in an overnight reaction at 4°C. 2µL of the ligated product was gently mixed into 50µL thawed DH5α competent cells (Zymo Research, USA). The cells were transformed as per manufacturer's specifications and plated on IPTG/XGal (Fermentas, Canada) (Appendix B.8) coated Luria agar (Sigma-Aldrich, USA) plates containing 50mg/mL ampicillin (Sigma-Aldrich, USA) (Appendix B.9). The plates were incubated for 16-24 hours at 37°C then refrigerated overnight to facilitate blue colour development. Single positive (white) colonies were inoculated in 5mL Luria-Bertani broth (Sigma-Aldrich, USA) containing 100mg/mL ampicillin (Appendix B.10) and grown in a 37°C shaking incubator at 185rpm for 12-16 hours.

2.3.3.5. Plasmid Miniprep

Cells were harvested by centrifugation in an Eppendorf 5810R (Eppendorf, Germany) at 3000 x g for 10 minutes at 4°C and purified using the QIAprep Miniprep kit (QIAGEN, USA) as outlined below. A volume of 250µL buffer P1 was used to resuspend the pellet and facilitate transfer to a 1.5mL microcentrifuge tube (not supplied in kit). Another volume of 250µL buffer P2 was added and mixed by inverting the tube 4-6 times followed by the addition of 350µL buffer N3. The tube was inverted a further 4-6 times. The mixture was then centrifuged at 13000 x g for 10 minutes in an Eppendorf 5418 (Eppendorf, Germany) and supernatant decanted into a QIAprep spin column. The supernatant was centrifuged at maximum speed for 1 minute and flow through discarded. The spin column was washed by the addition of 500µL buffer PB and centrifuged for 1 minute at maximum speed. Again, flow through was discarded. A further wash with 750µL buffer PB was carried out and the flow through discarded. The membrane was dried of residual wash buffer by centrifuging for an additional minute. The QIAprep spin column was placed into a new 1.5mL microcentrifuge tube and 50µL buffer EB pipetted directly onto the membrane and left to stand for 1 minute. The purified DNA was eluted at maximum speed for 1 minute. Product was quantified using a NanoDrop ND-1000 (ThermoScientific).

2.3.3.6. Restriction enzyme digest

The presence of the shRNA insert was confirmed by *Eco*RI restriction enzyme (Fermentas, Canada) digest (Appendix C.1.3, Figure 5.4). The reaction contained 1µg Miniprep DNA, 1µL *Eco*RI, 2µL *EcoRI* buffer and nuclease free water to make 20µL. The mixture was

incubated at 37°C for 2 hours. The digest product was separated on a 1.5% agarose gel prepared with 1X Tris-base EDTA buffer (TBE) containing 5μg/mL ethidium bromide, for 45 minutes at 85V. 1kb GeneRuler molecular weight marker (Fermentas, Canada) was used to identify two distinct bands at approximately 331bp (insert) and 3015bp (plasmid). The product was detected under UV in a Bio-Rad Chemidoc XRS+ imager (Bio-Rad, USA).

2.3.3.7. Sequencing

Clones containing the insert were verified by Sanger sequencing (Inqaba Biotec, South Africa) using M13 primers (Appendix C.1.4). Glycerol stocks of confirmed clones were prepared by infusing 800μL of cultured growth medium into 200μL autoclaved glycerol stock and stored at -80°C. The returned nucleotide sequence was confirmed in silico using the National Centre for Biotechnological Information (NCBI) Basic local alignment tool (BLAST) (Appendix C.1.2., Figure 5.2).

2.3.3.8. Plasmid Midiprep

5μL of the glycerol stock culture was inoculated into 100mL Luria-Bertani broth (Sigma-Aldrich, USA) containing 100mg/mL ampicillin and grown in a 37°C shaking incubator (New Brunswick Scientific, USA) at 185rpm for 16-20 hours. The cells were harvested by centrifugation in an Eppendorf 5810R (Eppendorf, Germany) at 3000g for 10 minutes at 4°C and purified using the QIAprep Midi/Maxiprep kit (QIAGEN, USA) as per manufacturer's specifications with an amended overnight elution step at 4°C.

2.4. Transfections

To assess the effect of *Foxc1* overexpression and knockdown on gene expression, POM cell lines were transiently transfected with p*Foxc1*-eGFP-N1 (Appendix C.2) and the generated *Foxc1*-pshRNA. For simplicity p*Foxc1*-eGFP-N1 and *Foxc1*-shRNA shall henceforth be p*Foxc*1 and psh*Foxc1* respectively. All transfections were carried out in 6cm culture dishes (Corning, USA), on 70-90% confluent monolayers using X-tremeGENE HP DNA transfection reagent (Roche, USA) in 5mL culture medium for 24 hours. Each transfection complex consisted of a 4:1 reagent to μg of DNA ratio in serum free medium up to 100μL, per 1mL culture medium. Thus, 4μg of DNA were diluted in the corresponding amount of serum free medium and 20μL X-tremeGENE HP DNA transfection reagent was added directly into the medium to prevent interaction between the reagent and the plastic

microcentrifuge tube. The complex was incubated at room temperature for 30 minutes before being added to the culture medium in a drop wise manner. The dishes were swirled to mix then returned to the incubator. POM cell lines were also transfected with Control shRNA Plasmid-A (Santa Cruz Biotechnology, USA) as a negative control (Appendix C.3). The scrambled shRNA has no target and does not degrade any known mRNA.

2.5. Lens treatments

In order to evaluate the role of the lens in POM development, whole chick lenses corresponding to developmental stages E12.5 and E13.5 were obtained from E6 and E8 chick embryos respectively. Fertilised chicken eggs supplied by Ukulinga poultry farms (Pietermaritzburg, South Africa) were incubated for 6 and 8 days at 37°C in a humidified incubator (Scientific Series 2000, USA). The eggs were turned at least once a day to simulate natural incubation.

2.5.1. Animal handling

Animal handling and animal cell manipulation was approved by the University of KwaZulu-Natal Animal Research Ethics Committee (ethics number 01/12/ANIMAL) and Humane Endpoint observation forms were completed regularly as requested by the National Council of Societies for the Prevention of Cruelty to Animals (NSPCA).

2.5.2. Lens dissections

Dissections were carried out under a Stemi DV4 stereo microscope (Zeiss, Germany) using sterilised tungsten needles electrochemically sharpened using 1M KOH at 150V (Appendix B.11). A firm mould made of Kimwipe™ (Kimberley-Clarke, USA) was prepared as an egg rest. Masking tape was wrapped around the wider circumference of the egg in order to contain egg shell shards. The egg was then pierced with a syringe and approximately 5mL of albumin was removed to prevent injury to the embryo by pulling the embryo sac away from the shell wall. The shell was then cut open along the midline of the masking tape and the embryo within revealed. With the egg settled in the mould, the embryo head was separated from the body by use of sterile scissors and kept in 1X PBS (Appendix B.12). The embryo head was cut along the sagittal plane and the retinal tissue removed to reveal the posterior surface of the aqueous humour. The humour was gently teased out pulling the lens with it. All remaining retinal tissue was dissected off and the lenses stored in minimal 1X PBS in 1.5mL microcentrifuge tubes at -80°C.

2.5.3. Assessing the effect of the lens on proliferation

48 wells of a 96 well plate (Corning, USA) were seeded with $1x10^3$ cells per well: 3 replicates per day (for 4 days) as controls and 3 replicates per day containing POM cells and a single lens, for both $E12.5^{+/+}$ and $E13.5^{+/+}$ lines. 3 negative controls were included per day containing culture medium only. An MTS assay was performed on the 9 wells at 24 hour intervals as described in Section 2.2.1.

2.5.4. Real time quantitative polymerase chain reaction (qPCR) analysis

When assessing the role of the lens in gene expression, ten E6 or E8 lenses were added to a 6cm culture dish (Corning, USA) containing $E12.5^{+/+}$ and $E13.5^{+/+}$ cells respectively, in 5mL culture medium. Similarly, E12.5 and E13.5 cells in which *Foxc1* had been silenced, were also treated with 10 lenses per dish for a period of 24 hours. After the initial 24 hour treatment with psh*Foxc1* and p*Foxc1*, the medium was replaced before the addition of lenses. RNA was isolated (Section 2.8) and cDNA synthesised (Section 2.9) for qPCR analysis (Section 2.10). As a control, similar experiments were carried out with boiled lenses (Appendix D). The basis for boiling lenses to inactivate the epithelium is provided by the experiments of Coulombre and Coulombre (1964).

2.6. TGFβ2 treatments

To investigate the effect of TGFβ2 on gene expression, normal POM cells, POM cells in which *Foxc1* was silenced and cells in which *Foxc1* was overexpressed, were treated with recombinant human TGFβ2 (PeproTech, Israel). 30ng/mL was found to have the most effect on gene expression in a concentration study carried out by another member of the laboratory, in a separate study. As controls, 30ng/mL TGFβ2 was added to 6cm culture dishes (Corning, USA) containing $E12.5^{+/+}$ and $E13.5^{+/+}$ cells, for 24 hours. Medium was removed from psh*Foxc1* and p*Foxc1* treated dishes and replaced with fresh medium containing 30ng/mL TGFβ2 and incubated for a further 24 hours. Thereafter, RNA was isolated and cDNA synthesised for qPCR as described in Section 2.8.

2.7. RNA isolation

RNA was isolated from cultured monolayers using the spin protocol of the QIAGEN RNeasy Mini Kit (QIAGEN, USA). To collect the cells, the culture medium was removed from each dish and the cells were treated with 1mL trypsin-EDTA for 6cm and 10cm for a maximum of 3 minutes. The trypsin-EDTA was neutralised with double volume culture medium

respectively. Cells were harvested by centrifugation for 5minutes at 3000g at 4°C, in 15mL centrifuge tubes (Corning, USA).

2.7.1. RNeasy Mini kit protocol

The pelleted cells were disrupted using 600µL of buffer RLT for 6cm and 10cm dishes. The resulting lysate was transferred to and homogenised in a QIAshredder spin column (QIAGEN, USA) at full speed for 2 minutes. Thereafter, 1 volume of 70% ethanol (Merck, USA) was mixed into the lysate by pipetting. Up to 700.0µL at a time of the sample mixture was pipetted into the RNeasy spin column which was assembled in a 2mL collection tube (supplied in the kit) and centrifuged at 9000g for 15 seconds. The flow through was discarded. 700µL buffer RW1 was used to wash the column membrane at 9000g for 15 seconds and the flow through discarded. A further two washes with 500µL buffer RPE were then carried out: the first for 15 seconds and the second for 2 minutes, both at 9000g. The flow through was discarded each time. An optional membrane drying step, 1 minute at full speed followed. To elute, the RNeasy spin column was then placed in a new 1.5mL collection tube (supplied in the kit) and 40µL nuclease free water (GIBCO, USA) added directly to the membrane. The column was then centrifuged at 9000g for 1 minute.

The RNA was immediately quantified using a NanoDrop 1000 run by ND V3.5.2 software and stored at -80°C in 1.5µg aliquots.

2.7.2 RNA gel electrophoresis

To assess the quality of RNA samples for cDNA synthesis and qPCR analysis, a 1.5% agarose 2.2M formaldehyde gel was used to identify the bands corresponding to the 28S and 18S ribosomal subunits. All equipment used for casting and running the gel – casting trays, combs, conical flasks, measuring cylinder, spatula, weigh boat, and tank – were soaked in 30% H_20_2 (Merck, USA) to deactivate RNAses and kept under a fume hood prior to use. 4µg of each RNA sample was treated with RNA Sample Loading Buffer (Sigma-Aldrich, USA) for 10 minutes at 65°C. The gel was prepared as follows: 1.5g TopVision agarose (Fermentas, Canada) was dissolved in 72mL DEPC water (Appendix B.13) in a microwave and cooled to approximately 55°C. 10mL 10x MOPS buffer (Appendix B.14), 18mL deionised formaldehyde and 100uL DEPC treated Ethidium Bromide (Appendix B.15) were then added, swirled to mix and instantly poured into a casting tray (Recipe, Appendix B.16). A 1x MOPS buffer (Appendix B.14) was used to separate products on the denaturing gel at 85V for 90 minutes.

2.8. cDNA synthesis

RNA samples were not DNAse treated in this investigation as this was shown to adversely affect the mRNA transcript copy numbers, by another member of the laboratory. cDNA was synthesised using SuperScript®III First-strand cDNA Synthesis (Invitrogen, USA) and SuperScript®VILO™ cDNA MasterMix (Invitrogen, USA). No reverse transcriptase controls were included for the samples as shown in Appendix E.4.

2.8.1. SuperScript®III First-strand cDNA Synthesis

1.5µg of RNA was combined with Oligo$(dT)_{15}$ (Promega, USA) 2µL of 2mM dNTPs (Fermentas, Canada) and made up to 10µL with nuclease free water (GIBCO, USA). The mixture was incubated at 65°C for 5 minutes and placed in ice immediately thereafter for 2 minutes. The reaction mixture was spun down before proceeding. A master mix of 4µL 5x RT Buffer, 1µL 0.1M DTT, 1µL RNase OUT and 1µL SuperScript®III Reverse Transcriptase was prepared and added to the reaction mixture. The new mixture was then incubated at 50°C for 50 minutes, 20°C for 10 minutes and 50°C for 50 minutes. The reaction was terminated at 85°C for 5 minutes after which the product was chilled on ice and used immediately or stored at -20°C.

2.8.2. SuperScript®VILO™ cDNA MasterMix

RNA was diluted into a volume of 16µL nuclease free water (GIBCO, USA), less the volume containing 1µg RNA. 4µL of the MasterMix was then added to make a total reaction volume of 20µL. The reaction mixture was incubated at 25°C for 10 minutes, then 42°C for 60 minutes followed by a termination step of 85°C for 5 minutes in a Bio-Rad MyCycler™ Thermal Cycler (Bio-Rad, USA). cDNA was diluted with 15µL nuclease free water (GIBCO, USA) and used immediately or stored for use within a week, at -20°C.

2.9. Real time quantitative polymerase chain reaction (qPCR)

qPCR was used to quantify the difference in expression of genes of interest (*Foxc1*, *N-cadherin*, *Slug*, *Tsc22* and *Pitx2*) against reference gene *Hprt,* between cell lines and treatments thereof. The same protocol was employed for all genes in a Mini Opticon MJ MINI™ Personal Thermal Cycler (Bio-Rad, USA) supported by the CFX manager software package on a dedicated Windows XP OS computer. All reaction preparations were made in triplicate and on ice to prevent undesired product synthesis and a 10µM primer concentration maintained throughout. A primer list is shown in Table 2.1 below, further

details of the targets and oligonucleotides are given in Appendix E.5. Two different master mixes were used as outlined below in Section 2.9.1 and 2.9.2 (Appendix E.6).

The $2^{-\Delta\Delta C_T}$ method (Livak and Schmittgen, 2001) was used to transform data from gene expression analyses. This involved normalising the quantification cycle (C_q), formerly threshold cycle (C_T), of the gene of interest (*Foxc1*, *Pitx2*, *Tsc22*, *Slug*, *N-cadherin*) (Appendix against the reference gene (*Rps12*, *Hprt*) to obtain a fold change in expression (Appendix E.7 and E.8). No-template controls (NTCs) (Appendix E.9) and as mentioned, no reverse-transcriptase (no-RT) controls were included for all samples (E.4).

Minimum information for publication of quantitative real time PCR experiments (MIQE) guidelines as outlined by Bustin *et al.* (2009) were adhered to as closely as possible (Appendix E).

Table 2.1: Primer sequences for reference genes *Hprt* and *Rps12*; and genes of interest, *Foxc1*, *Pitx2*, *Tsc22*, *Slug* and *N-cadherin*.

Gene of Interest	**Forward 5'→3'**	**Reverse 5'→3'**	**Product size (bp)**	**Accession number**	**Manufacturer**
Hprt	GTCCCAGCGTCGTGATTAGCGAT	GGGCCACAATGTGATGGCCTCC	206	NM_0135556.2	Inqaba Biotec, South Africa
Rps12	GGAAGGCATAGCTGCTGGAGGT	CGATGACATCCTTGGCCTGAG	364	NM_001016.3	Inqaba Biotec, South Africa
Foxc1	TCGCTTTCCTGCTCATTCGTC	TGCAGAAAACGCTGTAGGGG	559	NM_008592.2	IDT, USA
PitX2	AGCTGTGCAAGAATGGCTTT	CACCATGCTGGACGACATAC	232	NM_001042504.1	Inqaba Biotec, South Africa
N-cadherin	TTAAAAGCTGCTTGGCTTGG	AAGATTTGCATCCTGCGTGT	205	NM_007664.4	Inqaba Biotec, South Africa
Tsc22	GTAGACCAGTGGCGATGGAT	TCCAGCTGGGAGTTTTTCTC	256	NM_009366.3	Inqaba Biotec, South Africa
Slug	AAGAAGCCCAACTACAGCGA	GCTTTTCCCCAGTGTGAGTT	595	NM_011415.2	Inqaba Biotec, South Africa

2.9.1. qPCR using 5X HOT FIREPol® EvaGreen® qPCR Mix Plus

Each 20µL reaction contained 16µL nuclease free water (GIBCO, USA), 1µL cDNA, 0.5µL 10mM forward, 0.5µL 10mM reverse primer and 2µL 5X HOT FIREPol® EvaGreen® qPCR Mix Plus (Solis Biodyne, Estonia) (Appendix E.6.1). The protocol consisted of: denaturation at 94°C for 15 minutes; 40 cycles of 94°C for 15 seconds, 60°C for 30 seconds, 72°C for 1 minute; a plate read; and a 10 minute elongation step at 72°C (Appendix E.6.1., Figure 5.17). In quantifying *Foxc1* expression, 2µL of cDNA was used and reaction mixture adjusted to contain 1µL less water.

2.9.2. qPCR using SYBR® Green JumpStart *Taq* ReadyMix™

25µL reactions contained 9.5µL nuclease free water (GIBCO, USA), 1.0µL cDNA, 1µL forward primer, 1µL reverse primer and 12.5µL SYBR® Green JumpStart *Taq* ReadyMix™ (Sigma-Aldrich, USA) (E.6.2). The reaction mixtures were subjected to an initial step at 94°C for 2 minutes, followed by 40 cycles of 94°C for 15 seconds, 60°C for 30 seconds, 72°C for 1 minute; a plate read; and a 10 minute final elongation at 72°C (Appendix E.6.2., Figure 5.18). In the case of *Foxc1*, 2µL of cDNA was used and 1µL less water employed.

2.10. Confocal Microscopy

2.10.1. Monolayer Culture

To evaluate whether the lens could induce an epithelial phenotype from mesenchyme cells, POM cell monolayers were exposed to whole chick lenses then fixed for confocal microscopy. E12.5$^{+/+}$ and E13.5$^{+/+}$ cells were grown on UV treated, ethanol sterilised 12mm coverslips seated in 24 well plates (Corning, USA). 1x10^{3}cells in 300µL culture medium were seeded into each well covering the slip and cultured for 48-72hours. For the lens treatments, E6 and E8 lenses (one per well) were placed into each well. Growth was observed using a Nikon TMS-F inverted light microscope (Nikon, Japan).

2.10.2 Hanging drop Culture

To observe whether the lens could induce and epithelial phenotype from mesenchyme cells in 3D culture, hanging drops were prepared. Hanging drop culture was achieved by placing 30µL drops of culture medium containing 1x10^{3}cells on the inverted lid of a 6cm culture dish (Corning, USA). In the lens treatments, an E6 or E8 whole chick lens was placed on the lid and 30µL of culture medium containing 1x10^{3} E12.5 or E13.5 POM cells

respectively was placed over the lens before the dish was inverted. The culture dish base was filled with 3mL 1x PBS to prevent desiccation of the drops. The lid was then carefully reverted and replaced on top of the dish base. Cultures were allowed to grow for 72 hours. Spheroid growth was observed using a Nikon TMS-F inverted light microscope (Nikon, Japan).

Glass coverslips were coated with Poly-L-lysine (Sigma-Aldrich, USA) to facilitate adhesion of the spheroids to the coverslip. Under a Stemi DV4 stereo microscope (Zeiss, Germany), spheroids were transferred onto coverslips held by forceps, by gently touching the drop to the coverslip. Excess medium was carefully removed by pipetting and the spheroid-Poly-L-lysine interface allowed to air dry for 5 minutes. The drops were then fixed as described in Section 2.11.3.1 below.

2.10.3. Immunocytochemistry

2.10.3.1. Sample preparation

In preparation for staining, culture medium was removed and cells gently washed with 1x PBS using a Pasteur pipette rested against the well wall. Monolayers and hanging drops were fixed at room temperature for 10minutes with 4% paraformaldehyde (Merck, USA) in 1x PBS containing 0.15% Triton X-100 (Appendix B.17). 3 washes with 1x PBS followed. 0.5% Bovine Serum Albumin (BSA) Appendix (B.18) in 1x PBS was then used to block for 1 hour at room temperature.

2.10.3.2. *N-cadherin* staining

Polyclonal rabbit anti *N-cadherin* (Santa Cruz, USA) primary antibody in a 1:300 0.5% BSA in 1x PBS dilution was added to the cells and incubated overnight at 4°C. Each well was then subjected to 3 10minute washes in cold 1x PBS. The cells were then incubated in the dark for 1hr at room temperature with donkey anti-rabbit Cy3-conjugated secondary antibody (Jackson Immunolabs, USA) in a 1:1000 dilution with 0.5% BSA in 1x PBS. The slips were washed 3 times for 10 minutes in 1x PBS. Finally, cells were incubated with a 1:50 dilution of 50μg/mL DAPI in 1x PBS for 10 minutes, washed once in 1x PBS and mounted in one drop of Mowiol with DABCO (Appendix B.19). *N-cadherin* staining on hanging drops was carried out as above with extended 15 minute washes after each antibody incubation. The final wash, after incubation with DAPI was 20 minutes long.

No-primary and no-secondary antibody controls were also prepared in each instance (Appendix F).

2.10.3.3. Visualisation

N-cadherin localisation was imaged using a Zeiss LSM 710 Laser Scanning Confocal Microscope (Zeiss, Germany) and captured by the ZEN 2009 with the assistance of Shirley Mackellar and Celia Snyman of the Centre for Electron Microscopy, University of KwaZulu-Natal at Pietermaritzburg. Fixed cultures were viewed under LCI PlanNeofluar 25x/0.8 1mm Korr DIC M27 and 63x/1.3 1mm Korr DIC M27 objectives. N-cadherin was observed in the 488 channel (Mercury-Argon laser) under FITC filter, DAPI in the 405 and DIC in TPMT 488. The frame size was maintained at 1024 x 1024. The 8-bit depth images were taken at speed 9 with an averaging of 4. The pin hole was opened to 5.45 airy units, equal to an 11.8μm section.

CHAPTER 3: RESULTS

3.1. POM Cell morphology

Periocular mesenchyme cells are of neural crest origin and migrate to fill the space between the presumptive corneal epithelium (surface ectoderm) and the lens. Two cell lines were created by microdissection of mouse embryos at E12.5 and E13.5 as described in Appendix A. Both cell lines are fibroblastic and adherent. POM cells at E12.5 and E13.5 (Figure 3.1) had the same shape and maintained similar morphology throughout treatments.

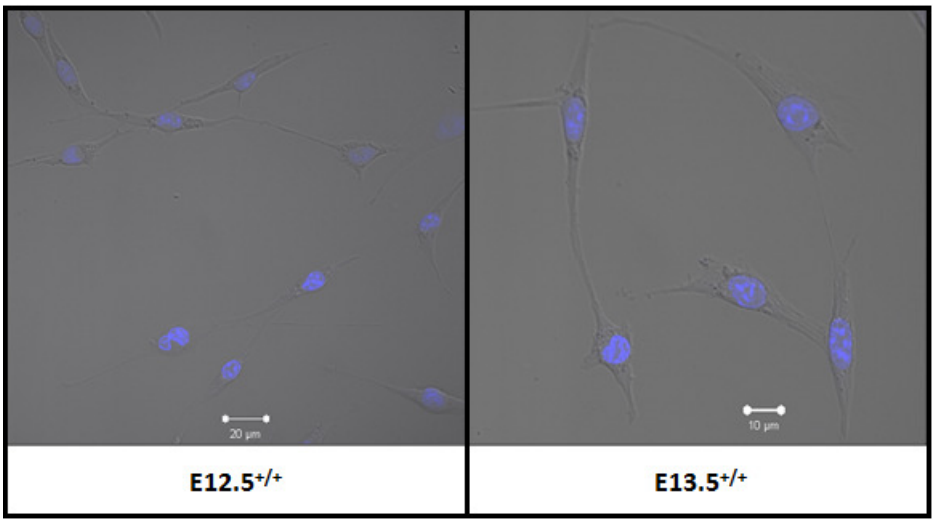

Figure 3.1: POM cell morphology. 25x Confocal microscopy merge of differential interference contrast (DIC) and DAPI stained image of fixed E12.5$^{+/+}$ (left) and E13.5$^{+/+}$ (right) POM cells. Scale bar is 20µm and 10µm respectively. The E13.5$^{+/+}$ image has been zoomed for better viewing.

3.2. SV40 large T-antigen

Immortalised POM cell lines at E12.5 and E13.5 were established by infection with retrovirus encoding a temperature-sensitive SV40 large T-antigen (SV40-Tag) with Geneticin (G418) resistance, by another member of the laboratory as described in Appendix (B). In theory, transformation by the retrovirus, the cell physiology can be manipulated as a response to temperature. Culture at 33°C causes the cells to proliferate while a higher temperature such as 37°C inhibits proliferation thus promoting differentiation. A 13 day G418 pressure study (Figure 3.2) was carried out to confirm whether the SV40-Tag was still encoded within the POM cells. Low passage POM cells (p=8) were cultured in 400µg G418/mL medium in 24 well plates seeded with 1x10^3 cells

per well. Observations were made every 24 hours. POM cell response to temperature was also investigated by cell counts (Figure 3.3) and MTS assay (Figure 3.4). MTS data was corrected as described in Section 2.2.1. For the cell counts, $1x10^3$ POM cells contained in 500 µL of medium per well were seeded in 24 well plates incubated at 33°C and 37°C for 96 hours and cell counts carried out every 24 hours. Cells were also observed using an inverted light microscope every 3 days at medium change.

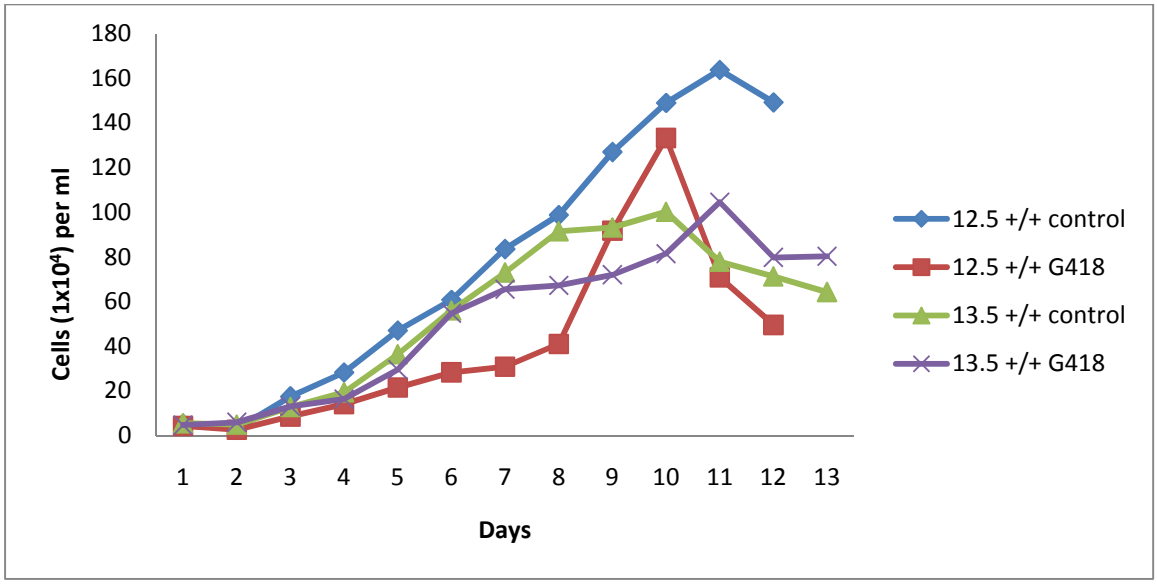

Figure 3.2: G418 antibiotic pressure study of $E12.5^{+/+}$ and $E13.5^{+/+}$ POM cells transformed with the temperature sensitive SV40 large T-antigen. 2 wells per control (untreated) and treatment (400µg/mL G418) were counted every 24 hours for 13 days. For clarity, standard error of the mean is not shown (SEM).

The $E12.5^{+/+}$ cells proliferated at a greater rate than the $E13.5^{+/+}$ cells. Both cell lines proliferated in the presence of G418 indicating that the G418 tag was still present in the cells. All samples were observed to be 80-85% confluent by day 9 after which the rapid decrease in cell count may be attributed to cell death as a result of diminishing resources and confluency.

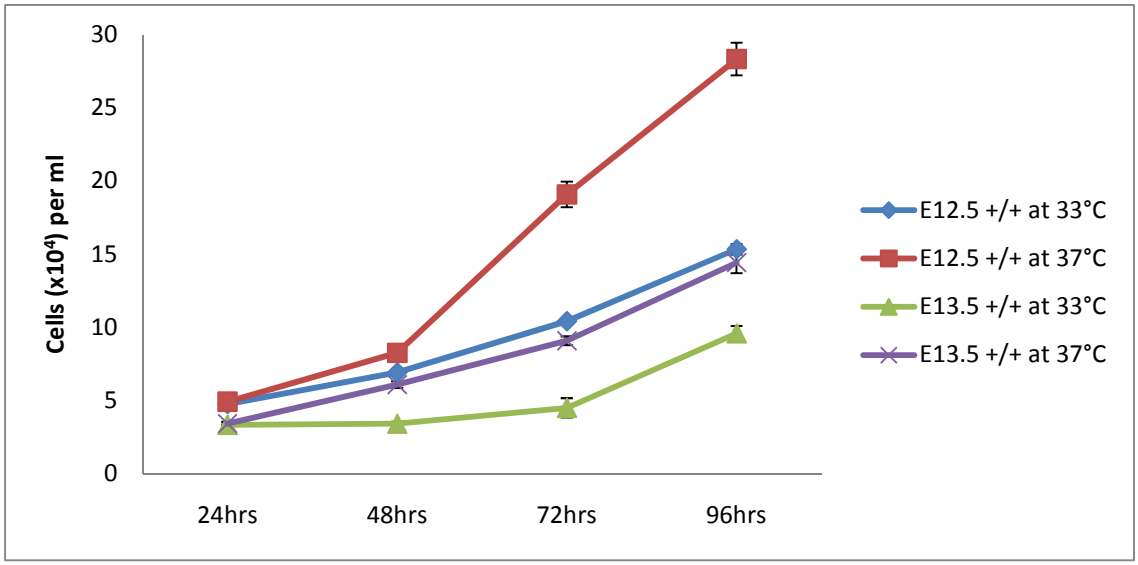

Figure 3.3: The effect of temperature on SV40-Tag transformed E12.5$^{+/+}$ and E13.5$^{+/+}$ POM cells. Cultures were incubated at 33°C and 37°C and counted at 24 hour intervals over 96 hours. (error bars = SEM).

E12.5$^{+/+}$ POM cultures proliferate more rapidly than their E13.5$^{+/+}$ counterparts at both 33°C and 37°C. The cell doubling time for E12.5$^{+/+}$ at 33°C and 37°C was approximately 48 hours and 24-48 hours respectively. For E13.5$^{+/+}$, the cell doubling time was about 52-56 hours and 24-28 hours respectively. Both cell lines proliferated more rapidly at 37°C than 33°C.

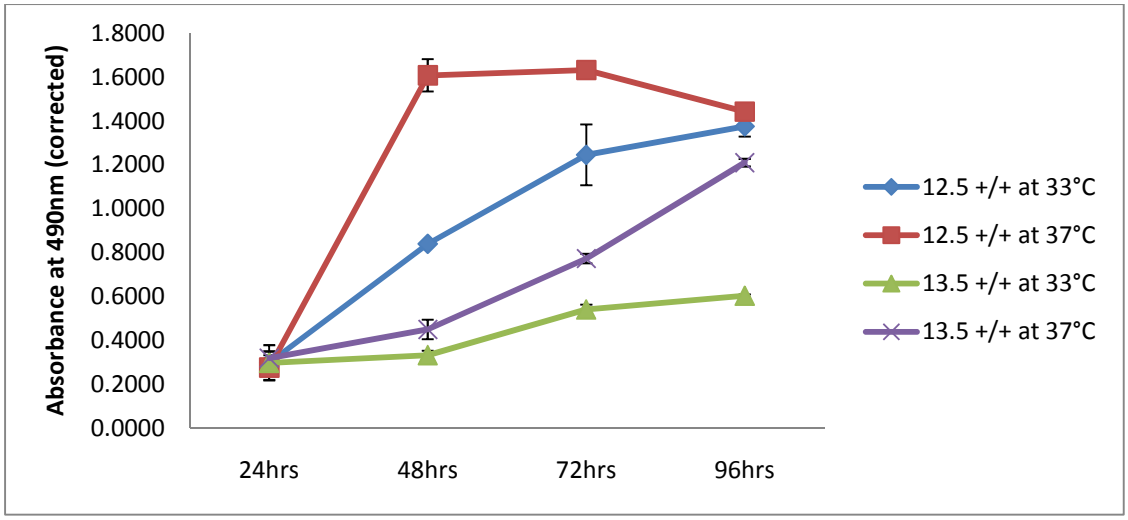

Figure 3.4: MTS assay of the effect of temperature on cell proliferation of E12.5$^{+/+}$ and E13.5$^{+/+}$ POM cells transformed with the temperature-sensitive SV40-Tag. Cells were incubated at 33°C and 37°C and assayed at 24 hour intervals over 96 hours. (error bars = SEM).

Continued growth throughout the 13 day pressure study confirms that the POM cells still encoded the SV40-Tag. However the results of the cell counts and MTS assay show that the protein is no longer temperature-sensitive. No morphological differences were observed in any of the investigations.

3.3. Real time quantitative PCR analyses

All treatments were carried out on passage 6≤p≥8 and higher passage (24≤p≥27) POM cells. Passage number did not significantly affect gene expression levels. Rigorous checks were carried out to ensure the integrity of the data according to MIQE guidelines (Bustin *et al.*, 2009) including no-RT (Appendix E.4) and no template controls (Appendix E.9.1). Expression was quantified as a fold change relative to the reference gene. Statistical analysis of qPCR data was carried out as described in E8. Results are presented as bar graphs with SEM bars.

3.3.1. Compliance with MIQE guidelines

MIQE guidelines (Bustin *et al.*, 2009) outline the minimum details required about qPCR experiments in order to maintain transparency, reliability, scientific integrity and allow reproducibility of results. They serve to evaluate experimental design and preserve consistency in interpretation of qPCR analyses. The guidelines were adhered to as closely as possible. A list of compliance is provided in Appendix E.

3.3.2. Validation of RNA purity and integrity

In accordance with MIQE guidelines, total RNA samples were quantified by Nanodrop 1000 (Thermo Scientific, USA) using ND V3.5.2 software, immediately after isolation. This form of spectrophotometry also gives an indication of RNA purity. RNA has an absorption maximum of 260nm and was measured at 260nm and 280nm to generate ratios allowing for the assessment of RNA purity. Pure RNA is considered to have an $A_{260/280}$ ratio between 1.8 and 2.1. Figure 3.5 shows the Nanodrop results of all RNA samples used to synthesize cDNA for real time quantitative PCR RNA. To asses RNA integrity for its use in qPCR, all RNA samples were run on a denaturing formaldehyde agarose gel with Ethidium Bromide stain for visualisation under UV light (Chemidoc XRS). The quality of the RNA was confirmed by two distinct bands of the 28S and 18S ribosomal subunits (Figure 3.6). As shown in Figures 3.5 and 3.6, RNA purity and quality was confirmed to be acceptable for analysis

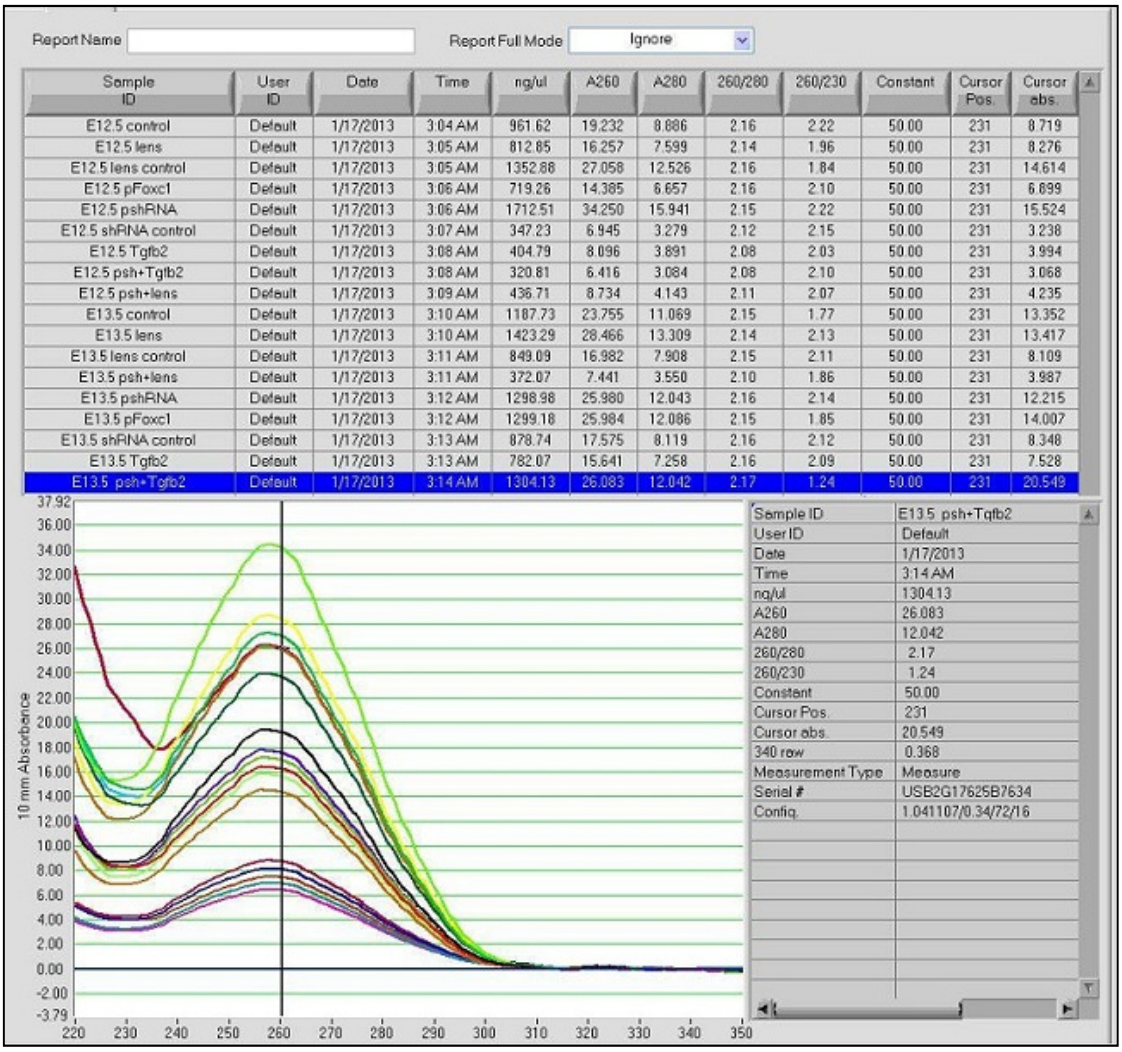

Report Name | Report Full Mode: Ignore

Sample ID	User ID	Date	Time	ng/ul	A260	A280	260/280	260/230	Constant	Cursor Pos.	Cursor abs.
E12.5 control	Default	1/17/2013	3:04 AM	961.62	19.232	8.886	2.16	2.22	50.00	231	8.719
E12.5 lens	Default	1/17/2013	3:05 AM	812.85	16.257	7.599	2.14	1.96	50.00	231	8.276
E12.5 lens control	Default	1/17/2013	3:05 AM	1352.88	27.058	12.526	2.16	1.84	50.00	231	14.614
E12.5 pFoxc1	Default	1/17/2013	3:06 AM	719.26	14.385	6.657	2.16	2.10	50.00	231	6.899
E12.5 pshRNA	Default	1/17/2013	3:06 AM	1712.51	34.250	15.941	2.15	2.22	50.00	231	15.524
E12.5 shRNA control	Default	1/17/2013	3:07 AM	347.23	6.945	3.279	2.12	2.15	50.00	231	3.238
E12.5 Tgfb2	Default	1/17/2013	3:08 AM	404.79	8.096	3.891	2.08	2.03	50.00	231	3.994
E12.5 psh+Tgfb2	Default	1/17/2013	3:08 AM	320.81	6.416	3.084	2.08	2.10	50.00	231	3.068
E12.5 psh+lens	Default	1/17/2013	3:09 AM	436.71	8.734	4.143	2.11	2.07	50.00	231	4.235
E13.5 control	Default	1/17/2013	3:10 AM	1187.73	23.755	11.069	2.15	1.77	50.00	231	13.352
E13.5 lens	Default	1/17/2013	3:10 AM	1423.29	28.466	13.309	2.14	2.13	50.00	231	13.417
E13.5 lens control	Default	1/17/2013	3:11 AM	849.09	16.982	7.908	2.15	2.11	50.00	231	8.109
E13.5 psh+lens	Default	1/17/2013	3:11 AM	372.07	7.441	3.550	2.10	1.86	50.00	231	3.987
E13.5 pshRNA	Default	1/17/2013	3:12 AM	1298.98	25.980	12.043	2.16	2.14	50.00	231	12.215
E13.5 pFoxc1	Default	1/17/2013	3:12 AM	1299.18	25.984	12.086	2.15	1.85	50.00	231	14.007
E13.5 shRNA control	Default	1/17/2013	3:13 AM	878.74	17.575	8.119	2.16	2.12	50.00	231	8.348
E13.5 Tgfb2	Default	1/17/2013	3:13 AM	782.07	15.641	7.258	2.16	2.09	50.00	231	7.528
E13.5 psh+Tgfb2	Default	1/17/2013	3:14 AM	1304.13	26.083	12.042	2.17	1.24	50.00	231	20.549

Sample ID	E13.5 psh+Tgfb2
User ID	Default
Date	1/17/2013
Time	3:14 AM
ng/ul	1304.13
A260	26.083
A280	12.042
260/280	2.17
260/230	1.24
Constant	50.00
Cursor Pos.	231
Cursor abs.	20.549
340 row	0.368
Measurement Type	Measure
Serial #	USB2G17625B7634
Config.	1.041107/0.34/72/16

Figure 3.5: *In silico* screen of Nanodrop assessment of RNA quality showing $A_{260/280}$ ratio and corresponding plots.

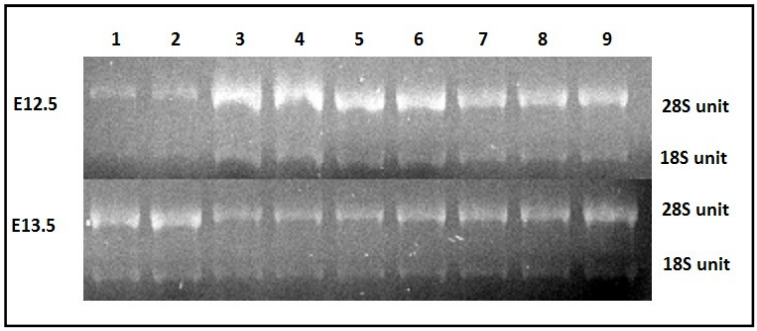

Figure 3.6: Denaturing formaldehyde agarose gel analysis of experimental RNA samples, taken from POM cells at E12.5 and E13.5. 1) Cells exposed to boiled whole chick lenses (lens experiment negative control) 2) Cells transfected with a scrambled shRNA 3) Untreated (control) POM cells 4) Transfected with p*Foxc1* 5) Transfected with psh*Foxc1* 6) Cells exposed to whole chick lenses 7) Transfected and exposed to lens 8) Treated with TGFβ*2* 9) Transfected with *Foxc1*-pshRNA and treated with TGFβ2.

3.3.3. The use of *Hprt* and *Rps12* as reference genes and validation of the $2^{-\Delta\Delta C_T}$ method of data analysis

Many variations can occur during qPCR analysis as a result of differing primer efficiency, amplification efficiency and extraction processes thus there is a need for an internal control to allow the reliable interpretation of data from the assay. Such an internal control is presented in the form of reference genes. mRNA data of the genes of interest are normalised against reference genes most suitable to the cell type and experimental design. The selected reference genes must be highly expressed in the sample and also across different tissue types, as well as stably and constantly transcribed under varying conditions. For this investigation, 40S Ribosomal protein 12 (*Rps12*) and Hypoxanthine phosphoribosyltransferase (*Hprt*) were chosen as two such acceptable mRNAs. Common practise is to use two reference genes however this was not possible in all assays due to limiting resources and thermo cycler capacity. *Rps12* was used for initial experiments and data obtained was correlated with assay data normalised against *Hprt* and there was no significant difference between the data obtained. Figure 3.7 below shows amplification data of *Hprt* normalised against *Rps12* (serving as the target gene in this case) in a cDNA serial dilution.

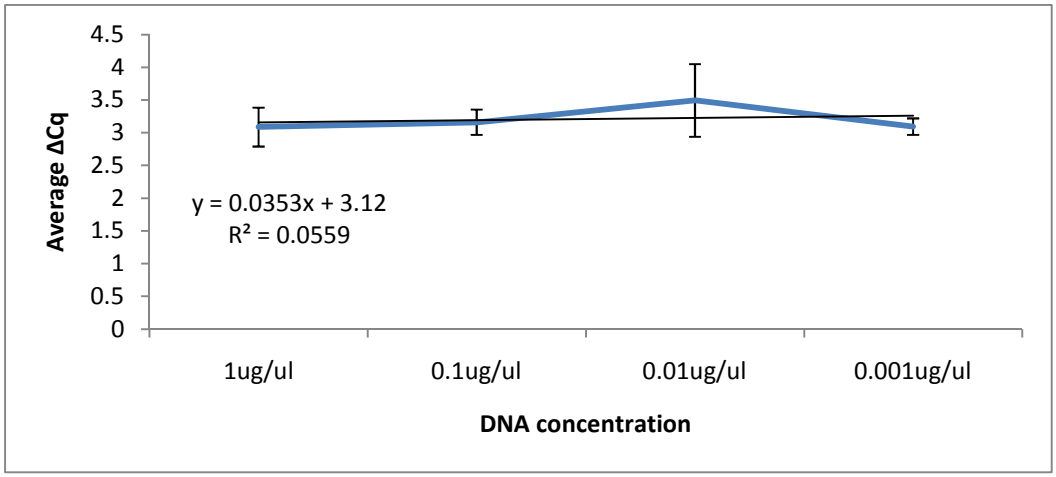

Figure 3.7: The mean change (ΔC_q) between *Hprt* and *Rps12* C_q values plotted against a dilution series of E12.5$^{+/+}$ cDNA. (error bars = SEM).

As seen above, the slope (m=0.0353) is close to zero showing that the mean difference in quantification cycle (C_q), formerly threshold cycle (C_t), remains relatively the same across dilutions. This validates the use of the $2^{-\Delta\Delta C_T}$ method as an appropriate means to analyse qPCR data studies. The defining assumption made by, and essential in the analysis of data by the $2^{-\Delta\Delta C_T}$ method (Livak and Schmittgen, 2001), requires that the amplification efficiency of the reference gene approximates the amplification efficiency of the target. An example of such an approximation is shown below for *Hprt and Rps12* expression in wild type E12.5 POM cells (Figure 3.8).

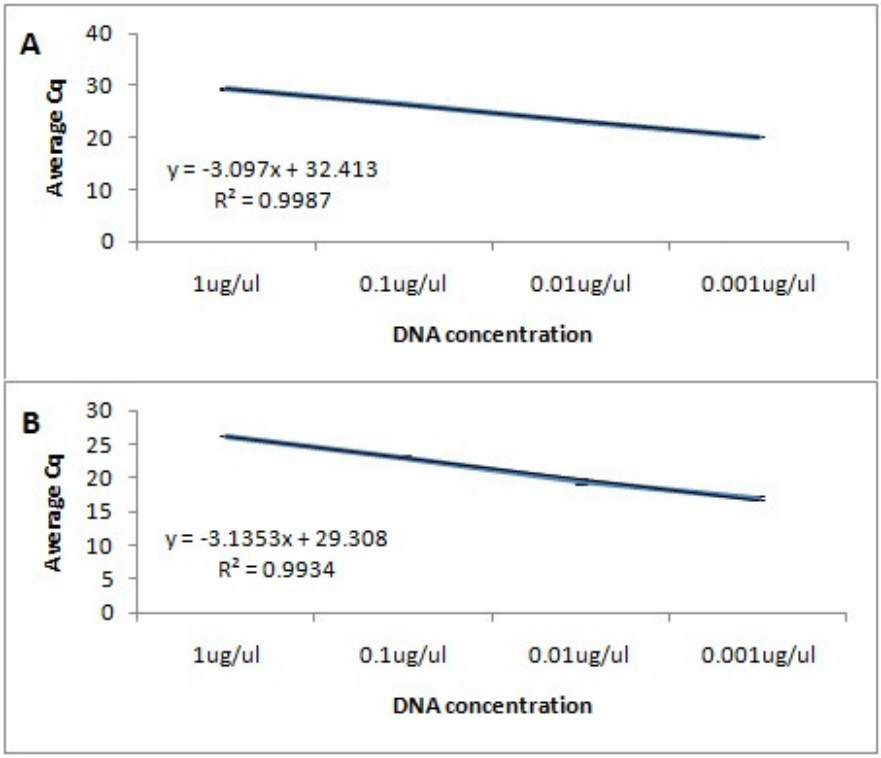

Figure 3.8: Plots of mean C_q of: A) *Hprt* and B) *Rps12* used to calculate amplification efficiency of the qPCR reaction. (error bars = SEM).

The amplification efficiency of *Hprt* was 110.33% and that of *Rps12* (serving as the target in this case) 108.42%, thus further validating the use of the $2^{-\Delta\Delta C_T}$ method.

3.4. Comparison of *Foxc1, Pitx2, Tsc22* and *Slug* expression levels in E12.5$^{+/+}$ and E13.5$^{+/+}$ POM cells

Foxc1 and *Pitx2* are two key genes directing the normal development of the eye and are regulated by other transcription factors and growth factors as well as lens derived signals. *Tsc22* has been identified as a downstream target of *Foxc1* and is downregulated by *Foxc1* in POM cells. *Slug* is a transcriptional repressor that facilitates epithelial to mesenchymal transition, a process requisite for cell differentiation and proliferation during development. Figure 3.9 below shows the relative expression of these genes of interest in POM cells at a developmental stage characterised by high proliferation, E12.5, and a more differentiated stage, E13.5.

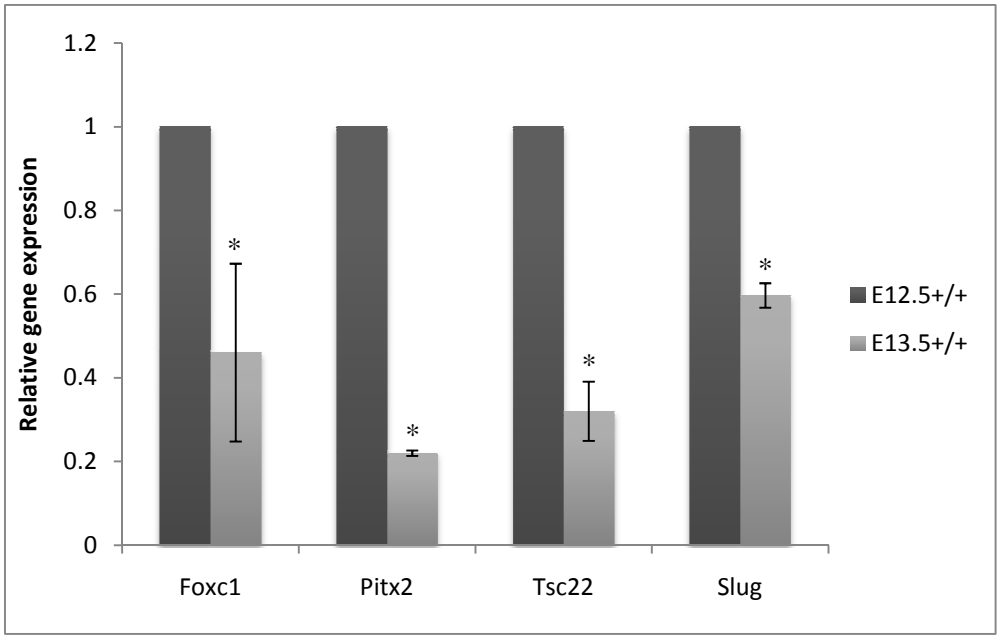

Figure 3.9: Real time qPCR analysis of *Foxc1, Pitx2, Tsc22* and *Slug* expression in POM cells at E13.5$^{+/+}$ relative to E12.5$^{+/+}$POM cells. (*=p<0.05, n=3; error bars = SEM).).

All genes are significantly downregulated at E13.5 with respect to E12.5 in POM cells (p<0.05). *Pitx2* is the most significantly downregulated by (up to 80%) while *Foxc1* expression is half that observed at E12.5 as seen in Figure 3.9.

3.5. Confirmation of transfection and functional efficiency of plasmids

To assess the effect of *Foxc1* overexpression and knockdown on the genes of interest *Pitx2*, *Tsc22* and *Slug*, E12.5$^{+/+}$ and E13.5$^{+/+}$ POM cell lines were transfected with p*Foxc1* and a short hairpin RNA targeting *Foxc1*, psh*Foxc1*.

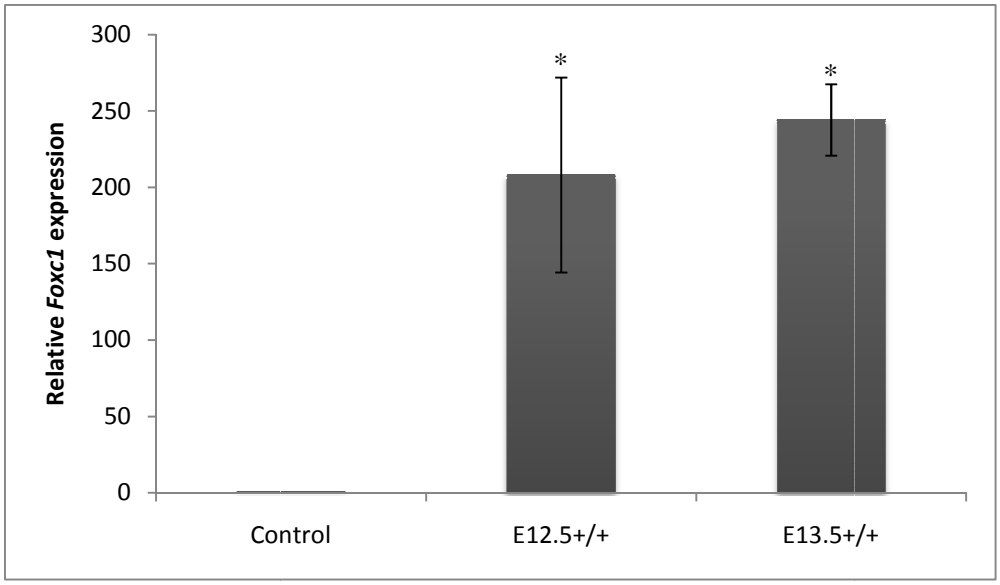

Figure 3.10: *Foxc1* overexpression efficiency analysis. Real time qPCR of p*Foxc1*-EGFP transfected E12.5$^{+/+}$ and E13.5$^{+/+}$ POM cells relative to control (untreated) POM cells. (*=p<0.05, n=3; error bars = SEM).

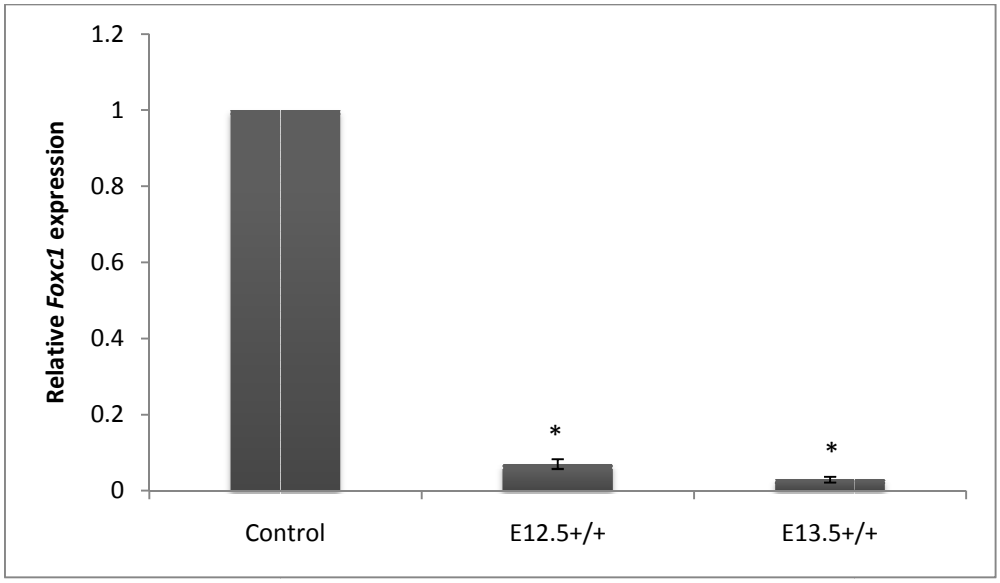

Figure 3.11: *Foxc1* knockdown efficiency analysis. Real time qPCR of the effect of psh*Foxc1* on *Foxc1* expression in E12.5$^{+/+}$ and E13.5$^{+/+}$ POM cell lines. (*=p<0.05, n=3; error bars = SEM).

Overexpression of *Foxc1* resulted in a 197 and 244-fold increase in *Foxc1* expression in E12.5$^{+/+}$ and E13.5$^{+/+}$ POM cells respectively (Figure 3.10). The corresponding knockdown efficiencies were 95% and 98% (Figure 3.11). These results indicate efficient transfection and both significant overexpression and knockdown of *Foxc1*.

3.6. The effect of overexpression and knockdown of *Foxc1* on *Pitx2, Tsc22* and *Slug* expression in POM cells at E12.5 and E13.5

As *Foxc1* is a transcription factor essential for normal development of the anterior segment of the eye, it was of interest to investigate the effect of silencing and overexpression on the expression of the genes of interest known to be expressed in the anterior segment.

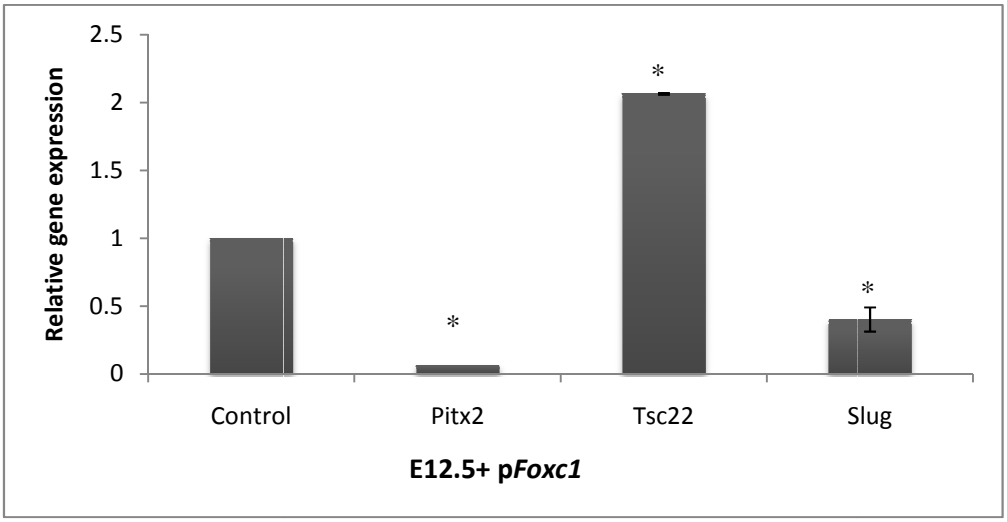

Figure 3.12: Real time qPCR analysis of *Pitx2, Tsc22* and *Slug* expression in response to *Foxc1* overexpression on at E12.5, relative to untreated $12.5^{+/+}$ POM cells. (*=p<0.05, n=3; error bars = SEM).

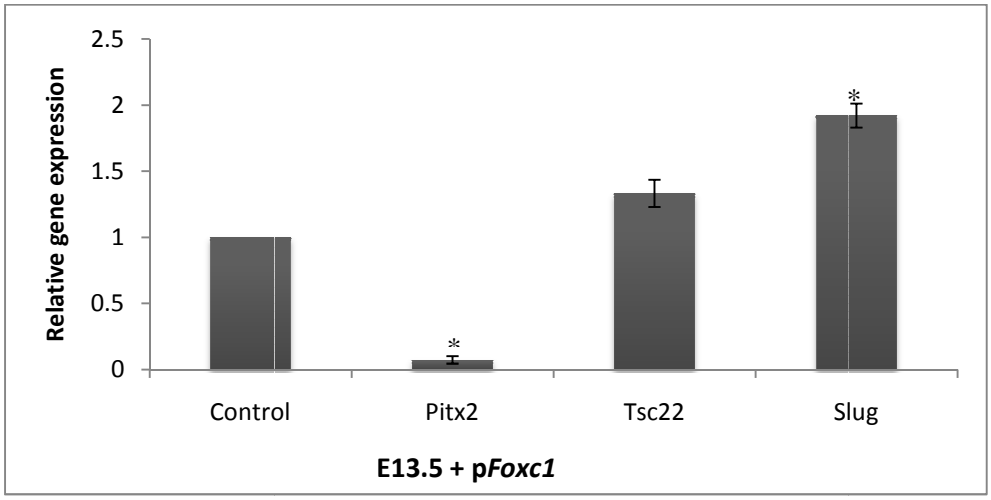

Figure 3.13: Real time qPCR analysis of *Pitx2, Tsc22* and *Slug* expression in response to *Foxc1* overexpression on at E13.5, relative to untreated $13.5^{+/+}$ POM cells. (*=p<0.05, n=3; error bars = SEM).

Overexpression of *Foxc1* at E12.5 significantly inhibits *Pitx2* and *Slug* expression ($p<0.05$) and promotes *Tsc22* expression (Figure 3.12). At E13.5, *Pitx2* is still inhibited by *Foxc1* overexpression ($p<0.05$) but *Tsc22* is not significantly affected. *Slug* seems to be upregulated 2-fold (Figure 3.13).

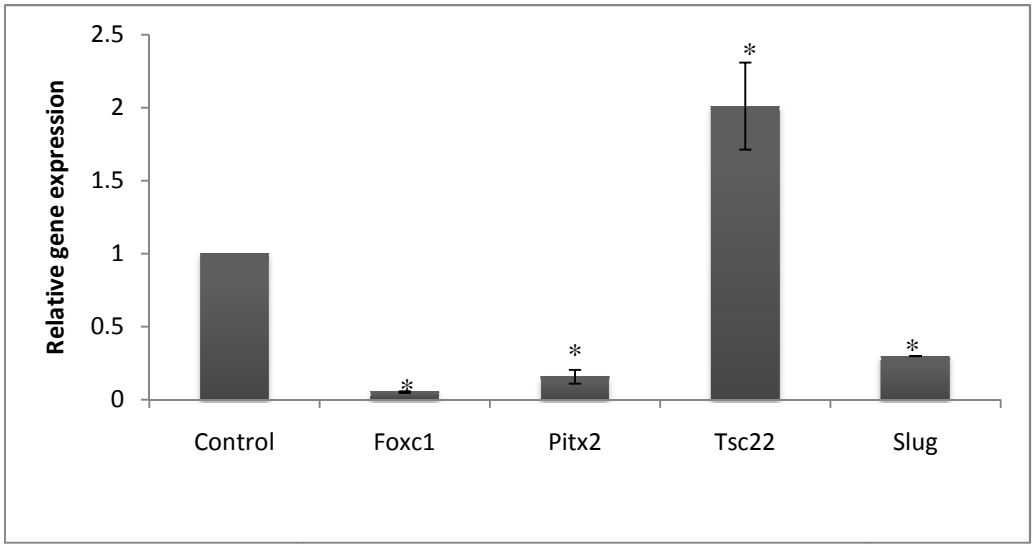

Figure 3.14: Real time qPCR analysis of the effect of *Foxc1* knockdown on *Pitx2, Tsc22* and *Slug* expression at E12.5, relative to untreated E12.5$^{+/+}$ POM cells. *Foxc1* knockdown is repeated for comparison. (*=$p<0.05$, n=3; error bars = SEM).

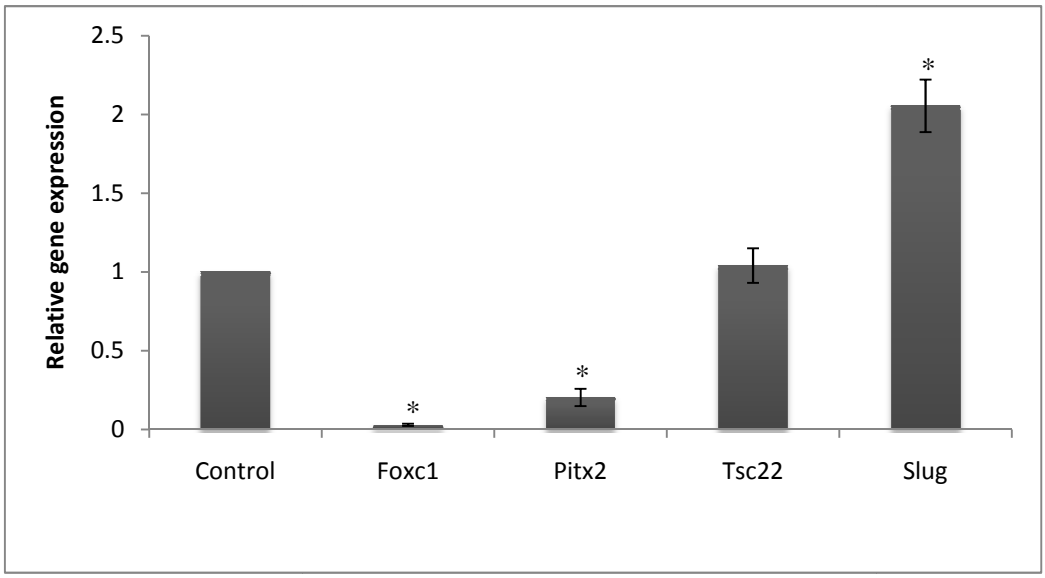

Figure 3.15: Real time qPCR analysis of the effect of *Foxc1* knockdown on *Pitx2, Tsc22* and *Slug* expression at E13.5, relative to untreated E13.5$^{+/+}$ POM cells. *Foxc1* knockdown is repeated for comparison. (*=$p<0.05$, n=3; error bars = SEM).

At E12.5, *Foxc1* knockdown significantly inhibits *Pitx2* and *Slug* expression ($p<0.05$) while appearing to enhance *Tsc22* expression (Figure 3.14). At E13.5, *Pitx2* expression is still reduced while *Tsc22* and *Slug* appear unaffected (Figure 3.15).

3.7. Real time quantitative qPCR of the effect of the lens on *Foxc1*, *Pitx2, Tsc22* and *Slug* expression at E12.5

To assess the effect of the lens on E12.5 wild type POM cells, cells were exposed to whole chick lenses for 24 hours and qPCR was performed on the RNA isolated. Results for *Foxc1* (Figure 3.16), *Pitx2* (Figure 3.17), *Tsc22* (Figure 3.18) and *Slug* (Figure 3.19) are shown below. Gene expression data was expressed relative to the control (untreated POM cells). The role of *Foxc1* in interpreting signals from the lens was determined by transfecting the cells with a *Foxc1* directed shRNA, then further treating by exposure to E6 whole chick lenses and comparing the data to lens treated cells. As a negative control, E12.5 and E13.5 cells were also exposed to boiled E6 and E8 lenses respectively (adapted from Coulombre and Coulombre, 1964). Boiled lenses had no effect on gene expression relative to the control (Appendix D).

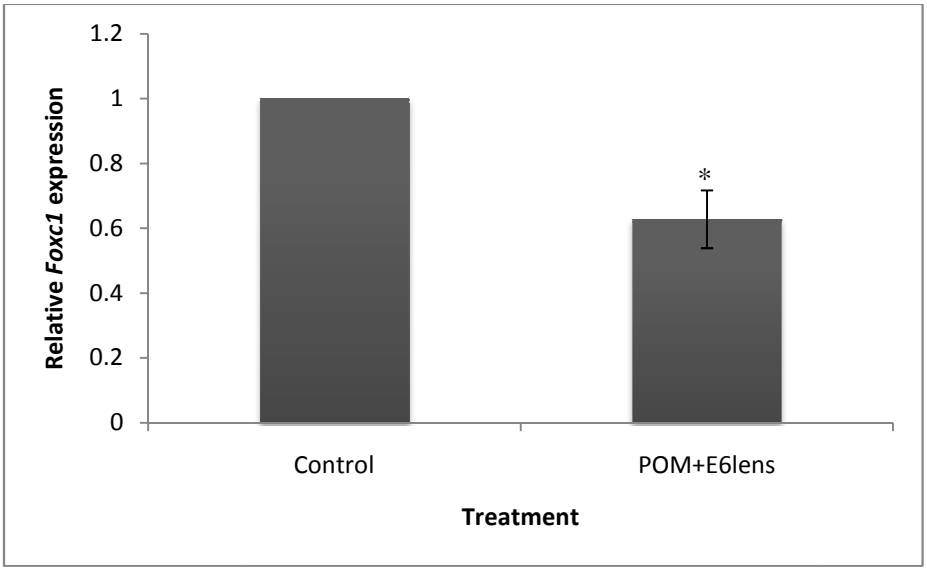

Figure 3.16: The expression of *Foxc1* in E12.5 POM cells in response to treatment with E6 lenses in normal cells relative to the control. (*=$p<0.05$, n=3; error bars = SEM).

Foxc1 expression is significantly downregulated by 40% as a response to E6 lens exposure ($p<0.05$).

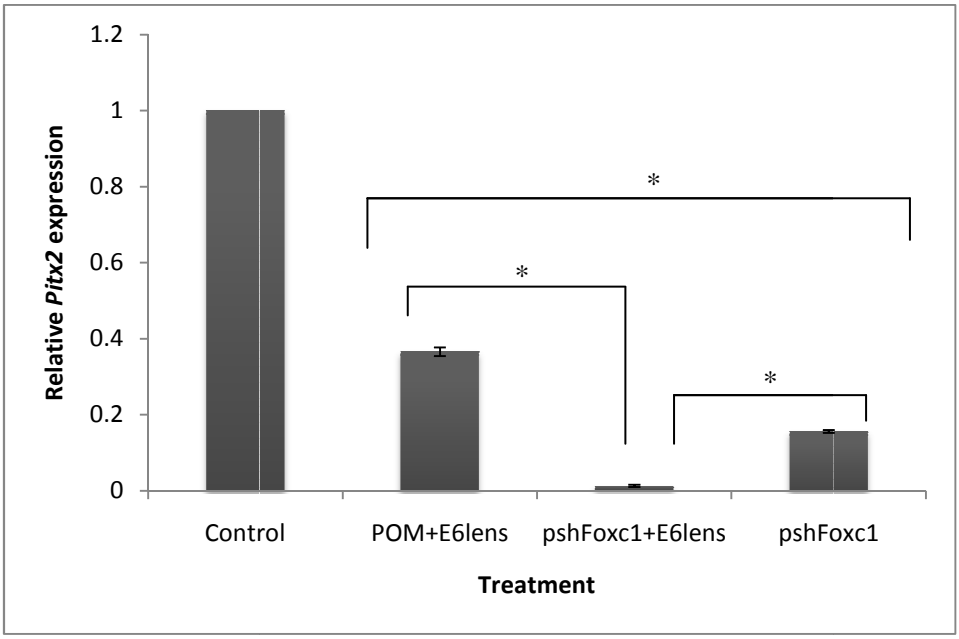

Figure 3.17: The expression of *Pitx2* in E12.5 POM cells in response to treatment with E6 lenses in normal cells and cells in which *Foxc1* expression has been silenced relative to the control. The effect of *Foxc1* silencing alone on *Pitx2* expression is repeated for comparison. (*=p<0.05, n=3; error bars = SEM).

Pitx2 expression in all treatments is significantly downregulated compared to the control. *Pitx2* is downregulated by approximately 60% in lens treated POM cells as compared to expression in the control. Its expression is reduced even more in the presence of the lens and the absence of *Foxc1.*

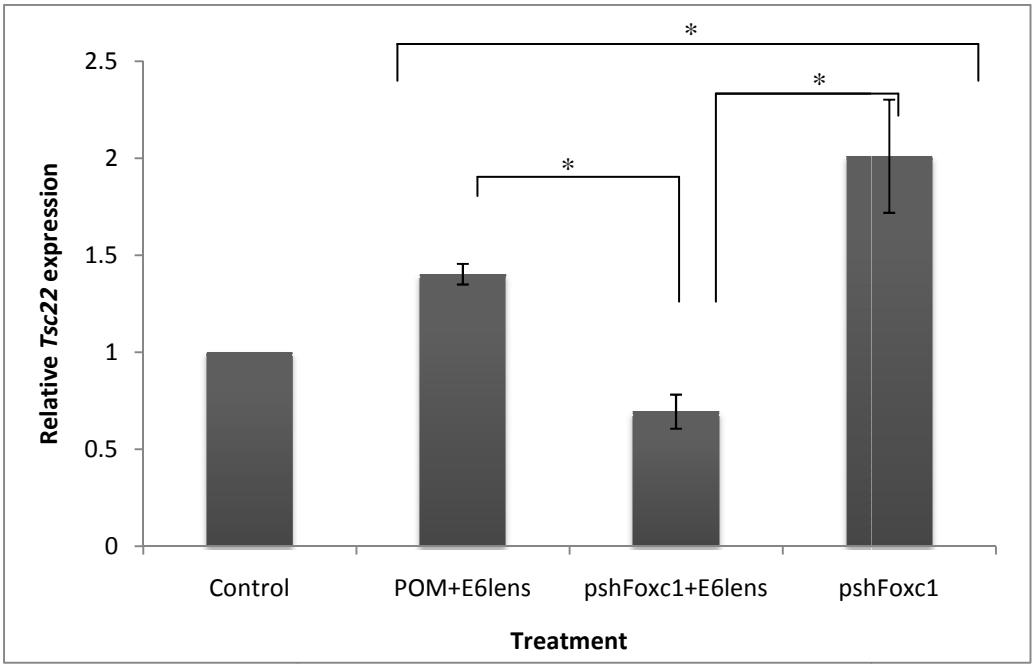

Figure 3.18: The expression of *Tsc22* in E12.5 POM cells in response to treatment with E6 lenses in normal cells and cells in which *Foxc1* expression has been silenced relative to the control. The effect of *Foxc1* silencing on *Tsc22* expression alone is repeated for comparison. (*=$p<0.05$, n=3; error bars = SEM).

When *Foxc1* is silenced, *Tsc22* expression is doubled. *Tsc22* expression is also increased by approximately 30% (relative to the control) when the POM cells are exposed to the lens ($p<0.05$). However when E12.5 cells are exposed to the lens and *Foxc1* knockdown, *Tsc22* expression is observed to decrease by 30% significantly with respect to the control.

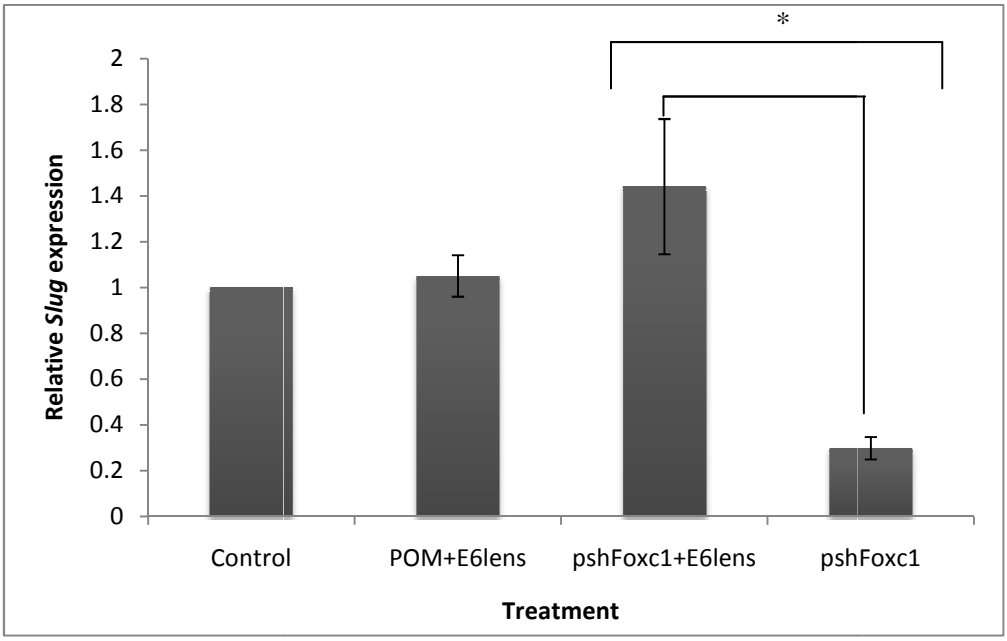

Figure 3.19: The expression of *Slug* in E12.5 POM cells in response to treatment with E6 lenses in normal cells and cells in which *Foxc1* expression has been silenced relative to the control. The effect of *Foxc1* silencing alone on *Slug* expression is repeated for comparison. (*=p<0.05, n=3; error bars = SEM).

E12.5$^{+/+}$ POM cells show no significant change in *Slug* expression when exposed to E6 lens. *Foxc1* silenced cells express 60% less *Slug* compared to the control. Expression of E12.5 cells to lens in the absence of Foxc1 results in a significant upregulation when compared to *Foxc1* knockdown alone.

3.8. Real time quantitative analysis of the effect of recombinant TGFβ2 on *Foxc1, Pitx2, Tsc22* and *Slug* expression of POM cells at E12.5

Lens secreted factors such as TGFβ2 have been implicated in the regulation of *Foxc1* and *Pitx2* during normal ocular development (Ittner *et al.*, 2005) and proteins of this family have been associated with epithelial-mesenchymal transition as well as differentiation of neural crest derived cells (Thut *et al.*, 2001). In this investigation, whole chick lenses were used to investigate the effect of the lens on POM cell lines at E12.5 and E13.5 by measuring gene expression and cell proliferation. Figures 3.20 (*Foxc1*), 3.21 (*Pitx2*), 3.21 (*Tsc22*), 3.23 (*Slug*) show the outcomes of the analyses.

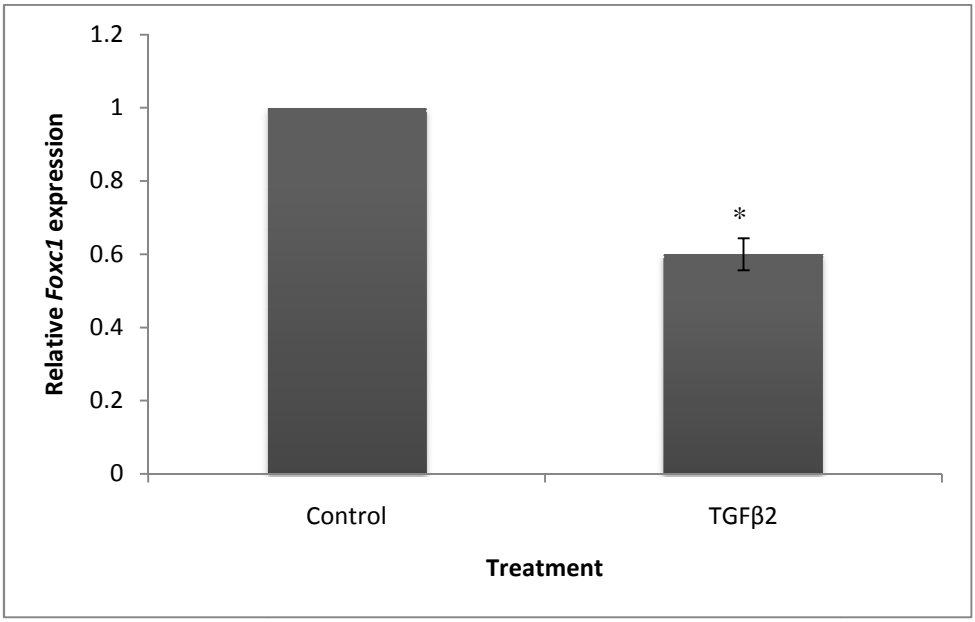

Figure 3.20: The effect of 30ng/mL TGFβ2 on *Foxc1* expression in normal cells relative to untreated (control) cells at E12.5. (*=p<0.05, n=3; error bars = SEM).

Foxc1 expression was observed to be 40% lower in TGFβ2 treated cells compared to the control (p<0.05).

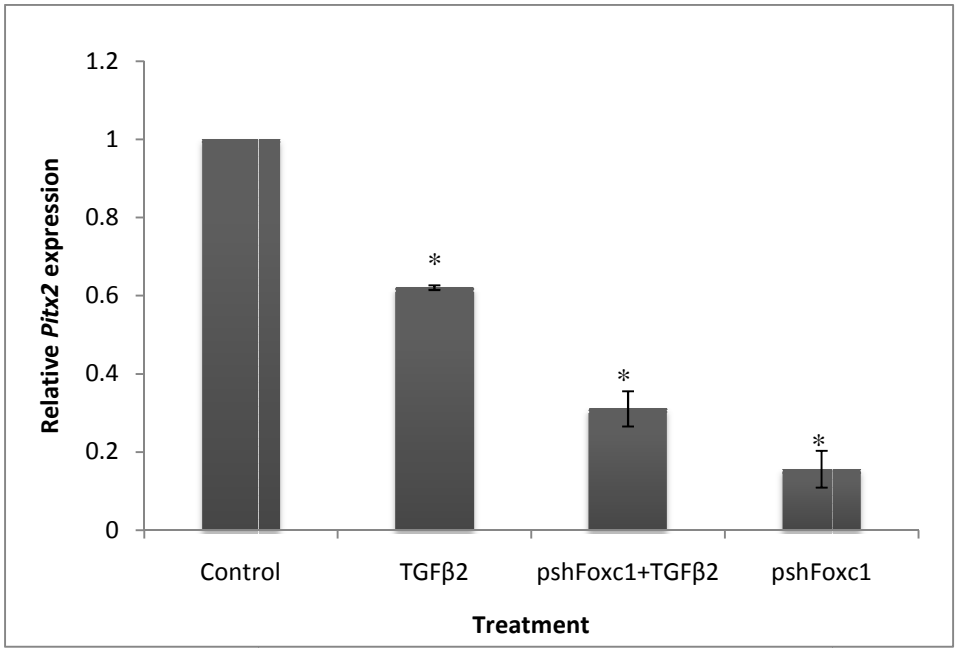

Figure 3.21: The effect of 30ng/mL TGFβ2 on *Pitx2* expression in normal cells and cells in which *Foxc1* has been silenced (psh*Foxc1*+TGFβ2), relative to untreated (control) cells at E12.5. The knockdown data is shown for comparison. (*=p<0.05, n=3; error bars = SEM).

Pitx2 is downregulated by 40% when treated with TGFβ2 and 85% in *Foxc1* silenced cells. *Pitx2* expression in E13.5 shRNA+TGFβ2 treated cells however is downregulated by 70% when compared to normal cells.

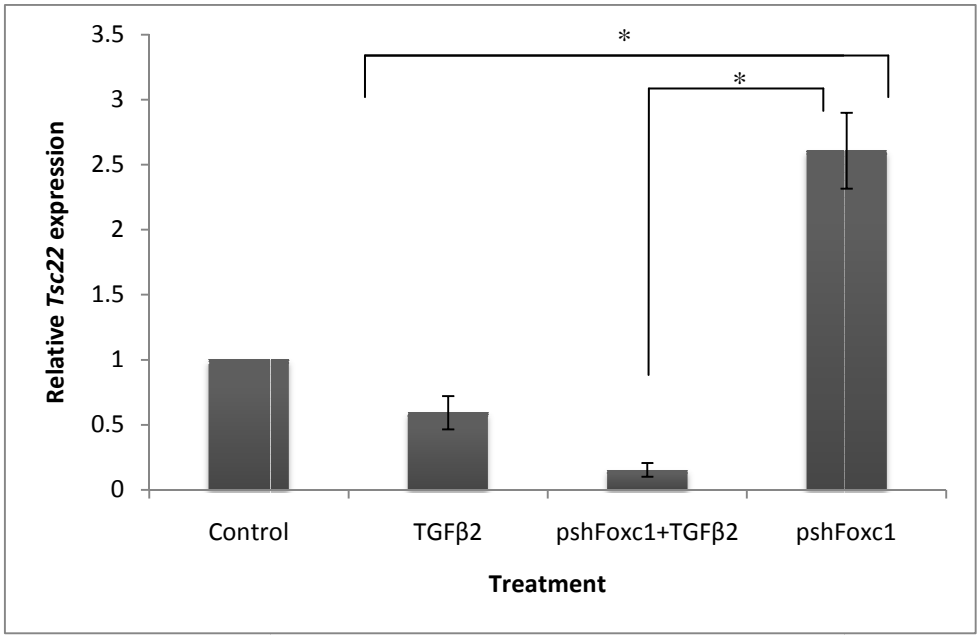

Figure 3.22: The effect of 30ng/mL TGFβ2 on *Tsc22* expression in normal cells and cells in which *Foxc1* has been silenced (psh*Foxc1*+ TGFβ2), relative to untreated (control) cells at E12.5. The knockdown data is shown for comparison. (*=p<0.05, n=3; error bars = SEM).

Tsc22 is 40% downregulated in TGFβ2 treated cells and upregulated by 2.5 times in *Foxc1* silenced POM cells (p<0.05). When both treatments are applied, 85% downregulation is observed compared to untreated cells (p<0.05).

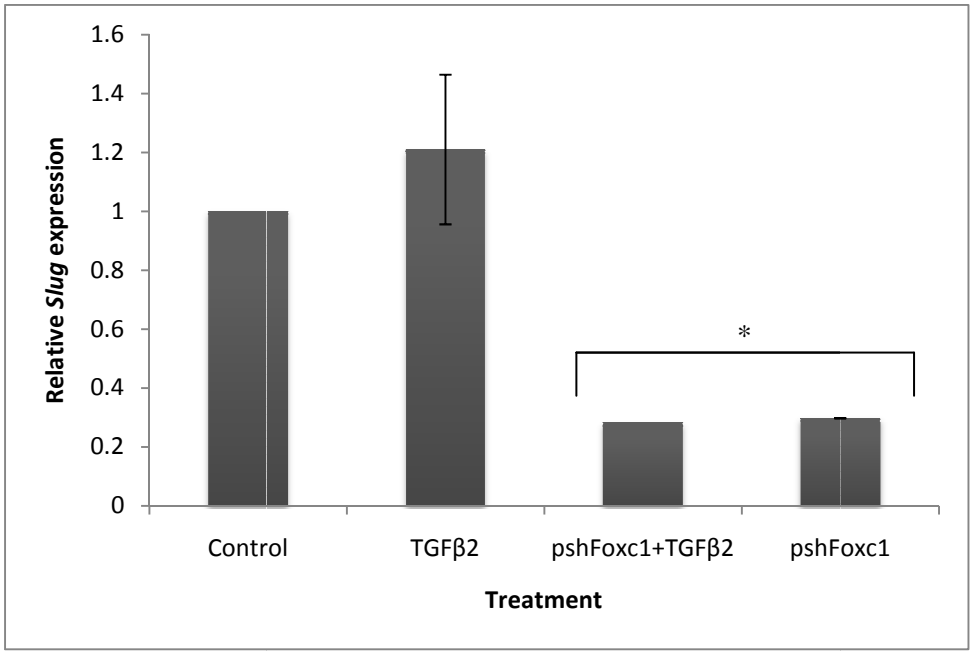

Figure 3.23: The effect of 30ng/mL TGFβ2 on *Slug* expression in normal cells and cells in which *Foxc1* has been silenced (shRNA+ TGFβ2), relative to untreated (control) cells at E12.5. The knockdown data is shown for comparison. (*=p<0.05, n=3; error bars = SEM).

Slug expression in TGFβ2 treated cells is slightly but insignificantly upregulated (p>0.05) as compared to the control. *Foxc1* silenced cells express about 30% of the normal levels of *Slug* (p<0.05). The same is observed in the psh*Foxc1*+TGFβ2 treatment. There is a slight but insignificant difference between the control and the TGFβ2.

3.9. The effect of the lens and TGFβ2 on *Foxc1, Pitx2, Tsc22* and *Slug* expression at E13.5

As mentioned in Section 3.7, TGFβ2 is a lens derived signal that has been speculated to regulate *Foxc1* expression in POM cells. To assess the nature of this association at E13.5, POM cells were exposed to recombinant TGFβ2 (30ng/mL of culture medium) for 24 hours. RNA was isolated from the cells and cDNA synthesised for qPCR analysis of *Foxc1* (Figure 3.24), *Pitx2* (Figure 3.25), *Tsc22* (Figure 3.26) and *Slug* (Figure 3.27).

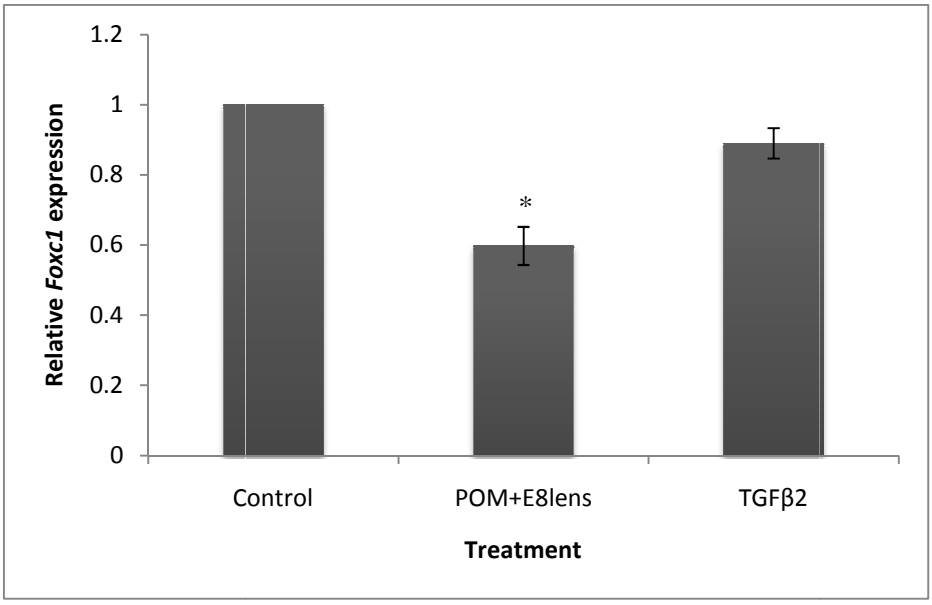

Figure 3.24: The expression of *Foxc1* in E13.5 POM cells in response to treatment with E8 lenses and TGFβ2 relative to the control. The effect of silencing alone is repeated for comparison. (*=p<0.05, n=3; error bars = SEM).

Foxc1 expression is significantly downregulated in lens exposed cells, relative to the control (p<0.05). TGFβ2 treatment causes a slight but non-significant decrease in *Foxc1* expression.

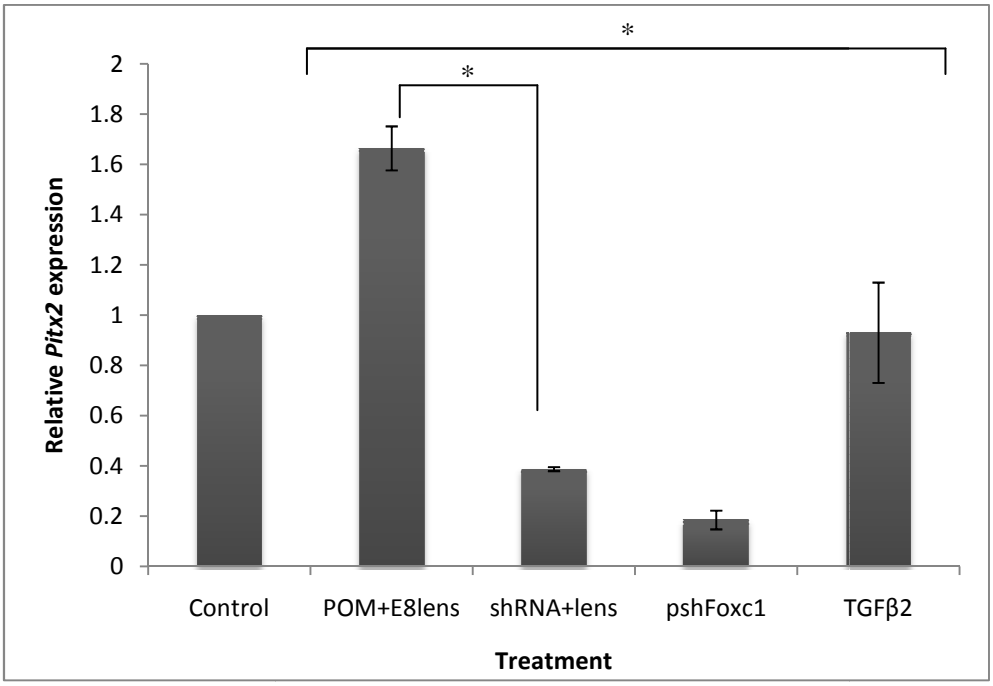

Figure 3.25: The expression of *Pitx2* in E13.5 POM cells in response to treatment with E8 lenses in normal cells and cells in which *Foxc1* expression has been silenced, and cells treated with TGFβ2 relative to the control. The effect of *Foxc1* silencing alone on *Pitx2* is repeated for comparison. (*=p<0.05, n=3; error bars = SEM).

Pitx2 expression is increased 1.6 times in response to E8 lens exposure in E13.5 POM cells (p<0.05). There is a significant difference between lens exposed cells and cells subjected to the knockdown and lens. In *Foxc1* silenced cells, *Pitx2* is expressed at about 20% of the levels seen in the control. E13.5 cells treated with the shRNA and exposed to E8 lenses also show a 40% decrease in *Pitx2* compared to the control (p<0.05). There is no significant change in expression in TGFβ2 treated cells.

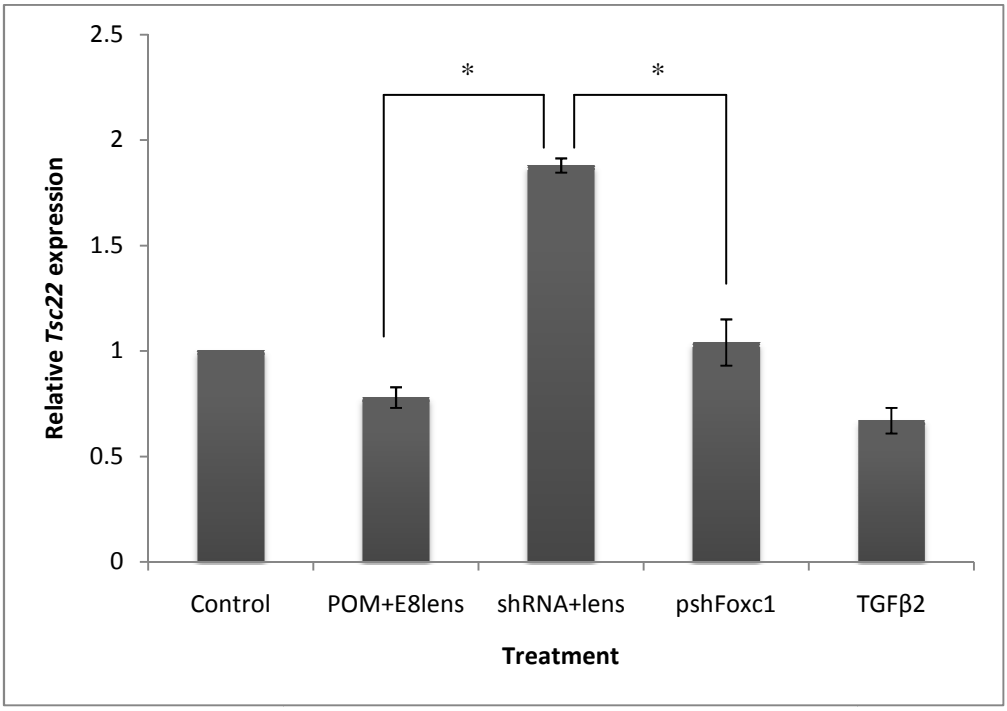

Figure 3.26: The expression of *Tsc22* in E13.5 POM cells in response to treatment with E8 lenses in normal cells and cells in which *Foxc1* expression has been silenced, and TGFβ2 relative to the control. The effect of silencing alone is repeated for comparison. (*=p<0.05, n=3; error bars = SEM).

Tsc22 expression remains relatively unchanged when *Foxc1* is silenced, when cells are exposed to lenses and when treated with TGFβ2. However psh*Foxc1*+lens treatments cause *Tsc22* expression to double relative to untreated POM cells. There is a significant downregulation in *Tsc22* expression between psh*Foxc1*+lens and lens exposed cells; and between psh*Foxc1*+lens treated cells and *Foxc1* silenced cells (p<0.05).

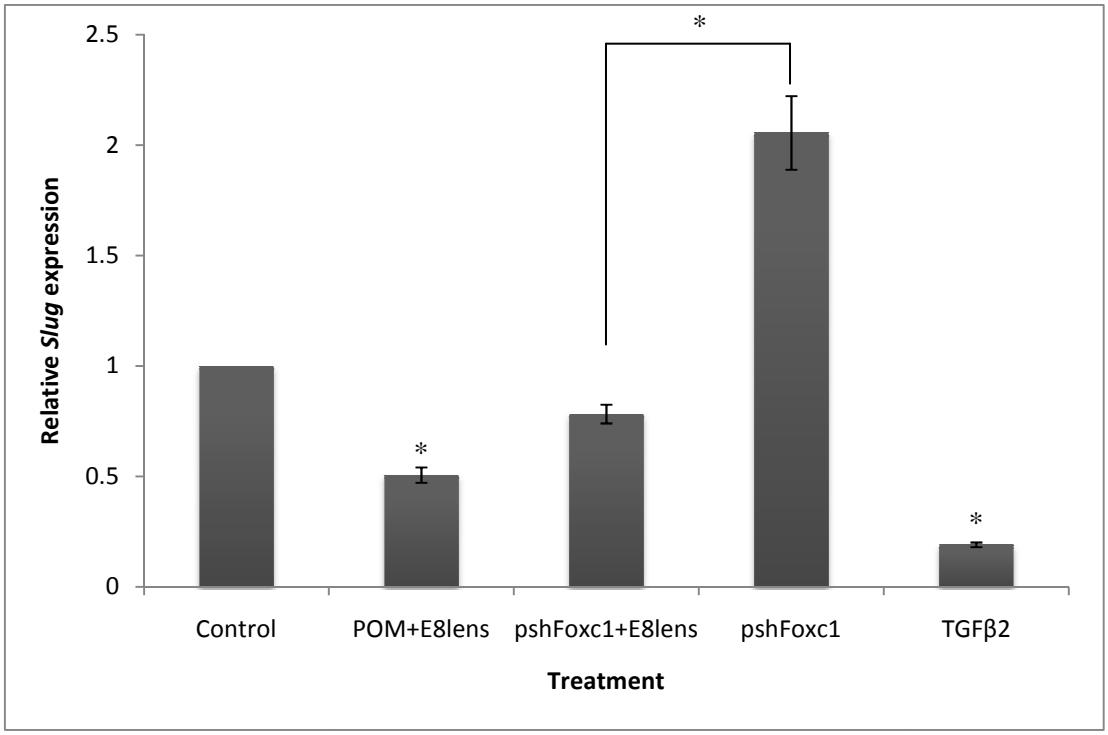

Figure 3.27: The expression of *Slug* in E13.5 POM cells in response to treatment with E8 lenses in normal cells, cells in which *Foxc1* expression has been silenced, and TGFβ2 treated cells relative to the control. The effect of *Foxc1* silencing alone on *Tsc22* expression is repeated for comparison. (*=p<0.05, n=; error bars = SEM 3).

Slug expression is significantly decreased in lens exposed and TGFβ2 treated cells (p<0.05). Expression in psh*Foxc1*+lens treated cells remains relatively unchanged. *Foxc1* silenced cells upregulated *Slug* expression 2-fold.

3.10. The effect of the lens on POM cell proliferation

To investigate any effect the lens may have on proliferation, E12.5$^{+/+}$ and E13.5$^{+/+}$ POM cells were exposed to E6 and E8 whole chick lenses respectively. 1x10^{3} E12.5$^{+/+}$ and E13.5$^{+/+}$ POM cells per well were seeded in 96 well plates and assayed made at 24 hour intervals, by measuring absorption at 490nm. Proliferation was quantified by MTS assay (Figures 3.28 and 3.29).

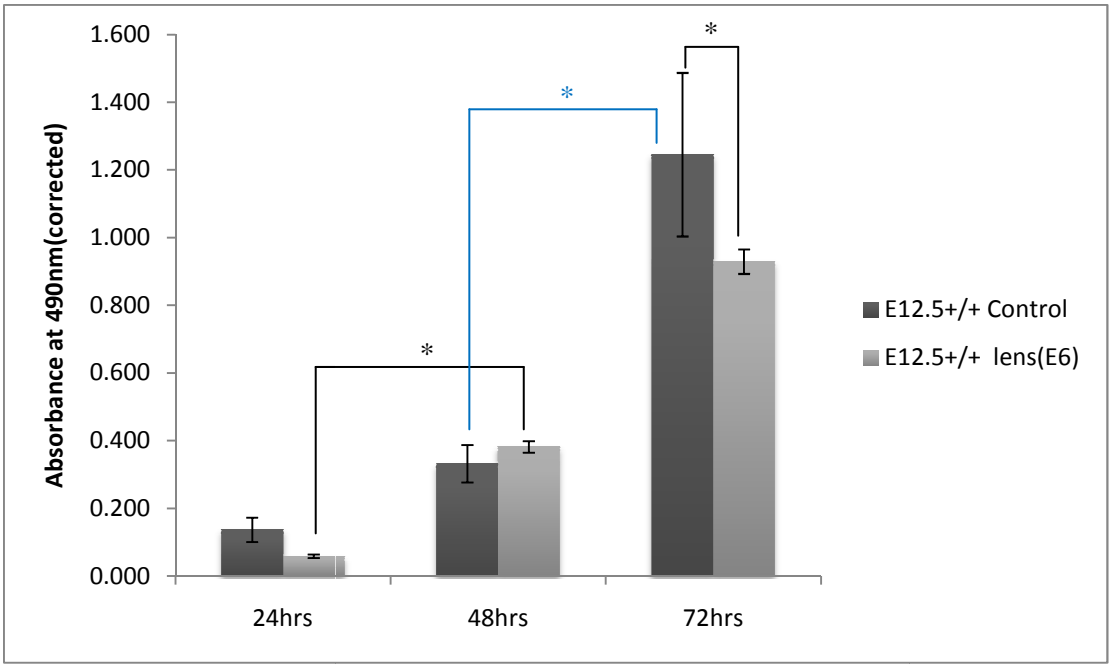

Figure 3.28: Cell proliferation at E12.5 quantified by MTS assay at 490nm. E12.5$^{+/+}$ POM cells were exposed to E6 whole chick lenses and proliferation compared to unexposed E12.5$^{+/+}$ POM cells. Measurements were made every 24 hours. Significant changes are indicated in different colours for clarity. (*=$p<0.05$, n=3; error bars = SEM).

There is a general, expected increase in proliferation across the time trial in both the control and treated cells (Figure 3.28). At 24 hours, there is no significant difference between the treated and untreated cultures ($p>0.05$). After 48 hours there is also no significant difference between treated and untreated cells. Interestingly, there is a 5.5-fold increase in proliferation between 24 and 48 hours in the lens treated POM cells ($p<0.05$); compared to the less than 1.5-fold increase in untreated cells. By 72 hours, there is a significant difference between the treated and untreated cells shown in blue ($p<0.05$). While a 3-fold increase is observed in the control ($p<0.05$) between 48 and 72 hours, the lens treated cells only showed a 1.5-fold increase in proliferation ($p<0.05$). Thus, the lens seems to stimulate proliferation of E12.5 POM cells between 24 and 48 hours but by 72 hours its presence appears to inhibit proliferation, relative to the control.

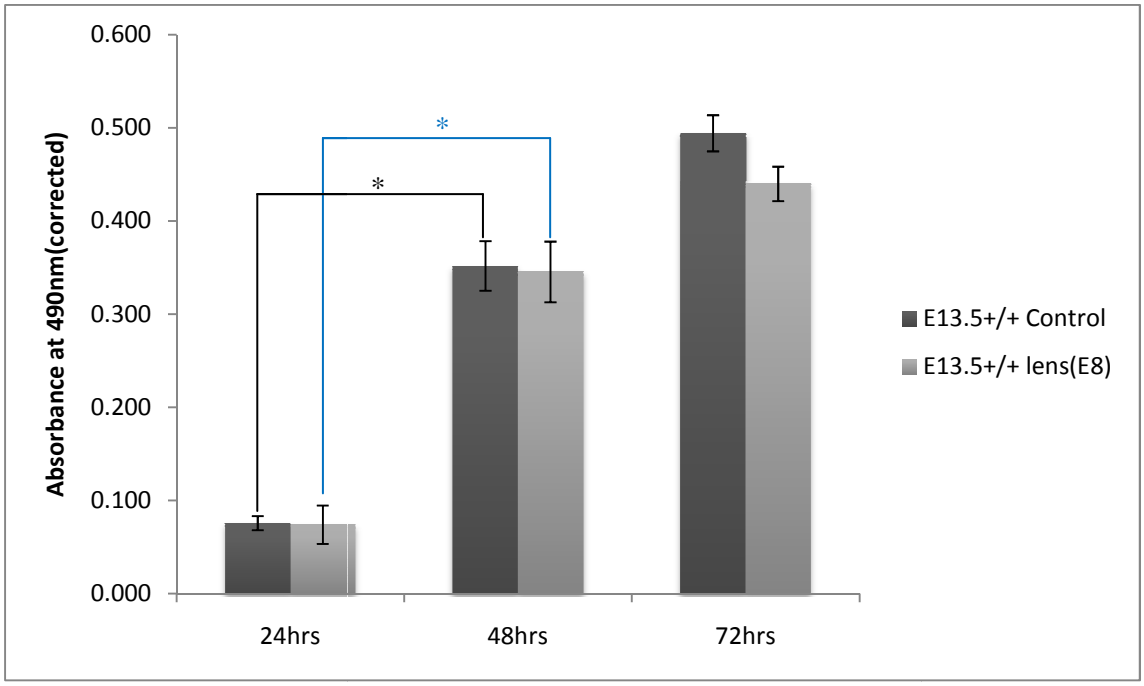

Figure 3.29: Cell proliferation at E13.5 quantified by MTS assay at 490nm. E13.5$^{+/+}$ POM cells were exposed to E8 whole chick lenses and proliferation compared to untreated E13.5$^{+/+}$ POM cells. Absorbances were read every 24 hours. Significant changes are indicated in different colours for clarity. (*=$p<0.05$, n=3; error bars = SEM).

As seen in Figure 3.29, after 24 hours of lens exposure, there was no significant difference in proliferation in E8 lens treated E13.5 POM cells compared to the control. After 48 hours, there was still no significant difference in proliferation between the treated and untreated cells. There was however a significant increase in proliferation between 24 and 48 hours in the control shown in black ($p<0.05$). Lens treated cells also showed a significant increase in proliferation between 24 and 48 hours indicated in blue ($p<0.05$).

3.11. Assessing mesenchyme to epithelial transition in POM cells at E12.5 and E13.5 using *N-cadherin* as a marker of cell differentiation

POM cells of neural crest origin differentiate into the ciliary body of the eye, sclera, iris, blood vessels and cornea through mesenchymal-epithelial transitions. *N-cadherin* is a protein expressed in cells derived from the neural crest, responsible for adhesion and forming tight junctions between cells. It plays an important role in embryonic development, by initiating changes in undifferentiated cells. *N-cadherin* was used in this study to assess the structural/inter-cellular changes in POM cells between E12.5 and E13.5.

3.11.1. Real time qPCR analysis of *N-cadherin* expression at E12.5 and E13.5

N-cadherin expression is noted from E9.5 in various tissues of mouse embryos. Its distribution and expression levels associated with cellular rearrangement, and its use as a marker of differentiation prompted this investigation. RNA was isolated from E12.5$^{+/+}$ and E13.5$^{+/+}$ cells for cDNA synthesis for use in qPCR analysis. *N-cadherin* expression at E13.5 relative to expression at E12.5 is show in Figure 3.30 below.

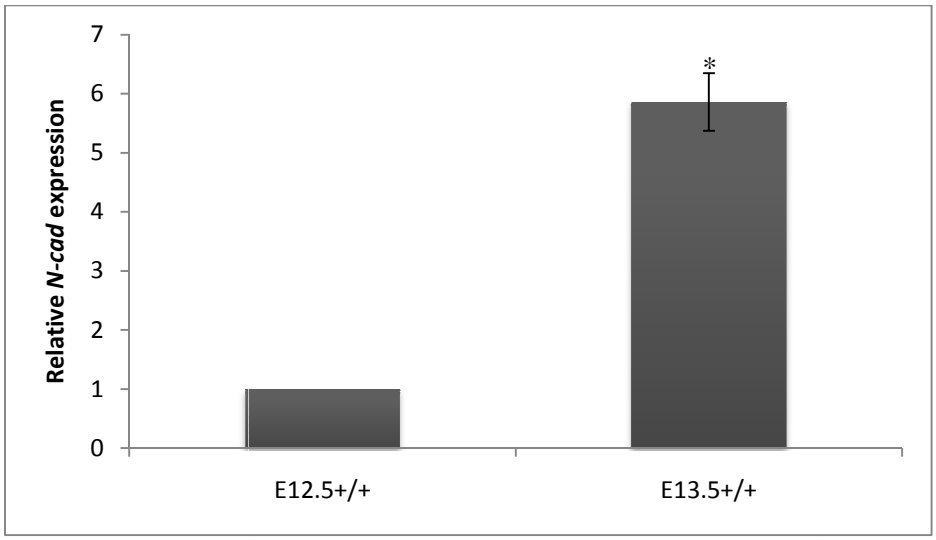

Figure 3.30: Real time quantitative analysis of *N-cadherin* expression in POM cells at E12.5 and E13.5. (*=p<0.05, n=3; error bars = SEM).

N-cadherin is upregulated at least 5-fold between E12.5 and E13.5 in POM cells.

3.11.2. Confocal Microscopy

Confocal microscopy is a fluorescence microscopy technique that uses point illumination as opposed to whole specimen illumination associated with conventional fluorescence microscopy. This allows the excitation of specific regions on the sample and fluorescence in that area only, eliminating unfocused light detection. The proximity of the pinhole (origin of illumination) to the focal plane also prevents detection of a large amount of background which is a limitation of traditional fluorescence microscopy. These qualities enhance the resolution of the image produced and can be used to generate a 3-dimensional image of the sample.

E12.5 and E13.5 POM monolayers (Figure 3.31) and hanging drops (Figures 3.32 and 3.33) were incubated with a fluorescent molecule conjugated to antibody. Cy3-conjugated to *N-cadherin* antibody excites at 488nm (Mercury-Argon laser) and is detected using a FITC

filter as green fluorescence (chosen by the investigator - Cy3 fluoresces red). Cell nuclei were stained with DAPI (blue), excited at 405nm (UV) and viewed using a DAPI filter. Differential interference contrast (DIC) images of the samples were also captured. This technique is similar to phase contrast microscopy but uses polarised light in a more complex light path to eliminate background fluorescence. Images were visualised on a Zeiss LSM 710 Laser Scanning Confocal Microscope (Zeiss, Germany) and captured by ZEN 2009 software.

3.11.2.1. Monolayer culture

E12.5 and E13.5 POM cells were cultured for 3 days prior to processing. Cells were grown and processed on cover slips. Cultures were fixed with 4% PFA and mounted in Mowiol with DABCO to prevent bleaching during visualisation. Images for the no-primary and no-secondary antibody controls can be seen in Appendix F.

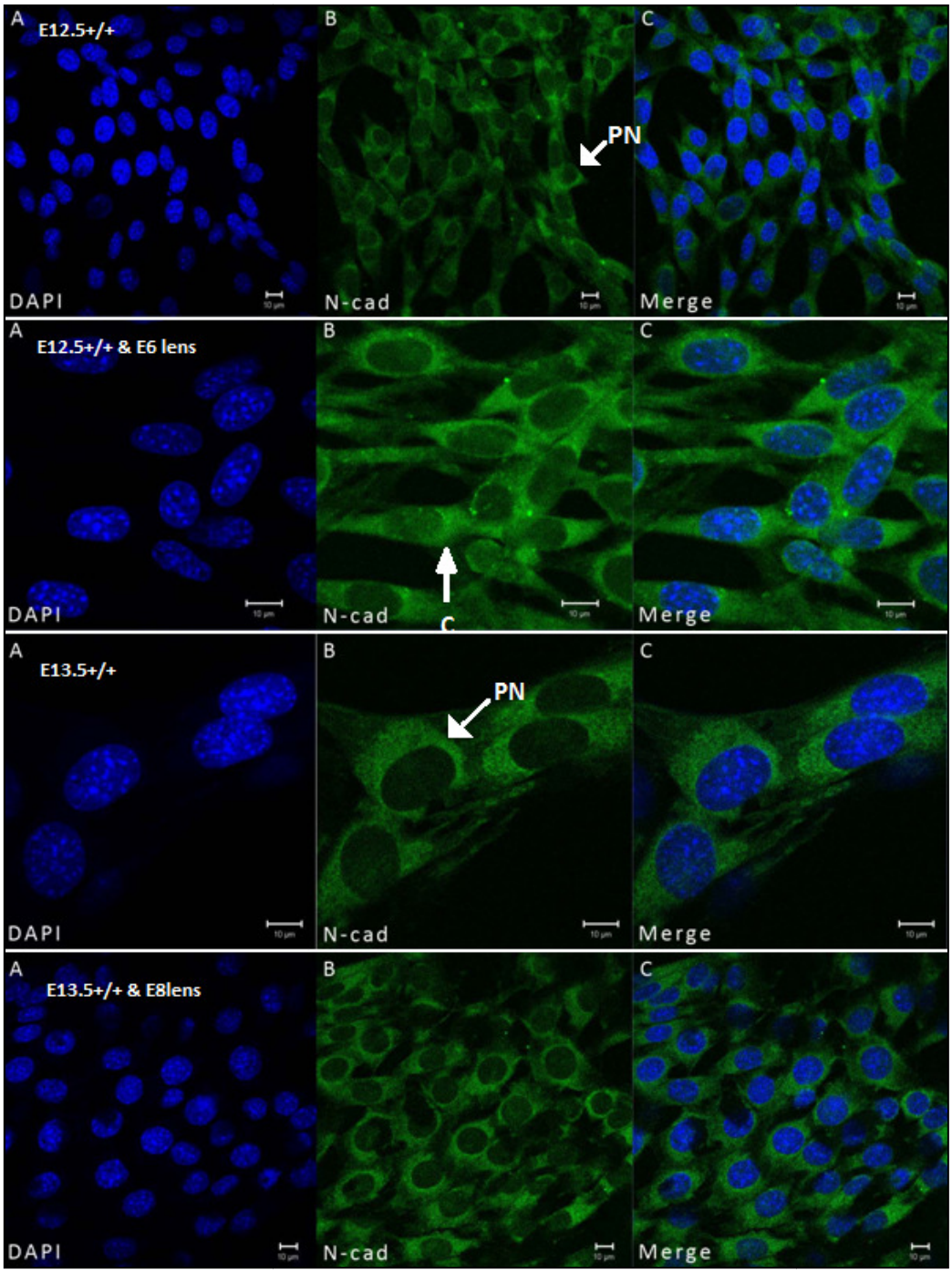

Figure 3.31: 63x confocal image of A) DAPI stained cells B) *N-cadherin* stained cells C) Merged DAPI and *N-cadherin* images. C = *N-cadherin* distributed in the cytoplasm. PN = peri-nuclear distribution of *N-cadherin*. Some images are zoomed for better examination; scale bar is 10μm.

N-cadherin is homogeneously distributed in the cytoplasm in E12.5 POM cells exposed to E6 lens compared to the control in which it is distinctly localised around the nucleus. Peri-nuclear *N-cadherin* is seen at E13.5 with no observed change in distribution with lens exposure.

3.11.2.2. Hanging drop culture

In order to further study *N-cadherin* localisation, E12.5 and E13.5 cells were grown in hanging drops in order to simulate the 3-dimensional conditions of an *in vivo* environment.

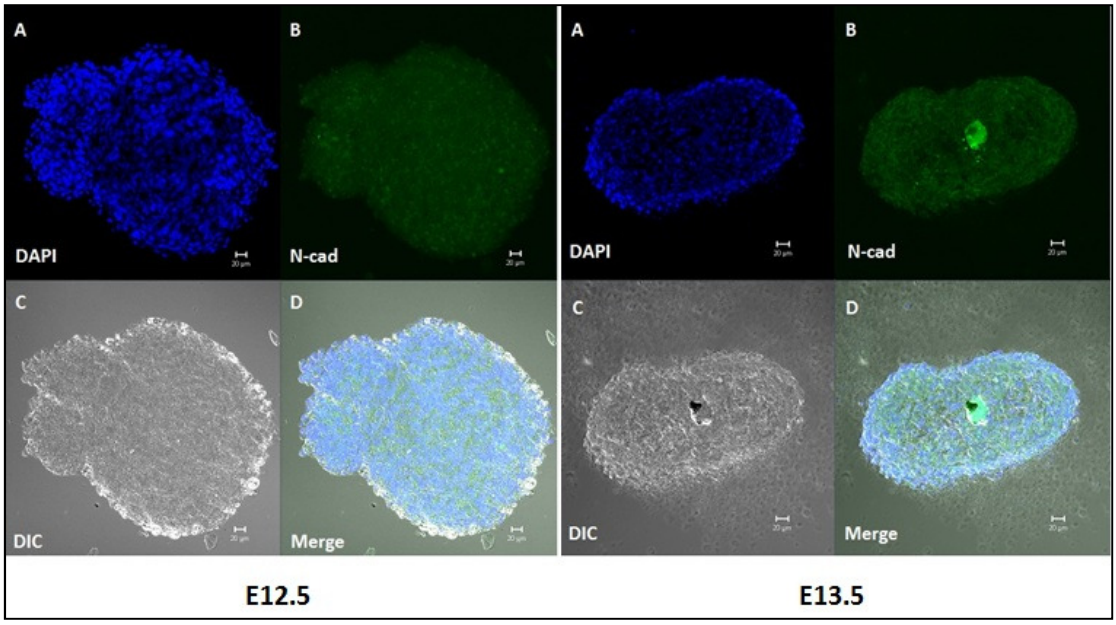

Figure 3.32: 25x confocal image of fixed and mounted E12.5 (left) and E13.5 (right) POM cells spheroids. A) DAPI image B) *N-cadherin* image C) DIC image D) Image merge. Scale bar is 20µm.

After 3 days of culture the E12.5 spheroid is much larger than the E13.5 culture as seen in Figure 3.32. The latter also shows a more regular shaped and regular edged spheroid. This was consistently observed across replicates.

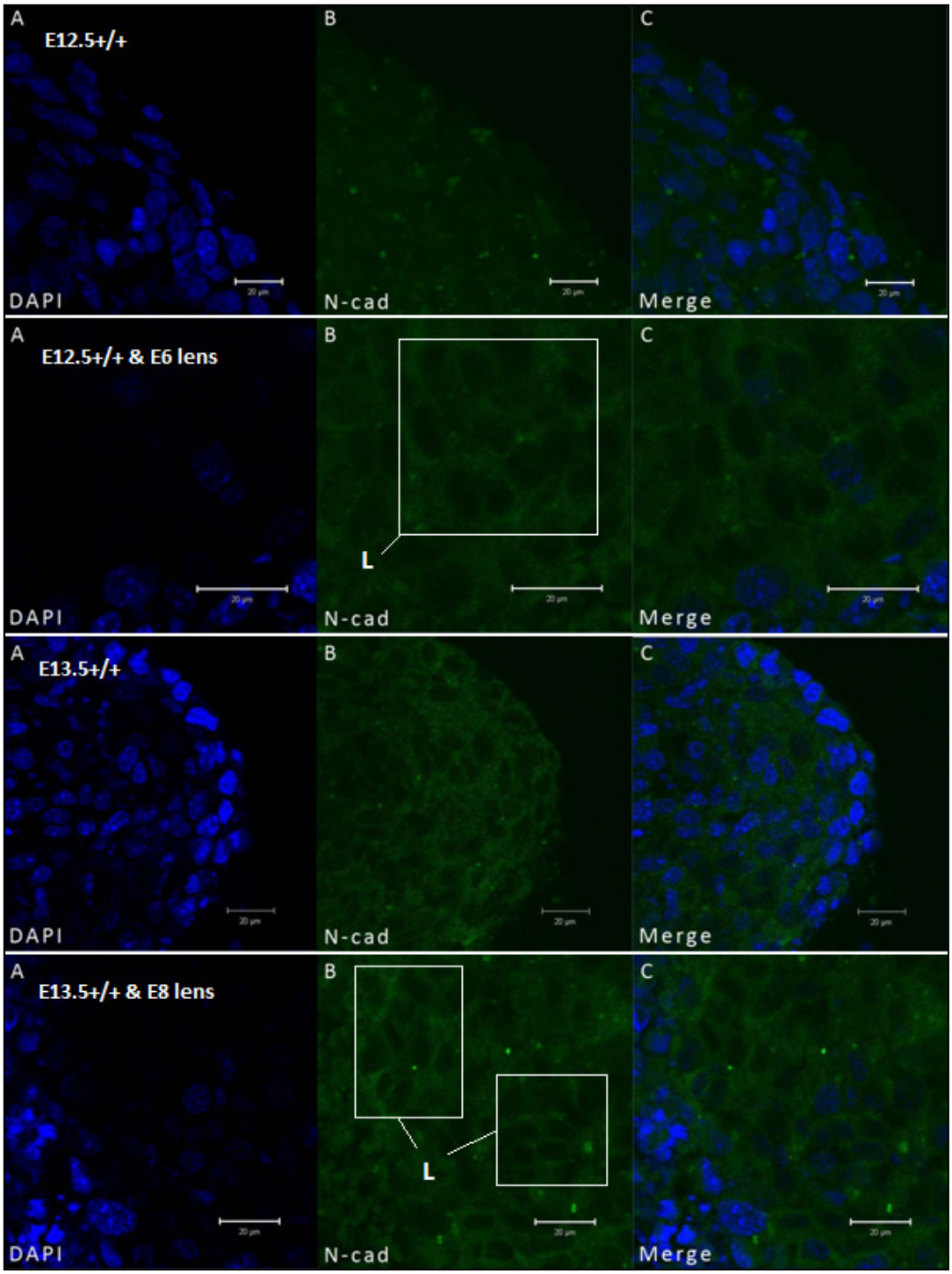

Figure 3.33: 63x confocal image of E12.5, E12.5 + lens treated and E13.5 and E13.5 + lens treated hanging drops. A) DAPI image B) *N-cadherin* image C) Image merge. L = lattice. Scale bar is 20µm.

Cells in the E12.5 control hanging drop are indistinguishable from each other. However when the cells are exposed to E6 lenses, a lattice framework can be observed. The same

lattice is observed in E13.5 hanging drops and the effect is more pronounced in E8 lens treated E13.5 POM cells.

CHAPTER 4: DISCUSSION

4.1. Overview of events preceeding normal anterior segment development

Normal eye development is coordinated by factors and signals interacting with cells and tissues to achieve a complex structure ensuring visual acuity. Development begins at gastrulation with the emergence of three germ layers from which different components of the eye are derived. In a series of inductions, cell-cell interactions give rise to the immature lens and presumptive corneal epithelium between which, POM of neural crest origin differentiate to form the corneal endothelium and corneal stroma (Ittner *et al.*, 2005; Cvekl and Tamm, 2004; Reneker *et al.*, 2000). In tandem, the various supporting structures of the anterior segment (ciliary body, lacrimal gland, irido-corneal angle) are also developed.

Key genes such as *Pitx2* and *Foxc1* are essential during these processes and are thought to be mediated by signals such as Tgfβ2 (Reneker *et al.*, 2000) secreted by the lens epithelium. The importance of these genes in eye development has been revealed by the various anterior segment disorders (ASDs) associated with their mutations. Mutations in the human homologues *PITX2* and *FOXC1,* manifest as the varying phenotypes of Peters' Anomaly and Axenfeld-Rieger Syndrome (Sowden, 2007; Matsuo *et al.*, 1993; Nishimura *et al.*, 2001; Ittner *et al.*, 2005). Also, the formation of a functional lens is pivotal for the correct development of the anterior segment as described by Beebe and Coats (2000) and Flügel-Koch *et al.* (2002).

Markers of epithelial-mesenchymal transition, *Slug* and the *Foxc1* downstream target, *Tsc22*, feature in the delicate development of the corneal endothelium although the specific nature of the interactions is unknown. The corneal endothelium is the most physiologically important tissue of the cornea as it regulates intraocular pressure and the transport of nutrients (Kivelä and Uusitalo, 1998; Tortora and Grabowski, 2003). During its formation, POM cells are directed to condense and form adherens junctions to assume an endothelial phenotype, possibly by *Slug* and *Tsc22* via a speculated interaction with Tgfβ2. This study attempted to determine the role of the lens and *Foxc1* in the expression of genes associated with the formation of the corneal endothelium: *Pitx2, Slug, Tsc22* and *N-cadherin*. A schematic diagram of known and hypothesised interactions is shown below in Figure 4.1.

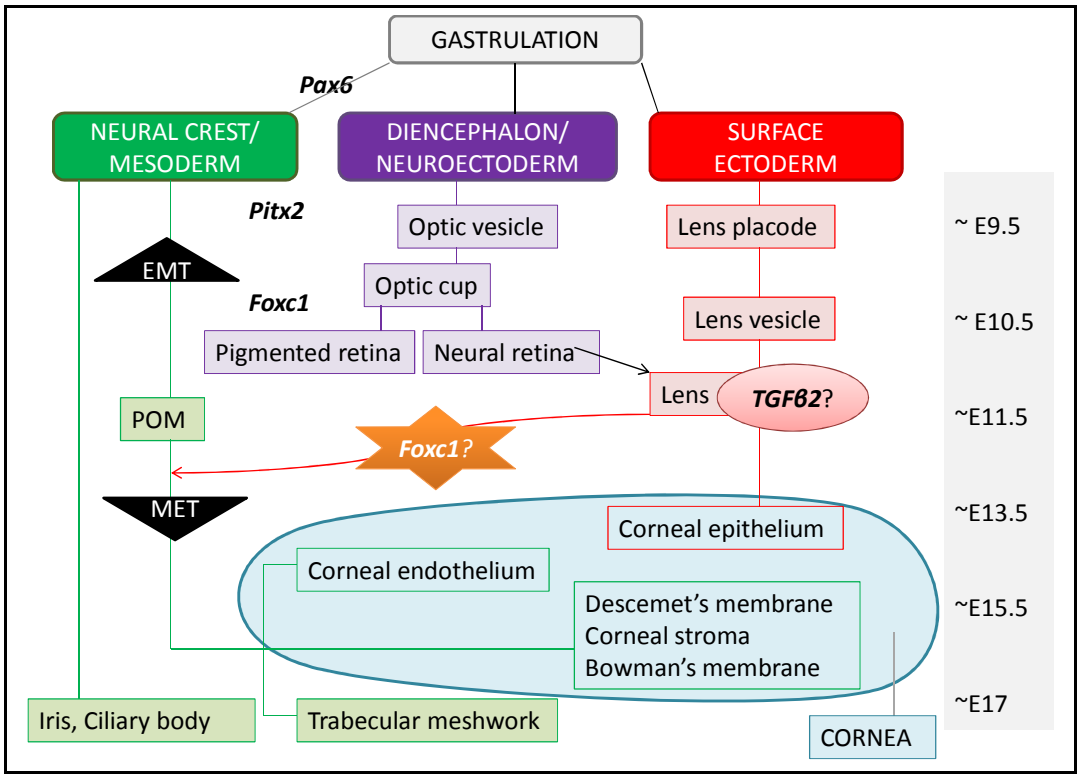

Figure 4.1: Schematic diagram of the events occurring during normal eye development in chronological order. The main objectives of this investigation are also shown.

4.2. SV40 Large T-antigen persists in POM cells, but is no longer temperature sensitive

In order to investigate murine POM cells at E12.5 and E13.5, immortalised cell lines at these stages of development were established by transformation with a temperature-sensitive SV40-Tag (developed by another member of the laboratory as described by Sommer *et al.*, 2006). Such a method of cell propagation allows consistency between handling and storage (cells can be stored in liquid nitrogen and returned to culture with ease) while eliminating errors associated with continuously isolating primary cultures (Ahuja *et al.*, 2005).

SV40 is a *Polyoma* virus associated with tumorigenesis, that contains a large T-antigen which directs infected cells to enter the synthesis phase (S-phase, during which DNA is replicated). Cells transformed by this virus gain extended survival potential and become immortalised by expressing the large T-antigen proteins and overcoming "mechanisms of mortality" (Ahuja *et al.*, 2005; Araki-Sasaki *et al.*, 2000). The large T-antigen binds the heat shock chaperone protein, hsp70, and the tumour suppressor, p53 (a transcriptional

activator), as part of cellular transformation. Upon infection, this protein encodes G418 resistance and is permissive to proliferation at 33°C and growth inhibiting at 37°C, thus permitting differentiation at a higher temperature (Prince *et al.*, 2001).

The investigation began with verification of the presence of the SV40-Tag in low passage (p=8) POM cells in culture. The results (Section 3.2.) show that cell morphology had not changed since infection and was not affected by subsequent treatments (Figure 3.1.); the SV40-Tag was still encoded as proven by a 13 day antibiotic pressure study (Figure 3.2.); and that although still encoded, the protein had lost temperature sensitivity (Figures 3.3. and 3.4.). Cell doubling times of SV40-Tag infected E12.5$^{+/+}$ and E13.5$^{+/+}$ POM cells were comparable to the 24.4 hours of human corneal endothelial cells, which are rarely immortalised as reported (Araki-Sasaki *et al.*, 2000). However, in this investigation, both cell lines proliferated more rapidly at 37°C than at 33°C. This differed from the studies of Prince *et al.* (2001) in which restricted proliferation at higher temperature was confirmed.

No characteristics associated with loss of SV40-Tag function as a result of mutation in the protein were observed (change in morphology or death in antibiotic medium), and extended passage could not be the cause as the cells tested were p=8. A potential cause of the SV40-Tag losing temperature-sensitivity is non-homologous recombination during integration into the cellular genome, a possibility described by Ahuja *et al.* (2005). As the cell lines were still immortalised and loss of temperature-sensitivity did not pose a hindrance to the investigation, the E12.5$^{+/+}$ and E13.5$^{+/+}$ POM cells were still an appropriate and satisfactory model on which to carry out the proposed study.

4.3. E12.5$^{+/+}$ and E13.5$^{+/+}$ POM cell lines are appropriate models to study corneal endothelial differentiation

E12.5 is characterised by rapid proliferation of POM cells that have filled the cavity between the lens and surface ectoderm (Cvekl and Tamm, 2004). By E13.5, the cells begin to condense as the process of differentiation into the corneal endothelium is initiated (Pei and Rhodin 1970; Kidson *et al.*, 1999). Gene expression analysis (by qPCR) at E13.5 relative to E12.5 showed that *Foxc1*, *Pitx2*, *Tsc22* and *Slug* must be downregulated for normal development to proceed (Figure 3.9). *Foxc1*, *Pitx2* and *Tsc22* expression was downregulated by at least 50% while *Slug* expression decreased 40% between E12.5 and E13.5. Previous studies have indicated the roles *Foxc1* and *Pitx2* play in cell proliferation and differentiation (Baulmann *et al.*, 2002; Kidson *et al.*, 1999). Kidson *et al.* (1999)

describe a general downregulation of *Foxc1* from E11.5 to E15 (with detachment of the lens vesicle from the surface ectoderm to 0.5 days before the cornea matures). Berry *et al.* (2006) demonstrated that *Foxc1* and *Pitx2* are co-expressed and follow a generally similar expression pattern. This direct interaction would implicate the expression of *Pitx2* to follow that of *Foxc1*, and also to be downregulated between these stages. The findings of this investigation are in agreement with this previous research.

Tsc22 is a transcription factor with both activation and suppression capacity depending on the tissue type it is expressed in. It is commonly noted at sites of EMT where it is upregulated (Hashiguchi *et al.*, 2004). During normal anterior segment development, *Tsc22* expression decreases between E12.5 and E13.5 (Sommer *et al.*, 2006). *Slug* is a transcriptional repressor that is capable of inducing EMT in epithelial cell lines and is a marker of this process as it is normally upregulated at these sites (Mani *et al.*, 2008; Baum *et al.*, 2008). As previously stated, genes that are highly expressed for EMT must be downregulated for MET to occur. In this investigation, both *Tsc22* and *Slug* were downregulated by E13.5 suggesting a more differentiated state at this stage of development. Additionally, in this investigation, Figure 3.3 illustrates the results of cell counts which clearly show that POM cells at E12.5 proliferate almost twice as fast as POM cells at E13.5 indicative of a more proliferative state comparative to a differentiated state as alluded to by Cvekl and Tamm (2004).

N-cadherin, a cell adhesion protein, is upregulated from E11 to the formation of the corneal endothelium at E15.5, and beyond in maintenance of the structure (Kidson *et al.*, 1999; Reneker *et al.*, 2000). As a junction protein, it plays a role in differentiation and as such would be expected to be present at higher levels during MET. This investigation found that *N-cadherin* expression increased at least 5-fold between E12.5 and E13.5 (Figure 3.30) further validating previous literature.

4.4. Successful *Foxc1* silencing (psh*Foxc1*) using RNA interference

RNA interference (RNAi), formerly known as post transcriptional gene silencing and quelling, describes a process in which specific mRNAs are destroyed thus inhibiting the expression of a particular gene. Small interfering RNAs (siRNA) are generated when the enzyme Dicer cleaves double stranded RNA. Each siRNA contains a passenger strand which is degraded, and a guide strand which becomes integrated into a silencing complex. This happens when the siRNA interact with messenger RNA (mRNA) and decrease its

ability (siRNA are also capable of activation) to produce a protein (Barsted, 2001; Hung *et al.* 2006). As these siRNA bind specific molecules, it is clear that the efficiency of any siRNA is dependent on the target sequence. RNAi has become a widely used tool *in vitro* and *in vivo*, especially in developmental regulation, as well as therapeutics (Hung *et al.* 2006). Relevant to this investigation, RNAi has been employed to study loss of function of genes that determine viability (Yang *et al.*, 2012). Short hairpin RNA (shRNA) as its name suggests is an RNA sequence that makes a loop or hairpin turn which can be used to prevent translation via RNAi. The target sequence is very important to the efficacy of an shRNA but also the choice of promoter and plasmid vector play an equally important role. The target chosen is a 21bp sequence corresponding to a section of chromosome 13 of the C57BL/6L mouse strain, where *Foxc1* has been mapped (Mears *et al.*, 1998). Human U6 promoter was chosen for this investigation as it has been demonstrated to be more effective than its murine homologue, in silencing gene expression of mammalian cells (Castanotto *et al.*, 2002). The template for the human U6 promoter was provided by DNA from Human Embryonic Kidney (HEK 293) cells. The chosen vector pGEM®T-Easy contains an M13 (sequencing primer) site and encoded Ampicillin resistance for identification of sh*Foxc1*-containing clones. After transfection into POM cells at E12.5 and E13.5, the efficiency of psh*Foxc1* was analysed by qPCR. In E12.5 POM cells, *Foxc1* was knocked down by 95% and in E13.5 by 98% (Figure 3.11). Thus psh*Foxc1* silencing using shRNA was found to be an appropriate tool to study the effects of *Foxc1* silencing on genes of interest in POM at E12.5 and E13.5.

4.5. *Foxc1* overexpression and knockdown affects *Pitx2*, *Tsc22* and *Slug* Expression

Aberrant expression of *Foxc1* is associated with ASD disorders demonstrating its various roles in cell fate determination, cell proliferation and differentiation (Mattiske *et al.*, 2006(a); Zhou *et al.*, 2002). The function of *Foxc1* is tissue-specific. Abnormal *Pitx2* expression is equally established in anterior segment dysgenesis in its somewhat overlapping expression pattern with *Foxc1*-linked disorder phenotypes. Part of normal *FOXC1*/*Foxc1* function is to regulate other factors and in this capacity, has been linked to BMP (Mattiske et. al, 2006(b)), *PITX2* (Smith *et al.*, 2000) and *Tsc22* (Sommer *et al.*, 2006). Conjecture here would be that anomalous *Foxc1* expression might have an effect on the associated factors. To investigate the role of *Foxc1* in the possible regulation of *Pitx2*, *Slug* and *Tsc22*, E12.5 and E13.5 cells were transiently transfected with plasmids

overexpressing or silencing *Foxc1*, and the effects on gene expression were determined by qPCR. The effects are summarised in Figure 4.2.

Foxc1 and *Pitx2* have been shown to be co-expressed in the developing eye and patterns thereof are dependent on the tissue and stage of development (Berry *et al.*, 2006). In this study, when *Foxc1* is overexpressed and silenced, *Pitx2* is downregulated at both E12.5 and E13.5, showing that *Foxc1* normally plays a role in upregulating *Pitx2* at both these stages. Downregulation as a result of *Foxc1* silencing may be explained by the *Foxc1*-*Pitx2* negative regulation relationship described by Berry *et al.* (2006) where lack of *Foxc1* would lead to low levels of *Pitx2*. By this assumption, it would follow that *Foxc1* overexpression would cause an increase in *Pitx2* expression. However, both overexpression and silencing of *Foxc1* resulted in a decrease in *Pitx2* expression. This indicates that *Foxc1* plays a role in regulating *Pitx2* and that this regulation is crucially dose-dependent (Lehmann *et al.*, 2003; Gould *et al.*, 2004). Mears *et al.* (1998) described *Foxc1* expression patterns in the mesenchyme in the developing eye as being very similar to those of *Pitx2*. *Foxc1* is known to be downregulated as development progresses. In this investigation, *Pitx2* was downregulated regardless of *Foxc1* overexpression and silencing at E12.5 and E13.5 possibly indicating an independent response.

Tsc22 is a documented downstream target of *Foxc1* (Sommer *et al.*, 2006) and was shown to be upregulated as a response to both *Foxc1* overexpression and silencing at E12.5 (Figures 3.12 and 3.14). Using a temperature-sensitive SV40-Tag, Sommer *et al.* (2006) showed that *Tsc22* is upregulated 3.5-fold in mutant (*Foxc1*$^{-/-}$) POM cells when compared to wild-type cells. This is comparable to the 2-fold upregulation observed in this investigation as a response to *Foxc1* silencing and corroborates this report. At E13.5, *Foxc1* knockdown and overexpression elicited no significant response in *Tsc22* expression. This, too, was in agreement with the findings of Sommer *et al.* (2006). At E12.5, *Slug* was downregulated when *Foxc1* was both overexpressed and silenced. At E13.5, *Slug* was upregulated. This shows that *Foxc1* normally plays a role in upregulation of *Slug* at E12.5 and that by E13.5, *Foxc1* plays a role in its downregulation. In both cases, the transcriptional activity is finely tuned to the dose. The difference in behaviour or response of the cells is a consequence of the two developmental stages. As differentiation is initiated (MET), *Slug* will be downregulated.

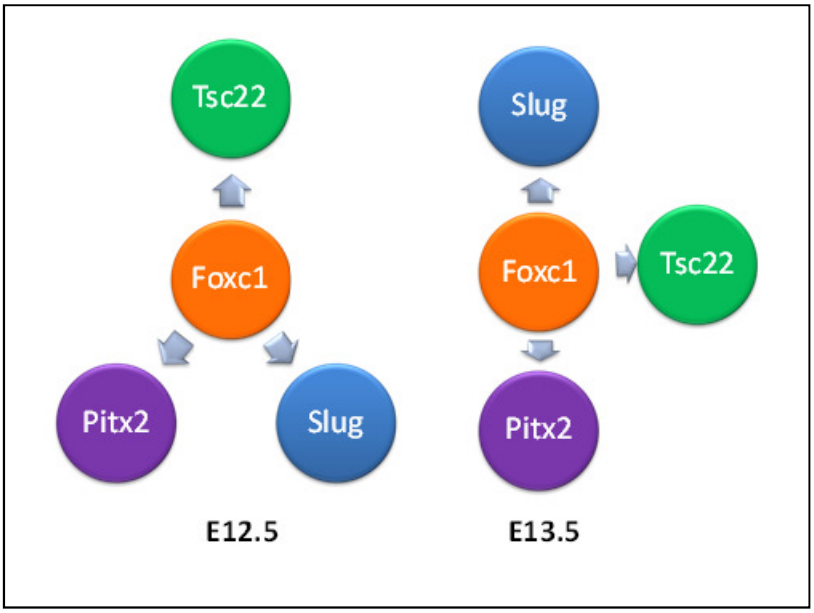

Figure 4.2: The effect of aberrant *Foxc1* expression on *Pitx2*, *Tsc22* and *Slug* expression at E12.5 and E13.5. At E12.5, *Pitx2* and *Slug* are downregulated significantly while *Tsc22* is upregulated ($p<0.05$). By E13.5 *Foxc1* overexpression and knockdown results in significant upregulation of *Slug* and downregulation of *Pitx2* but no significant change in *Tsc22* expression.

It is very interesting to note that *Foxc1* overexpression and silencing downregulated *Slug* at E12.5 but upregulated *Tsc22*. Also that *Slug* was upregulated at E13.5 but *Tsc22* seems unaffected. These responses seem linked to the stage of development. Both are factors associated with EMT so it would be tempting to assume that they may be switched on and off at the same time to effect MET. However, the observed effects reveal a complicated interplay of factors required in this complex development. It is likely that specific doses of these transcription factors are associated with varying degrees of adherens junction formation. Thiery (2003) and Baum *et al.* (2008) mention a relationship between *N-cadherin* expression and zinc-finger domain proteins (such as *Slug* and *Snail*). An investigation into the relationship between the *Snail* family, *Tsc22* and *cadherins* would be beneficial to fully understanding the interactions of MET. The common theme in all responses is that normal function of these *Foxc1* linked factors is dependent on a specific dose of *Foxc1*. These data are consistent with reports that precise levels of *Foxc1* are required for correct differentiation of the peri-ocular mesenchyme and that both mutations in *FOXC1* or duplication of *FOXC1* can result in abnormal anterior segment development and ARS (Strungaru *et al.*, 2007). The possibility of erroneous gene

expression due to the transfection treatment (plasmid or reagent) was ruled out by the use of a control plasmid encoding a scrambled plasmid that does not degrade any known mRNA transcript (Appendix C.3, Figure 5.6).

4.6. The lens has an effect on *Foxc1*, *Pitx2*, *Tsc22* and *Slug* expression at E12.5

The lens is pivotal in normal anterior segment development (Beebe and Coats, 2000). In order to assess the role of the lens on *Foxc1*, *Pitx2*, *Tsc22* and *Slug* expression at E12.5 and E13.5, wild type POMs were subjected to 24 hour treatments with E6 and E8 whole chick lenses respectively (Thut *et al.*, 2003). These are the corresponding stages in development. qPCR analysis was used to evaluate the gene expression levels after treatment. At E12.5, *Foxc1* decreased by approximately half in response to 24 hour exposure to the lens. This effect mimics the down-regulation of *Foxc1* at E13.5 and suggests that lens-derived signals are responsible for this downregulation. Kidson *et al.* (1999) describe a general downregulation in *Foxc1* expression by E15, supporting these data. Similarly, at E12.5, *Pitx2* is downregulated in response to the lens. *Pitx2* expression decreases 80% between E12.5 and E13.5 (Figure 3.9) while the lens elicits a 65% decrease (Figure 3.17). These effects mimic that of *Foxc1*. This is expected as Berry *et al.* (2006) reported that *Foxc1* and *Pitx2* have similar expression patterns (Berry *et al.*, 2006). *Pitx2* expression as a response to lens treatments was compared to expression patterns during psh*Foxc1* and psh*Foxc1*+lens treatments to ascertain whether *Foxc1* plays a role in interpreting the effect of the lens signal. When *Foxc1* is silenced, *Pitx2* is downregulated by approximately 90% and almost completely suppressed when POM cells are subjected to psh*Foxc1*+lens. The difference is significant ($p<0.05$) and shows that the lens and *Foxc1* act synergistically to downregulate *Pitx2* expression. Therefore, *Foxc1* is not required to interpret lens-derived effects on *Pitx2* expression.

Tsc22 was significantly upregulated in normal E12.5 POM cells exposed to lenses, showing that the lens has an upregulatory effect on *Tsc22* in the presence of *Foxc1*. As discussed before, *Tsc22* expression doubled when *Foxc1* was silenced. However, psh*Foxc1*+lens exposure caused *Tsc22* expression to be downregulated by 40% relative to the control. An over 50% decrease in *Tsc22* levels is expected when development progresses from E12.5 to E13.5 (Figure 3.9). Taken together, the results indicate that *Tsc22* is upregulated by the lens, and *Foxc1* deficiency in isolation, but that psh*Foxc1*+lens elicits the correct developmental response in moving from E12.5 to E13.5. Therefore *Tsc22* is responding directly to the lens independently of *Foxc1* during normal development. This is interesting

as Sommer *et al.* (2006) identified *Tsc22* as a downstream target of *Foxc1*, showing that *Foxc1* downregulates this factor. This investigation shows that the lens signal supersedes the transcriptional effect *Foxc1* has on *Tsc22*.

Slug expression in normal cells exposed to E6 lenses remained relatively unchanged while expression in *Foxc1*-silenced cells fell to approximately 20% compared to the control. psh*Foxc1*+lens treated cells however showed a 40% increase in *Slug* expression. This shows that lens signals induce *Slug* expression at E12.5, over-riding the inhibitory effect of *Foxc1*. Therefore, the presence of *Foxc1* is necessary to reduce the stimulatory effects of the lens on *Slug*. This is an interesting result as *Slug* upregulation is associated with EMT and invasiveness in cancer (Hemavathy *et al.*, 2000) and may cause malignancy in response to lens signals if unchecked. *Slug* levels decrease as development proceeds from E12.5 to E13.5 and results show *Foxc1* only stabilises the lens effects but does not cause the necessary downregulation. Therefore, other factors must be responsible for this downregulation. In chick limbs, FGF and retinoic acid have been shown to regulate *Slug* (Ros *et al.*, 1997; Buxton *et al.*, 1997).

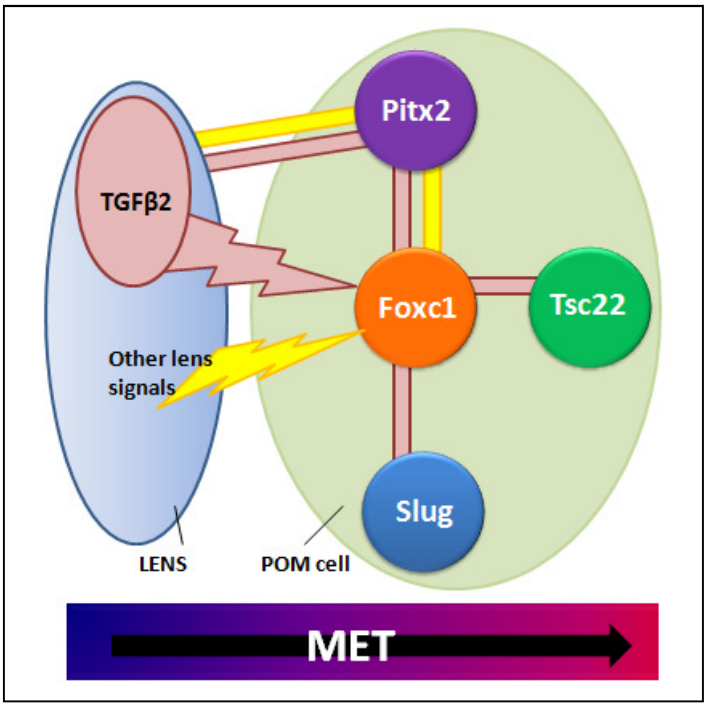

Figure 4.3: A summary of the lens and TGFβ2 effects on *Foxc1*, *Tsc22*, *Pitx2* and *Slug* expression at E12.5. The lens is shown in blue and the magnified POM cell in light green. Only the interactions necessary for normal development (as established between E12.5 and E13.5) have been shown. Unspecified lens-derived signals are shown in yellow, TGFβ2 is shown in pink. MET is progressing with development. *Foxc1* is necessary for the correct interpretation of TGFβ2 in *Tsc22* and *Slug*. *Foxc1* may be necessary for interpreting lens signals in *Pitx2* expression.

4.7. The lens-derived signal TGFβ2 has an effect on *Foxc1*, *Pitx2*, *Tsc22* and *Slug* expression at E12.5

TGFβ2 is a well documented lens-derived signal although its specific interactions with the various factors involved in anterior segment development are still under investigation. It is mostly expressed in the anterior segment between E13.5 and E15, stages which represent the initiation of differentiation (E12.5) and prior to specification of the cornea (E15). POM cultures were subjected to a 24 hour treatment in culture medium containing 30ng/mL TGFβ2. To determine whether any observed effects were directly caused by TGFβ2 and to establish whether *Foxc1* plays a role in mediating the signal, a different treatment group of POM cells were silenced for *Foxc1* and then subjected to the TGFβ2 treatment (psh*Foxc1*+TGFβ2). RNA was isolated from the cultures and used analysed by qPCR.

At E12.5, TGFβ2 exposure downregulates *Foxc1* by 40% ($p<0.05$). This result mirrors the outcome of the E6 lens exposure showing that TGFβ2 is most likely the lens signal that *Foxc1* is responding to in this culture system, and may be responsible for the normal developmental reduction of *Foxc1* from E12.5 to E13.5 (Figure 4.3). *Pitx2* expression is downregulated when exposed to TGFβ2. It is further downregulated when the cells have been both silenced for *Foxc1* and subjected to TGFβ2 for 24 hours. This parallels the effect the lens had on the E12.5 POM cells. As with *Foxc1*, TGFβ2 has an effect on *Pitx2*. However, these results show that *Foxc1* may not be necessary for the correct interpretation of lens signals in moving from E12.5 to E13.5. Pitx2 may also be responding directly to the factor (Figure 4.3). Iwao *et al.* (2009) described *Foxc1* and *Pitx2* as "downstream molecules" of TGFβ2 while studies using mice with Tgfβ2 receptor knockouts (Tgfβr2$^{-/-}$), showed that *Foxc1* and *Pitx2* expressions were synchronously reduced (Ittner *et al.,* 2005). The results of this investigation corroborates previous research.

Tsc22 is downregulated 40% in the presence of TGFβ2 and approximately 80% when POM cells are treated with psh*Foxc1*+TGFβ2. Thus, *Tsc22* is responsive to TGFβ2. When *Foxc1* is silenced in POM cells, *Tsc22* expression doubles compared to the control (as discussed in section 4.5) but, additional treatment with TGFβ2, overrides the *Foxc1* knockdown effect, almost suppressing *Tsc22* expression. Sommer *et al.* (2006) showed that *Tsc22* is a downstream target of *Foxc1* and also that a secreted factor may be necessary in its regulation of *Tsc22*. They proposed TGFβ1 as a candidate factor as it had been show to upregulate *Tsc22* (Dohrmann *et al.* 1999; Shibanuma *et al.* 1992). These experiments and the results of this investigation together show that *Foxc1* does play a role in interpreting TGFβ2 signals, allowing correct developmental progression to E13.5. Comparison with the lens experiments shows that *Tsc22* is responding to multiple lens signals.

As with lens exposures, exposure to TGFβ2 has no significant effect on *Slug* expression ($p>0.05$). Knockdown of *Foxc1* significantly reduced *Slug* expression as discussed previously and psh*Foxc1*+TGFβ2 also reduced *Slug* expression, suggesting here that *Foxc1* effects on *Slug* expression override any possible TGFβ2 effects. Therefore, other signal/s must be responsible for the normal developmental downregulation of *Slug* at between E12.5 and E13.5. As mentioned before, *Slug* needs to be downregulated in order for MET to occur, this data shows that *Slug* responds to decrease in *Foxc1* levels, thus linking *Foxc1* dosage to MET via regulation of *Slug* expression.

4.8. The lens and lens-derived signal TGFβ2 has an effect on *Foxc1*, *Pitx2*, *Tsc22* and *Slug* at E13.5

Correspondingly, lens exposures and TGFβ2 treatments were applied to E13.5 POM cells in order to assess whether the lens has an effect on this stage of development. E13.5 POM cultures were also subjected to 30ng/mL TGFβ2 to determine if this lens-derived signal is responsible for any effect the lens may have on *Foxc1*, *Pitx2*, *Tsc22* and *Slug* expression. Due to time constraints, the psh*Foxc1*+TGFβ2 treatment was not applied to the E13.5 POM cells. Gene expression analyses were done by qPCR.

Foxc1 expression was downregulated by the lens and slightly downregulated by TGFβ2 ($p>0.05$) showing that POM cells are still responsive to lens signals at E13.5 (Figure 4.4). *Foxc1* expression in POMs decreases till E15.5 (Kidson *et al.,* 1999) which marks the formation of the corneal endothelium. The downregulation associated with exposure to E8 lenses and TGFβ2 are consistent with the lens participating in the progression of development, specifically that TGFβ2 is still involved in *Foxc1* expression.

Pitx2 is downregulated by both *Foxc1* overexpression and silencing. Exposure to E8 lens induces *Pitx2* expression by over 60% compared to the control. However, when POM cells are subjected to psh*Foxc1*+lens treatment, *Pitx2* is downregulated by approximately 70%. This data shows that *Pitx2* is still responsive to lens signals at E13.5 and, at this stage, *Foxc1* expression is required for *Pitx2* to respond to these signals. TGFβ2 exposure does not affect *Pitx2* expression at E13.5, therefore, although, *Pitx2* is still responsive to secreted signals, TGβF2 is not one of them as shown in Figure 4.4.

Tsc22 remains relatively unaffected by *Foxc1* overexpression and knockdown at E13.5. Exposure to E8 lens results in a slight but significant 20% downregulation. psh*Foxc1*+lens treatment upregulates *Tsc22* by 80% demonstrating that at E13.5, *Tsc22* may still require *Foxc1* to mediate lens signals. TGFβ2 treatment mirrors the lens results.

Unlike at E12.5, *Slug* expression in E13.5 POM cells responds to lens exposure and TGFβ2 treatment. Both these treatments resulted in a 50% downregulation. psh*Foxc1*+lens treatment yielded a small (20%) but significant decrease in expression ($p<0.05$). *Foxc1* overexpression and silencing doubled *Slug* expression at E13.5. Altogether, this means that *Foxc1* has a regulatory effect on *Slug* expression but the lens overrides this effect and downregulates *Slug*. TGFβ2 treatment on normal POMS has a similar effect, but due to the

lack of psh*Foxc1*+TGFβ2 data, it cannot be conclusively identified as the molecule responsible.

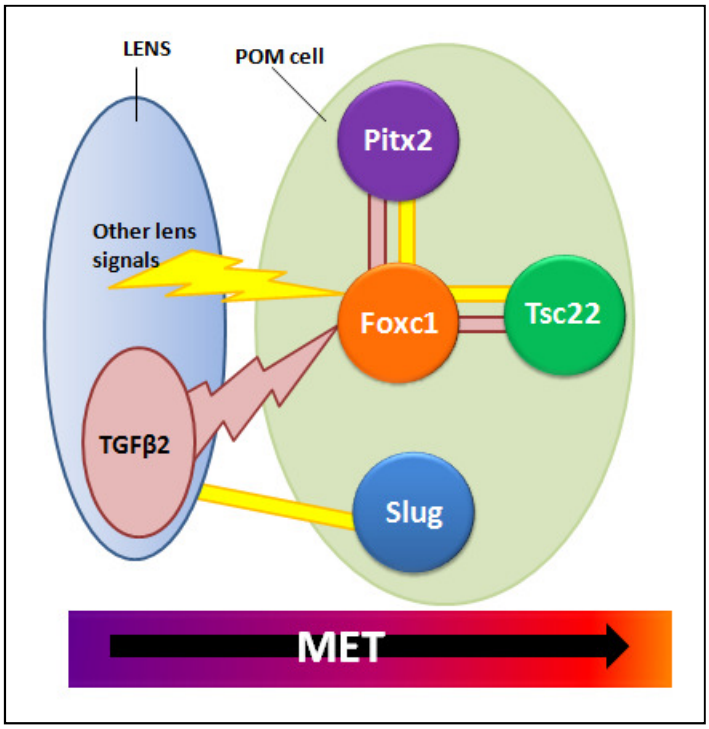

Figure 4.4: A summary of the lens and TGFβ2 effects on *Foxc1*, *Tsc22*, *Pitx2* and *Slug* expression at E13.5. The lens is shown in blue and the magnified POM cell in light green. All significant interactions are shown. Unspecified lens signals are shown in yellow, TGFβ2 is shown in pink. MET is progressing with development. *Foxc1* seems necessary for the correct interpretation of TGFβ2 in *Tsc22* and *Pitx2* expression. *Foxc1* no longer seems to be intercepting lens signals in *Slug* expression but rather *Slug* responds directly to the lens.

An analysis of *Foxc1*, *Pitx2*, *Tsc22* and *Slug* expression at the next stage of development, would have been instrumental in understanding the expression patterns observed at E13.5.

4.9. The lens regulates proliferation of E12.5 POM cells

Having explored the expression patterns associated with E12.5 and E13.5 POM cells, an investigation to determine the effect of the lens on cell proliferation was carried out. POMs in culture were exposed to whole chick lenses for 72 hours and proliferation assessed by calorimetric assay. In the course of this investigation, E12.5 cells have been shown to be more proliferative than E13.5 cells (Figures 3.3. and 3.4). A general increase in proliferation was noted in the E12.5 culture from 24 to 72 hours as expected, which was

consistent in the control. However, the lens treated cells showed a 5.5-fold increase between 24 and 48 hours that confirmed the lens promotes POM cell proliferation. Between 48 and 72 hours, the lens treated cells do proliferate but the change pales in comparison to the increase in the control ($p<0.05$) (Figure 3.16). At this point it is clear that the lens regulates proliferation. The results fit the proliferation-differentiation model thus far developed for E12.5 and E13.5 POM cells. At E12.5, the lens stimulates proliferation and at E13.5 proliferation is reduced as cells condense to form the corneal endothelium. It is also possible that the lens is inducing the POM cells to different stages of development. It must be noted that in this culture system, the POM cells are immortalised and the lens epithelium is not. Although the POMs may be manipulated to mimic a different stage of development, the lens epithelium is actually developing and senescing. If the POMs are indeed being induced to mimic different stages, the first 24 hours would represent condensing of the cells to begin forming the corneal endothelium. The 48 hour point would signify the rapid proliferation associated with forming cells of the corneal stroma and 72 hours, condensing of cells as the cornea becomes fully specified. In future, to clarify the outcome of this experiment, lenses will be replaced every 24 hours with lenses of the appropriate and corresponding developmental stage.

Meanwhile, the genetic profile elucidated in the course of this investigation may explain the trends observed. *Foxc1*, *Pitx2*, *Tsc22* and *Slug* are known to be involved in differentiation and proliferation. All four genes are downregulated in moving from E12.5 to E13.5. Subject to 24 hour lens exposure, *Foxc1* and *Pitx2* are downregulated while *Tsc22* is upregulated and *Slug* expression remains relatively unchanged. Dohrmann *et al.* (1999) noted that *Tsc22* expression was localised to the contact area between the surface ectoderm and optic vesicle of the developing eye prior to separation. It is possible the upregulation of *Tsc22* after lens exposure in E12.5 cells plays a role in MET. The unchanged *Slug* expression might be linked with inhibition of *N-cadherin* in the POM cells which would also be indicative of a mesenchymal state. When E13.5 POMs are exposed to lens for 24 hours, *Foxc1* and *Slug* are downregulated, *Tsc22* remains unchanged and *Pitx2* is upregulated. *Slug* downregulation is linked to the stimulation of *N-cadherin* expression so this would confer differentiation at this stage. The static *Tsc22* expression may be associated with MET as well. *Pitx2* upregulation at E13.5 is significant and Gould *et al.* (2004) associate this with formation of the keratocytes of the corneal stroma.

4.10. The lens can induce an epithelial-like phenotype from mesenchyme cells in 3D culture

In order to observe the role of the lens in developing an epithelial layer, POM cell monolayers and hanging drops were exposed to whole chick lenses. Cells were grown for 72 hours then immunostained for the junction protein N-cadherin and processed for confocal microscopy.

At both E12.5 and E13.5, N-cadherin was distributed around the nucleus in monolayer culture (Figure 3.31). Once exposed to the lens, N-cadherin seemed to be diffused in the cytoplasm of E12.5 POM cells. This result was inconclusive although a visible difference is apparent. There was no observed change in N-cadherin localisation in E13.5+lens POMs. The size of the hanging drops (Figure 3.32) follows the proliferation data mentioned before wherein E12.5 cultures proliferate faster than E13.5. The E12.5 spheroids were much larger than those of E13.5. Unlike the monolayers, E12.5 POM cells clearly responded to the lens and N-cadherin was observed to form an organised lattice structure (Figure 3.33) associated with formation of adherens junctions (Chen *et al.*, 2012) and differentiation. The control cells did not show organised structure and cell peripheries could not be distinguished from internal structures. E13.5 control cells showed an organised structure with observable network of cell membranes but this effect was more pronounced in the lens exposed hanging drops.

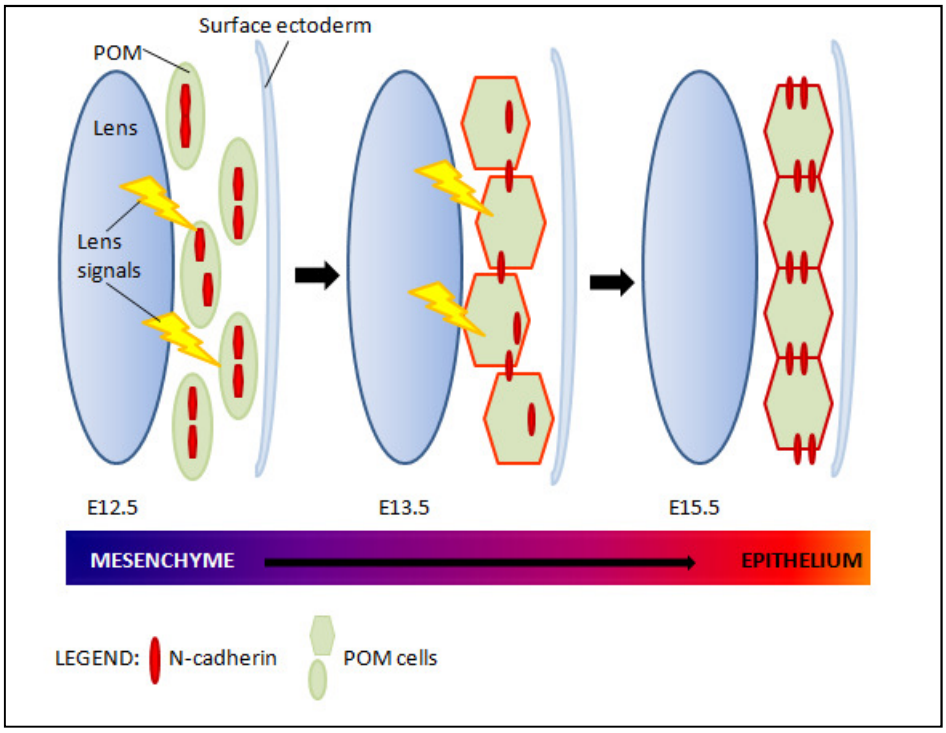

Figure 4.5: An illustration of the lens effects on development at E12.5 and E13.5 as demonstrated in the hanging drop investigation. The E15.5 stage was not investigated but has been shown for reference and *N-cadherin* is shown in red. Surface ectoderm has been included for clarity but was represented by the inverted droplet meniscus/surface tension in culture. As development progresses, lens signals interact with POM cells and MET is initiated. At E12.5, *N-cadherin* seemed to be distributed within the cell and by E13.5 the POM cells take on a more organised structure as *N-cadherin* becomes localised in the membrane and junctions are formed. By E15.5, establishment of the corneal endothelium, *N-cadherin* is highly expressed (Reneker *et al.*, 2000) as indicated by the intense red. Cell phenotype has changed and POMs are arranged in a monolayer.

Gene expression analysis of the lens exposures (discussed in Section 4.8) established that the lens in the presence of *Foxc1* downregulates *Slug*. *Slug* is known to have an interaction with *N-cadherin* (Baum *et al.*, 2008; Thiery, 2003). Therefore the lens is implicated in the *Slug-N-cadherin* interaction. The E13.5 3D culture + lens exposure support this association. Hence the lens does play a role in MET and can induce an epithelial/endothelial phenotype from peri-ocular mesenchyme cells at E13.5 as illustrated in Figure 4.5.

4.11. CONCLUSION

The interaction between lens epithelium and POM cells during the development of the corneal endothelium is complex and still under investigation. It is known that lens-derived signals mediate the expression of genes that drive this process. The major result obtained in *Foxc1* overexpression and knockdown investigations is that correct function of *Pitx2*, *Tsc22* and *Slug* in development from E12.5 to E13.5 is *Foxc1* dose dependant. At E12.5 and E13.5, *Foxc1* seems to plays a role in regulating *Pitx2* expression. Previous studies have shown that *Pitx2* regulates *Foxc1* expression. The results of this investigation show that the interplay between these two genes is much more complex with both genes being dependent on expression of the other. To assess the true nature of the role *Pitx2* plays in this relationship, a similar series of investigations could be carried out with a *Pitx2* knockdown in future. Overexpression and knockdown of *Foxc1* showed that the *Foxc1* target *Tsc22* is normally downregulated by *Foxc1* at E12.5 and is unaffected at E13.5. Slug was shown to be normally upregulated by *Foxc1* at E12.5 and downregulated by *Foxc1* at E13.5.

At E12.5, the lens downregulates *Foxc1* and *Pitx2* and stimulates *Tsc22* expression. Further investigation showed that TGFβ2 was the signal responsible for downregulating *Foxc1* and *Pitx2*. However, it may not be the only lens-derived signal/s responsible for these effects. The results show that *Foxc1* may not be responsible for interpreting lens signals in *Pitx2* expression but that *Pitx2* may be directly influenced by these secreted molecules. *Tsc22* also responded directly to TGFβ2 and *Foxc1* was necessary for the correct interpretation of this signal in development at E12.5. However, *Tsc22* was definitively stimulated by other lens signal/s that override *Foxc1* transcriptional regulation. *Slug* expression was induced by the lens but stabilised by *Foxc1*. Yet, the lens did not seem to be involved in the downregulation associated with this stage of development. The results of this investigation show that *Slug* expression is significantly linked to *Foxc1* expression.

At E13.5, *Foxc1* was still responsive to lens signals and TGFβ2 was shown to be one of those signals downregulating its expression. Although *Pitx2* expression was induced by the lens, TGFβ2 did not appear to be the inducing factor. Noteworthy is that *Foxc1* dose was especially key for *Pitx2* expression at this stage. *Foxc1* insufficiency quelled the lens effect. *Tsc22* was slightly but significantly downregulated by the lens and TGFβ2, and *Foxc1* was still required to mediate these signals. The previously potent effect *Foxc1* expression had on *Slug* was overcome as *Slug* was downregulated by the lens at E13.5 and

TGFβ2 seemed to be involved. Future psh*Foxc1*+TGFβ2 treatments could verify the role of TGFβ2 in *Pitx2*, *Tsc22*, and Slug expression.

The lens definitively played a role in the proliferation of E12.5 cells. The time trial demonstrated that the lens is capable of both promoting and inhibiting proliferation. Furthermore, the lens was proven to induce an epithelial/endothelial phenotype when E13.5 POM cells were exposed to E8 lenses. Thus a signal from the lens was implicated in *N-cadherin* expression. By compiling all these data, the interactions responsible for normal corneal endothelial development are summarised in Figure 4.6 below:

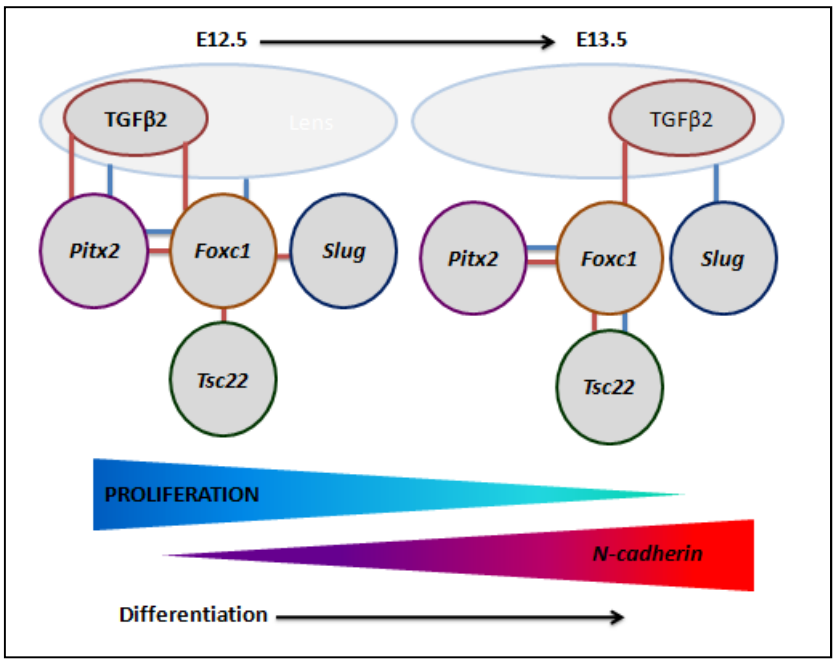

Figure 4.6: The summary of findings. The lens is necessary in normal development of the corneal endothelium and *Foxc1* plays a crucial role in interpreting the lens-derived signals required for this process. Proliferation decreases from E12.5 to E13.5 and *N-cadherin* expression is upregulated as POM cells undergo mesenchymal-endothelial transition.

4.12. FUTURE DIRECTIONS

To fully understand corneal endothelial development, an E15.5 POM cell line representing the differentiated corneal endothelium is crucial. The expression levels of *Foxc1*, *Pitx2*, *Tsc22* and *Slug* expression as done for the E12.5 and E13.5 cell lines should be determined to understand their role in the mature corneal endothelium. Using this cell line, we could:

- Assess the role of *Pitx2* in *Foxc1*, *Tsc22* and *Slug* expression using *Pitx2* overexpression and knockdown

- characterise the nature of the *Snail/Slug-N-cadherin* interaction

A full analysis of the lens-secreted factors by next-generation sequencing would discern all possible factors secreted by the lens. Using this information, we could:

- Discern which lens signals are responsible for downregulation of *Tsc22* and *Slug* during corneal endothelial development.

These expression patterns should be verified using an '*in vivo'* model using microdissected optic cups in culture. Furthermore, investigation of a postnatal stage of the corneal endothelium, when it is fully functional, would provide better insight into the complete developmental process. Altogether, this information could be used for manipulation of induced pluripotent cells to corneal endothelium. This would be of benefit in alleviating the global shortage of corneal donor material.

APPENDICES

Appendix A: Immortalisation of E12.5 and E13.5 POM cells (Sommer *et al.*, 2006)

To obtain primary cultures, 0.05mm^3 wedges of POM cells were dissected from the anterior eye of wild type E12.5 and E13.5 mouse embryos and expanded in culture medium (Appendix B.2) at 37°C for 48-72 hours. The cultures were then immortalised by infection with a retrovirus encoding the temperature-sensitive SV40 large T-antigen and G418 resistance using 8µg/mL Polybrene (Sigma, USA). Cells were incubated at 37°C for 2 hours after which medium was replaced and they were left overnight in DMEM containing 20% FBS. A 48 hour growth period at 33°C followed. 400µg/mL G418 was used to select SV40-Tag transformed cells over 10-14 days.

Appendix B: Recipes

B.1. 70% ethanol

70% Ethanol	1L
Absolute (99.9%) ethanol	700mL
Distilled water	300mL

70% ethanol was required for the QIAGEN Midiprep kit as it was not supplied. Ethanol was mixed into the distilled water and the solution stored at room temperature.

B.2. Medium for maintaining cell cultures

Culture medium	100mL
FBS	10mL
Penicillin-Streptomycin	2mL
DMEM	88mL

The culture medium was prepared and used under a laminar flow hood. FBS and Pen-Strep were added to the DMEM and mixed. The medium was stored at 4°C.

B.3. Trypsin-EDTA

Trypsin-EDTA	**100mL**
10x Trypsin	10mL
Na-EDTA	90mL

Trypsin was mixed into Na-EDTA solution, aliquoted into 10mL centrifuge tubes and stored at 4°C. 1mL or 2mL per 60mm or 10cm culture dish respectively was used to trypsinise cells, for 3 minutes and neutralised with double volume of culture medium.

Na-EDTA

Na-EDTA	**500mL**
EDTA	1g
NaCl	45g
Distilled water	500mL

NaCl and EDTA were dissolved in 500mL distilled water. The solution was stored at room temperature.

B.4. Cryostorage

5% DMSO	**1.5mL**
DMSO	75µL
Culture medium	1425µL

POM cells were stored at -80°C in a 5% DMSO mixture. Cells were centrifuged and resuspended in 1.5mL medium containing 75µL DMSO on ice.

B.5. 1.5% Agarose gel

1.5% Agarose gel	**100mL**
Agarose powder	1.5g
1X TBE	100mL

The agarose powder was dissolved in 100mL TBE in a microwave and allowed to cool to approximately 55°C before casting.

B.6. 10x Tris-borate EDTA

10X TBE	500mL
Boric acid	27.51g
EDTA	1.86g
Tris-base	53.91g
Distilled water	500mL

The salts were dissolved in 450mL distilled water and pH adjusted to pH8.3 and the solution made up to 500mL with distilled water. The solution was autoclaved before use, covered with foil and stored at 4°C.

1x TBE

1X TBE	1L
10X TBE	100mL
Distilled water	900mL

100mL of TBE was mixed into 900mL water and stored at room temperature.

B.7. Tris-EDTA buffer

10x Tris-EDTA buffer	1L
100mM Tris-HCl	12.11g
10mM EDTA	2.92g
Distilled water	1L

The EDTA and Tris salts were dissolved in 1L of distilled water with stirring. The solution was adjusted to pH 7.5. The buffer was stored at 4°C in the dark.

1x Tris-EDTA buffer	1L
10x Tris-EDTA	100mL
Distilled water	900mL

100mL 10x Tris-EDTA buffer was mixed into 900mL distilled water. The buffer was stored at room temperature.

B.8. IPTG/X-Gal master mix for blue/white selection

IPTG/X-Gal master mix	per plate
100mM IPTG	100µL
50mg/mL X-Gal	20µL

The master mix was made up as above, applied to the plate and incubated at 37°C prior to use.

B.9. Agar plates

Amp+ Luria agar	100mL ~ 10 plates
Luria agar	2g
Distilled water	100mL
100mg/mL Ampicillin	100µL

The agar was dissolved in distilled water and autoclaved before use. Ampicillin was added after the mixture had cooled to about 55°C, but before pouring into dishes. Agar plates were stored at 4°C.

B.10. LB broth

Amp+ Luria-Bertani broth	1L
Luria-Bertani broth	40g
Distilled water	1L
100mg/mL Ampicillin	1mL

The broth powder was dissolved in distilled water and autoclaved. Ampicillin was added after the mixture had cooled. The broth was stored at 4°C.

B.11. 1M KOH

1M KOH	200mL
Potassium hydroxide (KOH)	11.22g
Distilled water	200mL

Tungsten needles for microdissection were sharpened on a whetsone and further sharpened electrochemically using a 1M KOH and 150V power supply. The KOH was dissolved in distilled water and stored at room temperature.

B.12. 10x Phosphate buffered solution

10X PBS	500mL
Monosodium phosphate, (NaH_2PO_4)	2.28g
Disodium phosphate (Na_2HPO_4)	11.5g
Sodium chloride, NaCl	43.84g
Distilled water	500mL

The sodium salts were dissolved in 450mL distilled water and pH adjusted to 7.4, then made up to 500mL with distilled water. The solution was autoclaved before use, and stored at room temperature.

1x Phosphate buffered solution

1X PBS	1L
10X PBS	100mL
Distilled water	900mL

10x PBS was added to the distilled water and stored at room temperature.

B.13. DEPC treated water

DEPC water	1L
Distilled water	999mL
DEPC	1mL

The DEPC was added to the distilled water and incubated at 37°C for 2 hours before autoclaving to deactivate the DEPC. The solution was stored at 4°C in the dark.

B.14. 10x MOPS buffer

10x MOPS buffer	100mL
MOPS	4.18g
1M NaOAC (in DEPC water)	20mL
0.5M EDTA (in DEPC water, pH8)	20mL
DEPC water	make up to 100mL

MOPS, NaOAc and EDTA (recipes given below) were dissolved in 90mL DEPC water. The solution was adjusted to pH8.3 and made up to 100mL with DEPC water. The buffer was stored at room temperature.

1x MOPS buffer

1x MOPS buffer	1L
10x MOPS buffer	100mL
DEPC water	900mL

100mL of 10x MOPS buffer was mixed into 900mL DEPC water and stored at room temperature.

0.5M EDTA

0.5M EDTA	100mL
EDTA	14.61g
DEPC water	100mL

EDTA was dissolved in 100mL DEPC treated water. The solution was stored at room temperature.

1M NaOAc

1M NaOAc	100mL
NAaOAc	8.2g
DEPC water	100mL

The salt was dissolved in DEPC water and stored at room temperature.

B.15. DEPC treated Ethidium bromide

DEPC treated Ethidium Bromide	10mL
0.5mg/mL Ethidium Bromide	2mL
Distilled water	8mL
DEPC	10µL

2mL of pre-mixed Ethidium Bromide was added to 8mL of water and 10µL of DEPC added. The mixture was incubated at 37°C for 2 hours then autoclaved. The solution was stored in the dark at room temperature.

B.16. Denaturing RNA gel

1.5% agarose 2.2M Formaldeyde gel	**100mL**
Agarose	1.5g
DEPC water	72mL
10x MOPS buffer	10mL
Formaldehyde	18mL
DEPC treated Ethidium Bromide	100µL

1.5g agarose was dissolved in 72mL DEPC water in a microwave. 10mL of 10x MOPs buffer was added thereafter, followed by 18mL Formaldehyde and 100µL Ethidium bromide. The mixture was swirled and poured immediately.

B.17. 4% PFA

4% PFA	**100mL**
PFA	4g
1x PBS	100mL

The PFA was dissolved in 100mL 1x PBS by heating at 65°C. Drops of 1M NaOH were used to clarify the solution with stirring. The solution was then filtered through a 0.2µm filter and stored at -20°C in 5ml single use aliquots. Left over PFA was discarded.

B.18. 0.5% BSA

0.5% BSA	**50mL**
BSA	0.25g
1x PBS	50mL

0.26g of Bovine Serum Albumin was weighed out and dissolved in 1x PBS with vortexing. The solution was prepared fresh and used immediately or stored at -20°C.

B.19. Mowiol with DABCO

10% MOWIOL with DABCO	100mL
Mowiol	8g
0.2M Tris buffer	12mL
Glycerol	25mL
DABCO	1g
Distilled water	25mL

The Tris was heated with water at 60°C on a magnetic stirrer in a foil covered container. Mowiol was added to the solution and allowed to dissolve overnight. DABCO and glycerol were added and allowed to dissolve with further mixing for several hours. The Mowiol was aliquoted into 1.8mL Eppendorf tubes.

Appendix C: Plasmids

C.1. p*Foxc1*-shRNA

C.1.1. *Foxc1*-shRNA primers

5 shRNA primers were designed by Dr Marco Weinberg of the University of Witwatersrand and ordered from IDT, USA. shRNA-2 was chosen as it had been shown to have one of the two highest knockdown efficiency. The primers, given below in Figure 5.1, were HPLC purified.

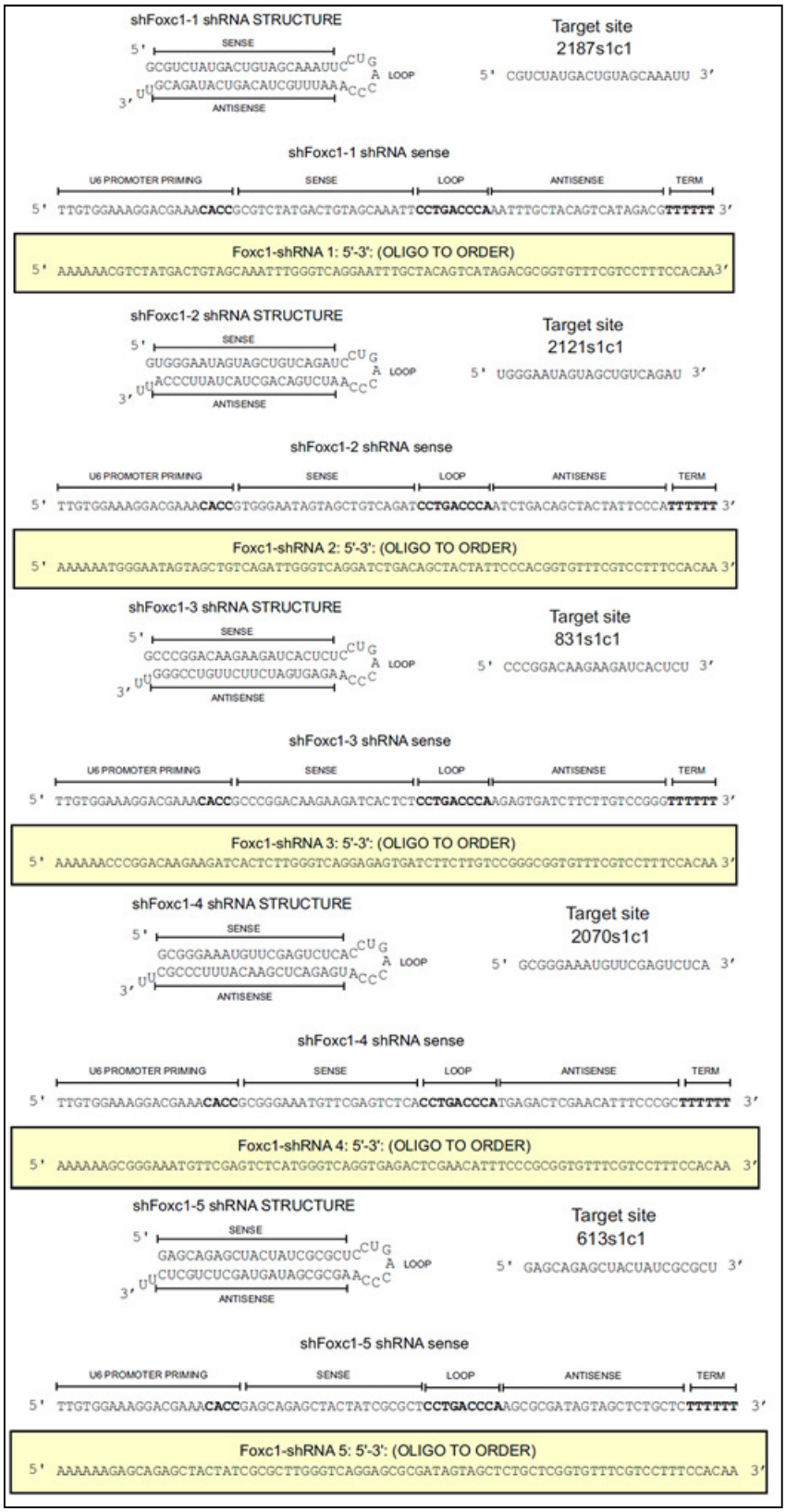

Figure 5.1: shRNA primers targeting *Foxc1*, designed by Dr Marco Weinberg, University of Witwatersrand.

C.1.2. *Foxc1*-shRNA-2 target sequence

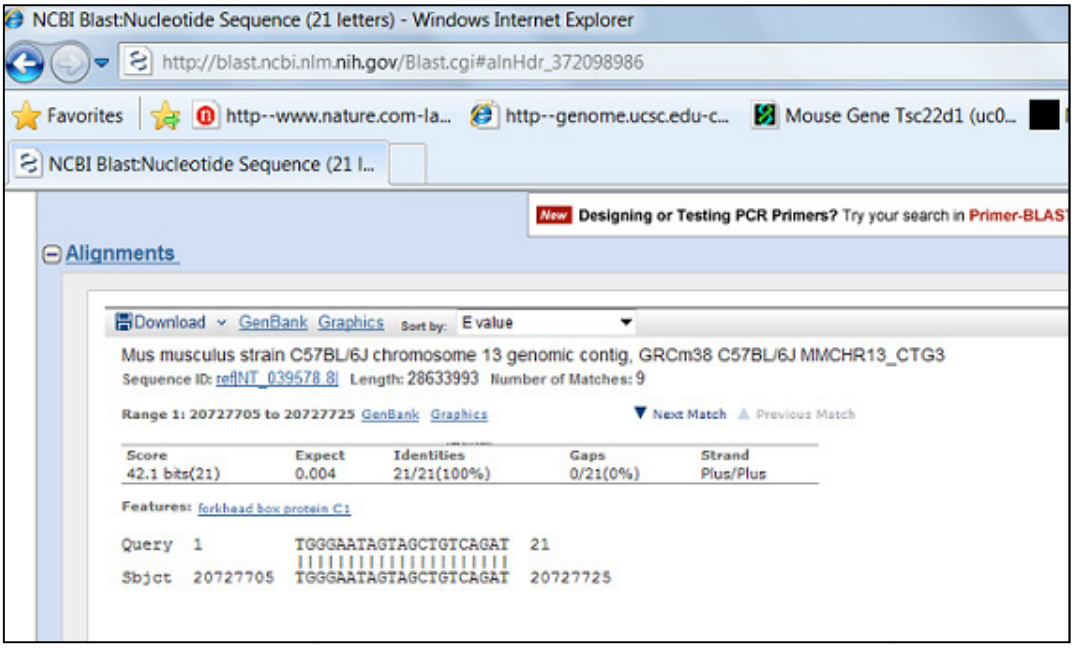

Figure 5.2: *In silico* screen of *Foxc1* shRNA-2 target sequence. The sequence was run through the National Centre for Biotechnology Information (NCBI) Basic Local Alignment Tool (BLAST) against the *Mus musculus* genome. The result generated shows the sequence is a 100% match to a sequence on chromosome 13 of C57BL/6J strain.

C.1.3. Ligation, transformation and restriction digest

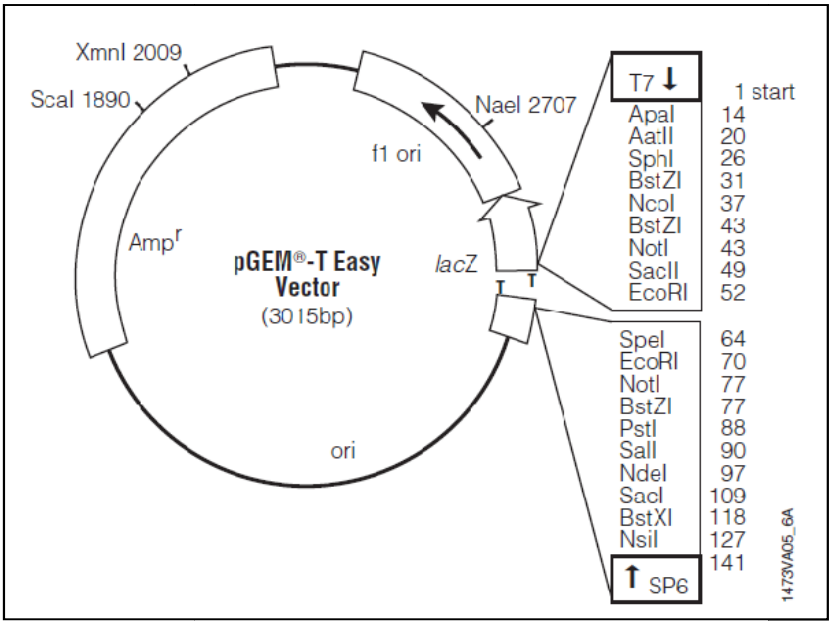

Figure 5.3: pGEM®-T Easy Vector map (Promega, USA).

PCR amplified shRNA product was ligated into pGEM®-T Easy vector overnight at 4°C, according to the reaction below:

Component	Standard Reaction	Positive Control
2x Rapid Ligation Buffer, T4 DNA Ligase	5µL	5µL
pGEM®-T Easy Vector (50ng)	1µL	1µL
PCR product	*x*µL	-
Control insert	-	2µL
T4 DNA Ligase (units/µL)	1µL	1µL
Nuclease free water	3-*x*µL	1µL
TOTAL	10µL	10µL

Presence of the insert was confirmed by *EcoRI* restriction enzyme digest and gel electrophoresis. The digest reaction was incubated for 3 hours at 37°C and product run on a 1.5% agarose gel. The digest reaction was composed of:

Component	Volume µL
Nuclease free water	17-*x*
10x Buffer *Eco*RI	2
DNA (0.5-1µg/µL)	*x*
*Eco*RI	1
TOTAL	20

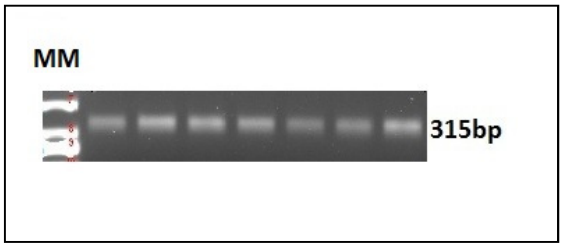

Figure 5.4: 1.5% agarose gel electrophoresis of *EcoRI* restriction digest on pGEM®-T Easy plasmid. The 315bp *Foxc1*-shRNA insert is shown. MM = Molecular marker

C.1.4. Sequencing

Clones containing the insert were verified by Sanger sequencing (Inqaba Biotec, South Africa) using M13 primers given below:

M13 R(-26)	CAGGAAACAGCTATGAC
M13 F(20)	GTAAAACGACGGCCAGT

The returned sequences were uploaded onto BLAST, and compared to sequences in the *Homo sapiens* database. BLAST generated the following result:

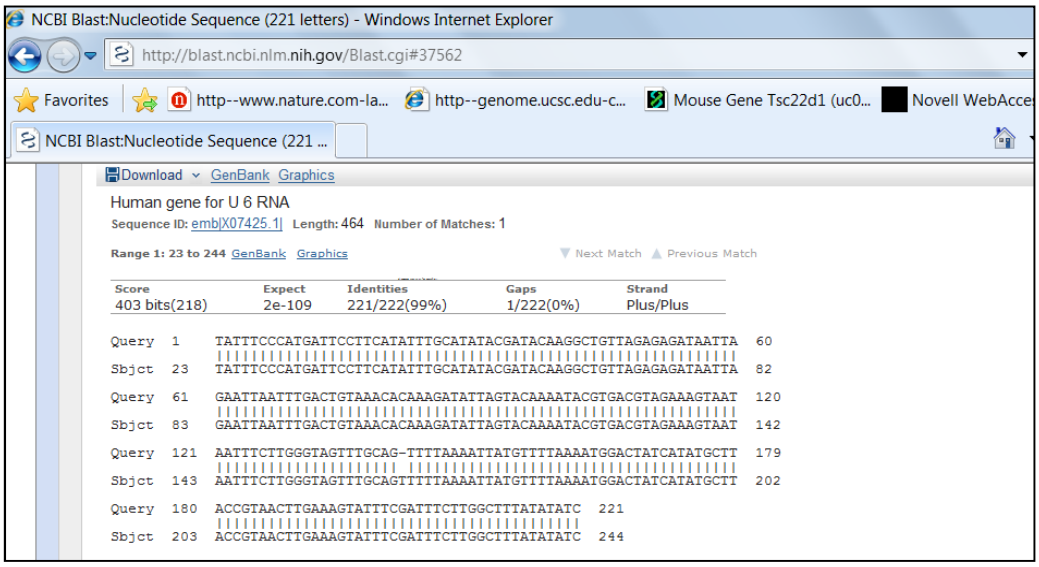

Figure 5.5: *In silico* screen of BLAST search result of a p*Foxc1*-shRNA 2 clone. The sequence showed a match to the Human gene for U6 RNA, accession X07425.1. This shows that the U6 promoter had been successfully cloned out.

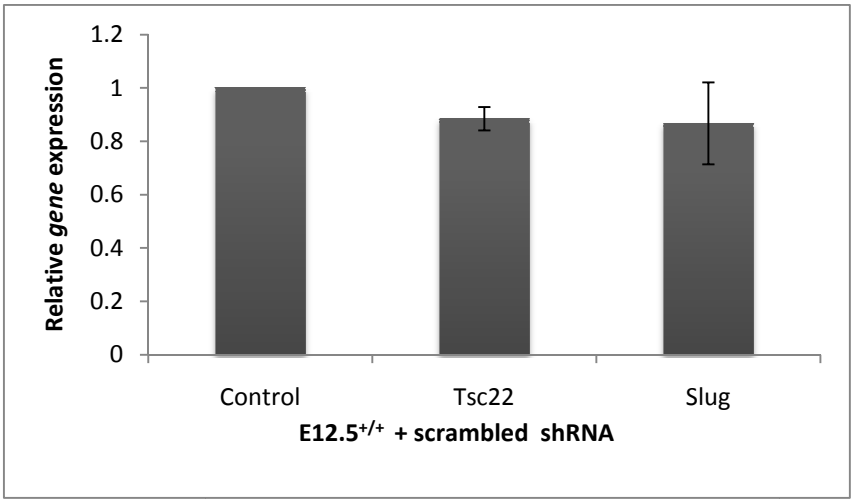

Figure 5.6: qPCR analysis of E12.5+/+ POM cells transfected with a control plasmid encoding a scrambled shRNA sequence that does not target any known mRNA. From the results it can be seen that the plasmid did not have any significant effect on gene expression. ($p<0.05$, n=3; error bars = SEM).

There was no significant difference between the expression of *Tsc22* and *Slug* in the untreated and treated cells.

C.2. p*Foxc1*-eGFP-N1

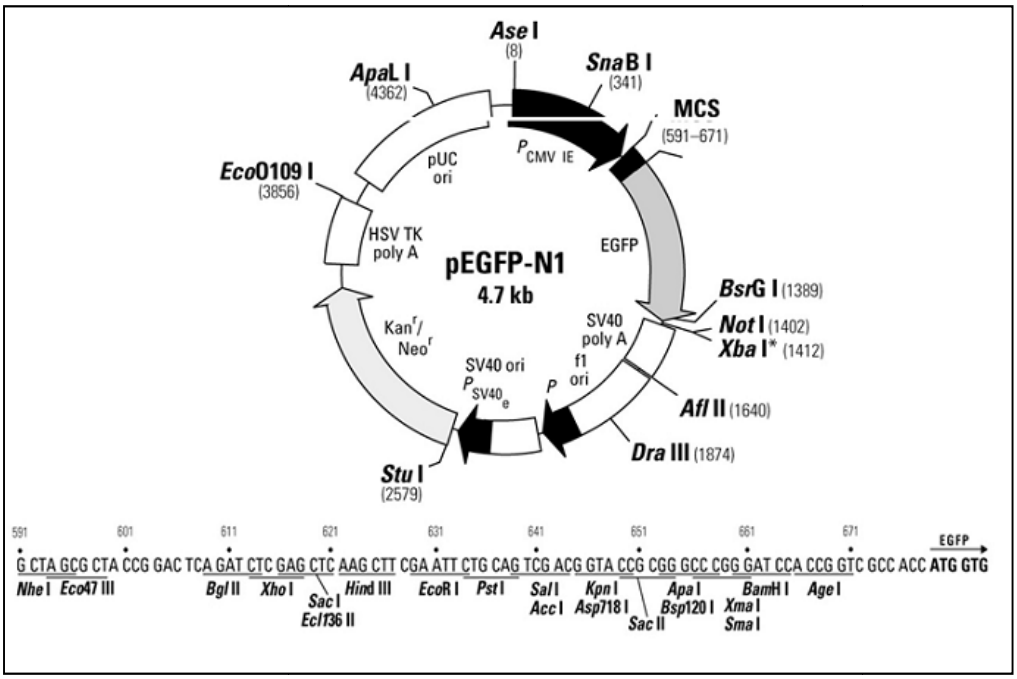

Figure 5.7: peGFP-N1 vector map.

Presence of the insert was confirmed by double digest with enzymes *EcoRI* and *BamHI* (Fermentas, Canada). Restriction digest was carried out in microcentrifuge tubes, incubated at 37°C for 3 hours. The 20µL reactions were composed of the following:

Component	Volume (µL)
Nuclease free water	15-*x*
10x Buffer R	2
DNA (0.5-1µg/µL)	*x*
*Eco*RI	1
*Bam*HI	2
TOTAL	20

C.3. Scrambled shRNA control

Control shRNA Plasmid-A (Santa Cruz Biotechnology, USA; sc-108060) encoding a scrambled shRNA sequence was used as a negative control for the *Foxc1* overexpression and knockdown experiments. The shRNA sequence does not target any cellular mRNA. The control plasmid was transfected into E12.5$^{+/+}$ POM cells as described in Section 2.5. RNA was isolated from the cells and cDNA synthesised for qPCR analysis of gene expression against the control (untreated POM cells). The analysis is given below. Due to reagent limitations, only data for *Tsc22* and *Slug* could be obtained. Figure 5.6 shows the results.

Appendix D: Lens treatment controls

Lenses were steeped in boiling water for 15 minutes in order to deactivate cellular activities in the lens epithelium. The boiled lenses were used as a negative control for the lens experiments described in Section 2.6.4. The results from qPCR analyses of the control experiments are given below:

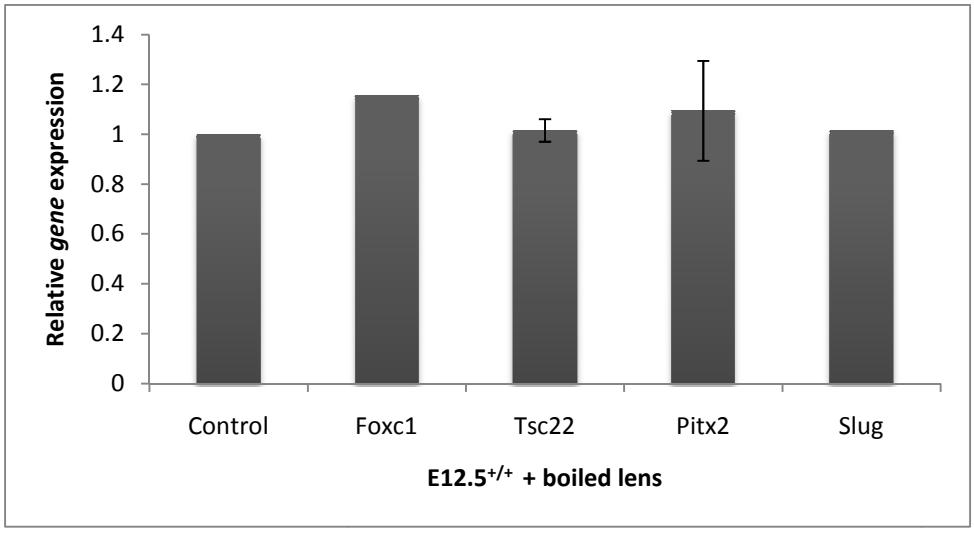

Figure 5.8: qpCR analysis of *Foxc1*, *Tsc22*, *Pitx2* and *Slug* expression in E12.5 POM cells after 24 hour exposure to boiled E6 lens, relative to the control (untreated POM cells). ($p<0.05$; error bars =SEM).

There was no significant difference in gene expression between the treated and untreated E12.5 POM cells.

Appendix E: MIQE checklist

E.1. Experimental design

For the investigation, immortalised POM cell lines representing two distinct developmental stages were established from wild type mouse embryos. These were E12.5$^{+/+}$ characterised by high proliferation and E13.5$^{+/+}$, a more differentiated state. Cells of passage $6 \leq p \geq 8$ and $24 \leq p \geq 27$ were used for the experiments and untreated E12.5$^{+/+}$ and E13.5$^{+/+}$ POM cells were used as the control.

The effect of *Foxc1* overexpression on *Pitx2*, *Tsc22* and *Slug* expression was assessed by transfecting E12.5 and E13.5 POM cells with p*Foxc1*-eGFP and performing qPCR on the isolated RNA. An shRNA targeting *Foxc1* was developed to assess the effect of *Foxc1* knockdown on the genes of interest, also by qPCR. A plasmid encoding a scrambled shRNA was used as a negative control. The effects of lenses on proliferation and gene expression were elucidated by exposure of E12.5 and E13.5 wild type POM cells to E6 and E8 whole chick lenses respectively. Proliferation was measured by cell counts and MTS assay and gene expression evaluated by qPCR. The effect of lens derived signals on *Foxc1*, *Pitx2*, *Tsc22* and *Slug* expression was studied by exposing POM cells that had been *Foxc1* silenced

to whole chick lenses. Exposure of POM cells to boiled lenses was used as a negative control. The effect of recombinant TGFβ2 on *Foxc1*, *Pitx2*, *Tsc22* and *Slug* expression was also investigated by qPCR analysis. E12.5 and E13.5 cells were subjected to a 24 hour treatment of 30ng/mL TGFβ2 before RNA was isolated. The localisation of *N-cadherin* was observed by immunostaining with an *N-cadherin* antibody conjugated to a fluorescent molecule and visualised by confocal microscopy. E12.5$^{+/+}$ and E13.5$^{+/+}$ monolayers and hanging drop cultures were studied.

Experiments were carried out at the University of KwaZulu-Natal, School of Life Sciences in the research laboratory of Dr Paula Sommer.

E.2. Sample

RNA was isolated, as described in Section 2.8.1, from confluent POM cell cultures grown in 60mm dishes (Corning, USA). Cells were trypsinised as in Section 2.1.1 and spun down before washing in 1x PBS. Cells were then harvested by centrifugation and RNA extracted. Long term storage was achieved by freezing cell stocks in 5% DMSO in culture medium (Section B.4).

E.3. Nucleic acid extraction

RNA was isolated using a QIAGEN RNeasy kit as per manufacturer's instructions. RNA purity was assessed by NanoDrop as shown in Figure 3.5 of Section 3.3.2. Quality of the RNA was established by running samples on a denaturing formaldehyde gel (Figure 3.6, Section 3.3.2). RNA was not DNase treated as this was shown to negatively affect qPCR data in a previous study by another member of the laboratory.

E.4. Reverse transcription

Conditions for reverse transcription using SuperScript®III First Strand Synthesis System for RT-PCR and SuperScript®VILO™cDNA MasterMix outlined in Sections 2.9.1 and 2.9.10 respectively.

Results for No-Reverse Transcriptase (No-RT) experiments are shown in the figure below:

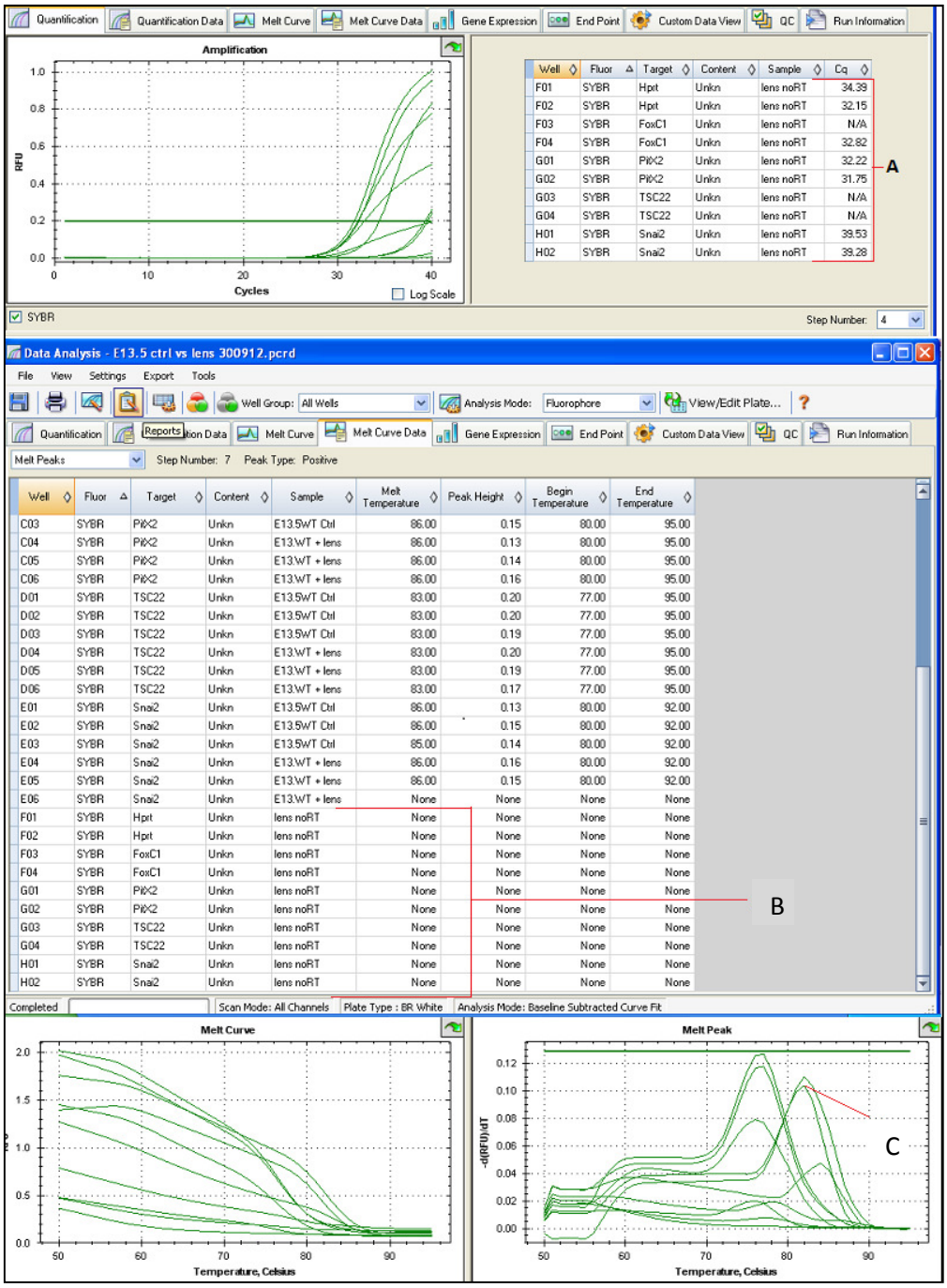

Figure 5.9: *In silico* screen of results for No-RT experiments showing A) Amplification data – the C_q values for each product. Although a Cq value was generated for some of the replicates, futher analysis of B) The corresponding melt curve data the melt curves, showed that the amplification was due to primer-dimer C) Peaks corresponding to the melt curve.

E.5. Target information and qPCR oligonucleotides

Details of qPCR primers are given in Table I, Section 2.10. Primers used in the investigation were subjected to BLAST against the *Mus musculus* genome in NCBI database. The Figures below are the screen results for each BLAST, including the accession number of the transcript and product size.

Primer-BLAST — Primer-Blast results

NCBI/ Primer-BLAST : results: Job id=JSID_01_36518_130.14.22.10_9002 more...

Input PCR template: none
Specificity of primers: Target templates were found in selected database: Refseq mRNA (Organism limited to Mus musculus)
Other reports: Search Summary

Detailed primer reports

Primer pair 1

	Sequence (5'->3')	Length	Tm	GC%	Self complementarity
Forward primer	GTCCCAGCGTCGTGATTAGCGAT	23	64.99	56.52	4.00
Reverse primer	GGGCCACAATGTGATGGCCTCC	22	66.03	63.64	8.00

Products on target templates

>NM_013556.2 Mus musculus hypoxanthine guanine phosphoribosyl transferase (Hprt), mRNA

```
product length = 180
Forward primer  1    GTCCCAGCGTCGTGATTAGCGAT  23
Template        160  .......................  182

Reverse primer  1    GGGCCACAATGTGATGGCCTCC  22
Template        339  ......................  318
```

Figure 5.10: *In silico* screen of of *Hprt* primer BLAST against *Mus musculus* genome.

Primer-BLAST — Primer-Blast results

NCBI/ Primer-BLAST : results: Job id=JSID_01_36683_130.14.22.21_9002 more...

Input PCR template: none
Specificity of primers: Target templates were found in selected database: Refseq mRNA (Organism limited to Mus musculus)
Other reports: Search Summary

Detailed primer reports

Primer pair 1

	Sequence (5'->3')	Length	Tm	GC%	Self complementarity
Forward primer	TCGCTTTCCTGCTCATTCGTC	21	61.00	52.38	2.00
Reverse primer	TGCAGAAAACGCTGTAGGGG	20	60.61	55.00	4.00

Products on target templates

>NM_008592.2 Mus musculus forkhead box C1 (Foxc1), mRNA

```
product length = 559
Forward primer  1     TCGCTTTCCTGCTCATTCGTC  21
Template        2559  .....................  2579

Reverse primer  1     TGCAGAAAACGCTGTAGGGG  20
Template        3117  ....................  3098
```

Figure 5.11: *In silico* screen of *Foxc1* primer BLAST against *Mus musculus* genome.

Primer-BLAST Primer-Blast results

NCBI/ Primer-BLAST : results: Job id=JSID_01_48181_130.14.22.10_9002 more...

Input PCR template none
Specificity of primers Target templates were found in selected database: Refseq mRNA (Organism limited to Mus musculus)
Other reports Search Summary

Detailed primer reports

Primer pair 1

	Sequence (5'->3')	Length	Tm	GC%	Self complementarity
Forward primer	AGCTGTGCAAGAATGGCTTT	20	58.66	45.00	4.00
Reverse primer	CACCATGCTGGACGACATAC	20	58.71	55.00	6.00

Products on target templates

>NM_001042504.1 Mus musculus paired-like homeodomain transcription factor 2 (Pitx2), transcript variant 1, mRNA

```
product length = 233
Forward primer  1    AGCTGTGCAAGAATGGCTTT  20
Template        560  ....................  579

Reverse primer  1    CACCATGCTGGACGACATAC  20
Template        792  ....................  773
```

Figure 5.12: *In silico* screen of *Pitx2* primer BLAST against *Mus musculus* genome.

Primer-BLAST Primer-Blast results

NCBI/ Primer-BLAST : results: Job id=JSID_01_37140_130.14.22.21_9002 more...

Input PCR template none
Specificity of primers Target templates were found in selected database: Refseq mRNA (Organism limited to Mus musculus)
Other reports Search Summary

Detailed primer reports

Primer pair 1

	Sequence (5'->3')	Length	Tm	GC%	Self complementarity
Forward primer	GTAGACCAGTGGCGATGGAT	20	59.25	55.00	5.00
Reverse primer	TCCAGCTGGGAGTTTTTCTC	20	57.43	50.00	8.00

Products on target templates

>NM_009366.3 Mus musculus TSC22 domain family, member 1 (Tsc22d1), transcript variant 2, mRNA

```
product length = 256
Forward primer  1    GTAGACCAGTGGCGATGGAT  20
Template        224  ....................  243

Reverse primer  1    TCCAGCTGGGAGTTTTTCTC  20
Template        479  ....................  460
```

Figure 5.13: *In silico* screen of *Tsc22* primer BLAST against *Mus musculus* genome.

Primer-BLAST Primer-Blast results

NCBI/ Primer-BLAST : results: Job id=JSID_01_36932_130.14.22.21_9002 more...

Input PCR template	none
Specificity of primers	Target templates were found in selected database: Refseq mRNA (Organism limited to Mus musculus)
Other reports	Search Summary

Detailed primer reports

Primer pair 1

	Sequence (5'->3')	Length	Tm	GC%	Self complementarity
Forward primer	AAGAAGCCCAACTACAGCGA	20	59.31	50.00	2.00
Reverse primer	GCTTTTCCCCAGTGTGAGTT	20	58.31	50.00	3.00

Products on target templates

>NM_011415.2 Mus musculus snail homolog 2 (Drosophila) (Snai2), mRNA

```
product length = 595
Forward primer  1    AAGAAGCCCAACTACAGCGA  20
Template        158  ....................  177

Reverse primer  1    GCTTTTCCCCAGTGTGAGTT  20
Template        752  ....................  733
```

Figure 5.14: *In silico* screen of *Slug/Snai2* primer BLAST against *Mus musculus* genome.

Primer-BLAST Primer-Blast results

NCBI/ Primer-BLAST : results: Job id=JSID_01_36799_130.14.22.21_9002 more...

Input PCR template	none
Specificity of primers	Target templates were found in selected database: Refseq mRNA (Organism limited to Mus musculus)
Other reports	Search Summary

Detailed primer reports

Primer pair 1

	Sequence (5'->3')	Length	Tm	GC%	Self complementarity
Forward primer	TTAAAAGCTGCTTGGCTTGG	20	57.18	45.00	7.00
Reverse primer	AAGATTTGCATCCTGCGTGT	20	58.46	45.00	4.00

Products on target templates

>NM_007664.4 Mus musculus cadherin 2 (Cdh2), mRNA

```
product length = 205
Forward primer  1     TTAAAAGCTGCTTGGCTTGG  20
Template        2933  ....................  2914

Reverse primer  1     AAGATTTGCATCCTGCGTGT  20
Template        2729  ..C....C............  2748
```

Figure 5.15: *In silico* screen of *N-cadherin* primer BLAST against *Mus musculus* genome.

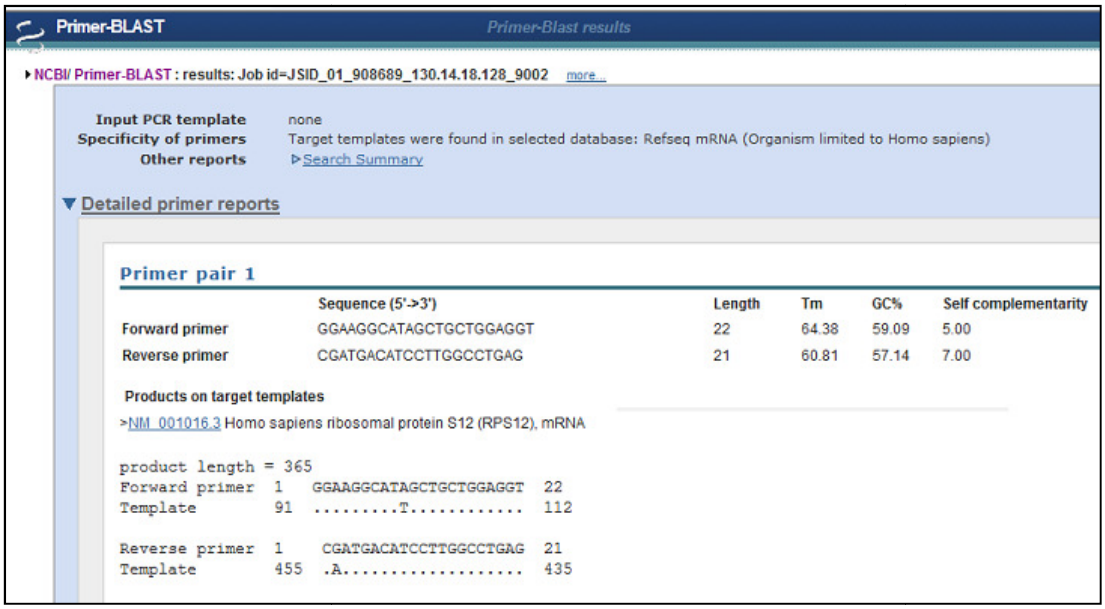

Figure 5.16: *In silico* screen of *Rps12* primer BLAST against *Mus musculus* genome.

E.6. qPCR protocol

All qPCR was carried out in a Mini Opticon MJ MINI™ Personal Thermal Cycler (Bio-Rad, USA) in individual Bio-Rad 0.2mL PCR tubes. The FAM and SYBR channels were used for reading fluorescence set at 0.2 relative fluorescence units (RFU) as a baseline. Reaction conditions were as shown below in Figures 5.15 and 5.16 and are described in Section 2.10.

E.6.1. qPCR protocol using 5x HOT FIREPol®EvaGreen®qPCR Mix Plus

The composition was as follows:

5x HOT FIREPol®EvaGreen®qPCR Mix Plus
Solis BioDyne Catalog no.: 08-24-00001
Composition
HOT FIREPol®DNA Polymerase
5x EvaGreen® qPCR buffer
12.5 mM $MgCl_2$
dNTPs
EvaGreen® dye
ROX dye

Fluorescence was measured in the FAM channel according to the protocol below, also outlined in Section 2.10.1:

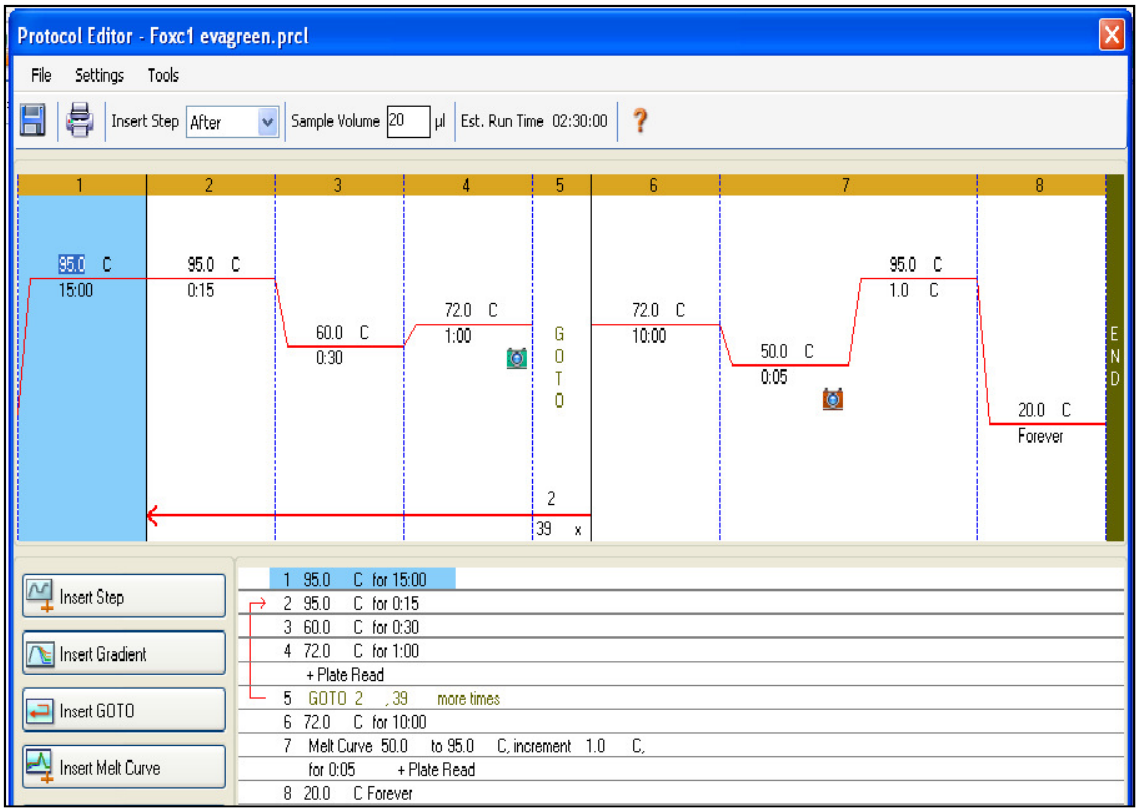

Figure 5.17: qPCR protocol for use with 5x HOT FIREPol®EvaGreen®qPCR Mix Plus

E.6.2. qPCR protocol using SYBR®Green JumpStart™ Taq ReadyMix™

Composition was as follows:

SYBR®Green JumpStart™ Taq ReadyMix™
SIGMA-ALDRICH Catalog no.: S4438
Composition
20nM Tris-HCl, pH8.3
100nM KCl
7nM $MgCl_2$
0.4mM of each (dATP,dCTP,dGTP, dTTP)
0.05unit/mL Taq DNA Polymerase
JumpStart Taq antibody
SYBR Green I
Stabilisers

Fluorescence was measured in the SYBR channel according to the protocol below also described in Section 2.10.2:

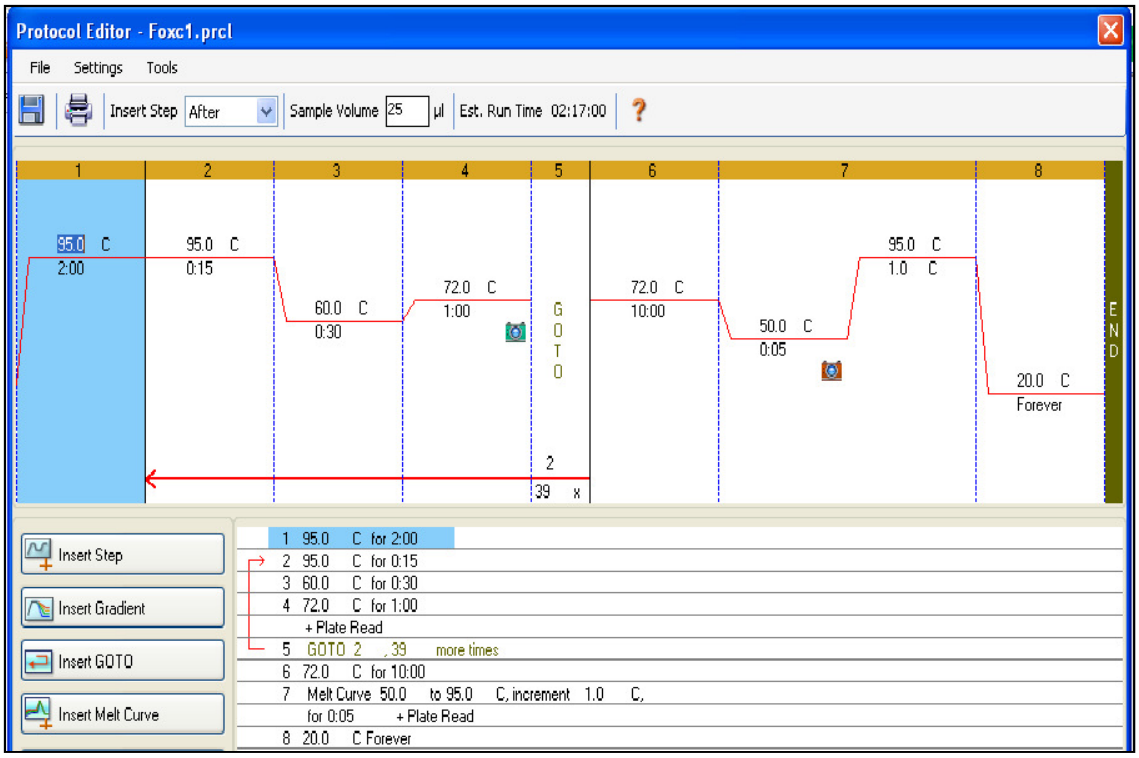

Figure 5.18: qPCR protocol for use with SYBR®Green JumpStart™ Taq ReadyMix™

E.7. qPCR validation

Below are screen images from qPCR data analysis generated by CFX software manager which supports the Mini Opticon MJ MINI™ Personal Thermal Cycler. Figures are comprised of combined screen shots of the A) Melt curve B) Melt peak window C) Amplification (quantification) window D) Melt temperature data E) C_q values read at the RFU intercept and F) 1.5% agarose gel electrophoresis of the qPCR product run against Fermentas 50bp ladder.

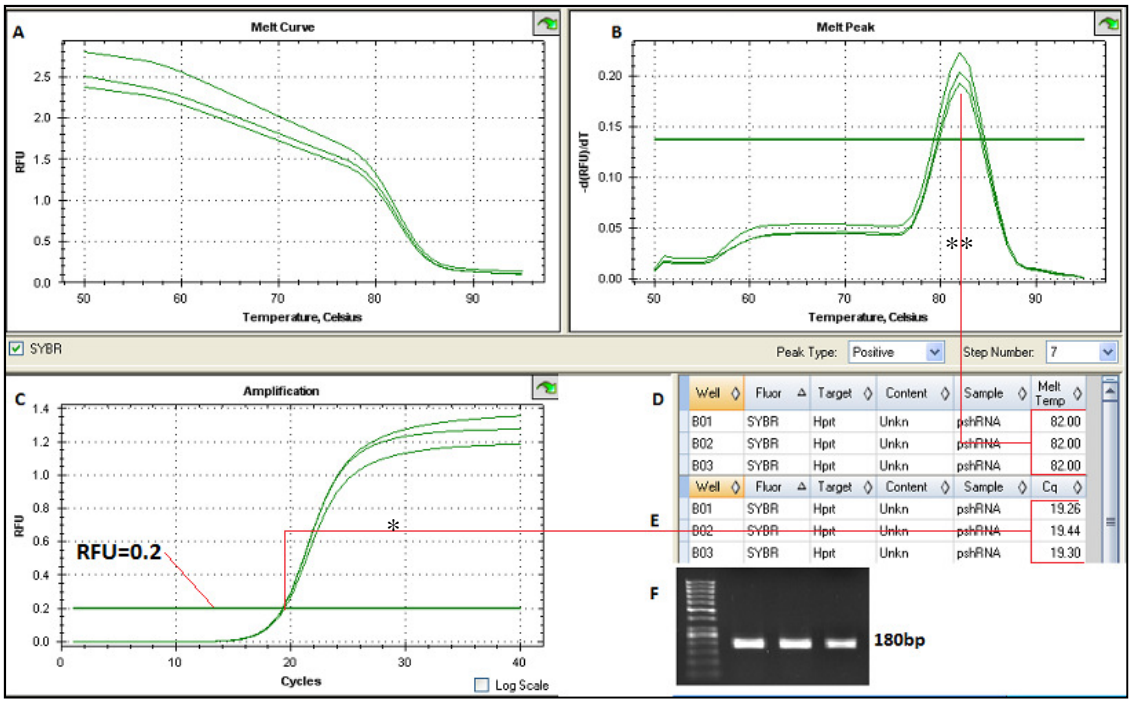

Figure 5.19: Melt curves, amplification curves and gel electrophoresis of qPCR product for *Hprt* primer set. Asterisk shows the C_q data generated and double asterisk shows the corresponding melt temperatures. A) The melt curve B) Melt peak C) Amplification curves D) Melt temperature data E) Amplification data F) Gel electrophoresis of product.

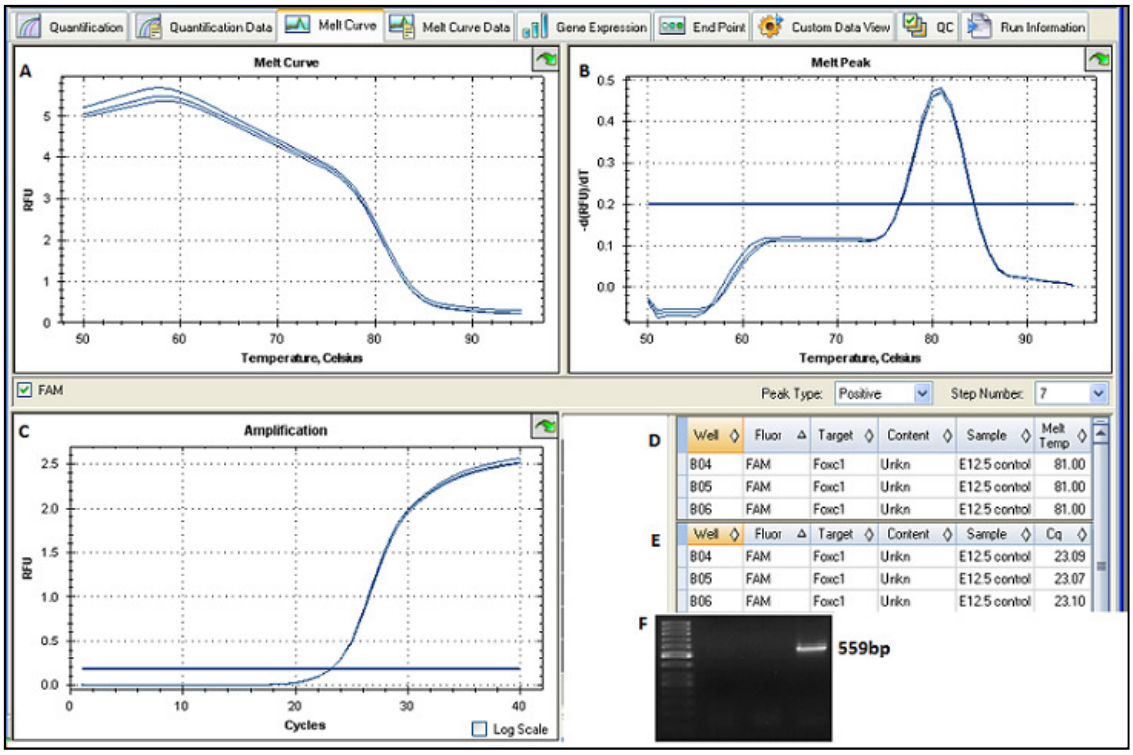

Figure 5.20: Melt curves, amplification curves and gel electrophoresis of qPCR product for *Foxc1* primer set. A) The melt curve B) Melt peak C) Amplification curves D) Melt temperature data E) Amplification data F) Gel electrophoresis of product.

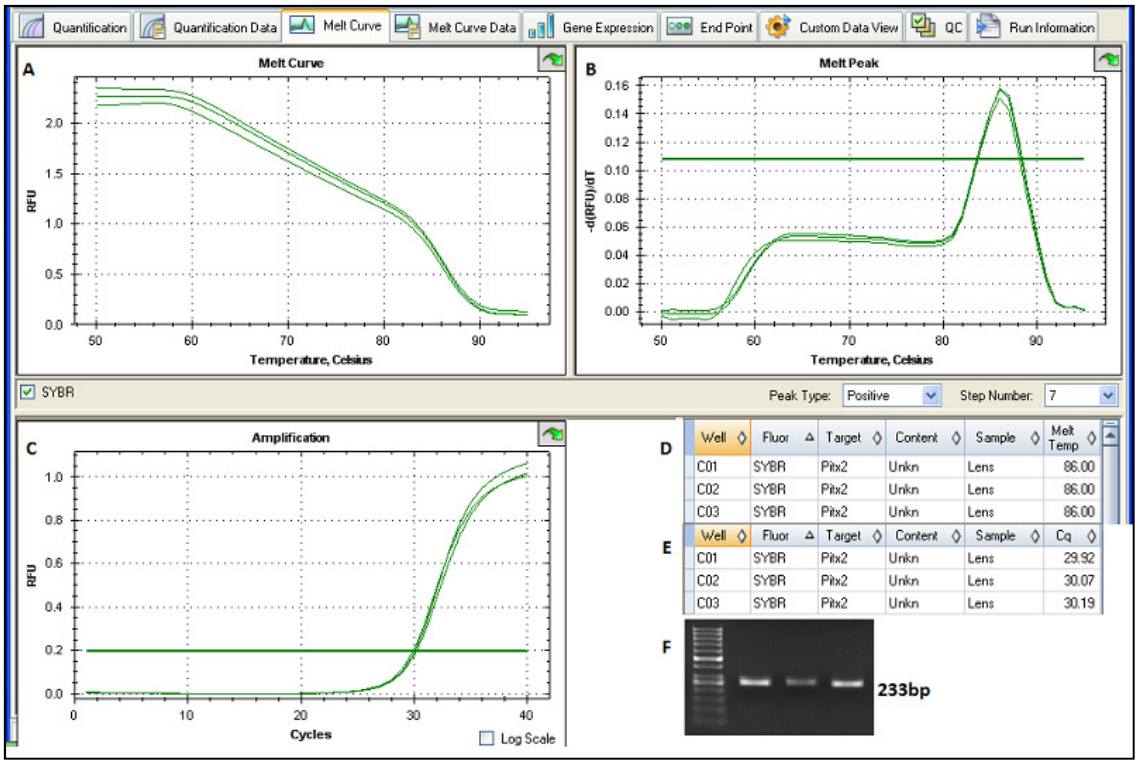

Figure 5.21: Melt curves, amplification curves and gel electrophoresis of qPCR product for *Pitx2* primer set. A) The melt curve B) Melt peak C) Amplification curves D) Melt temperature data E) Amplification data F) Gel electrophoresis of product.

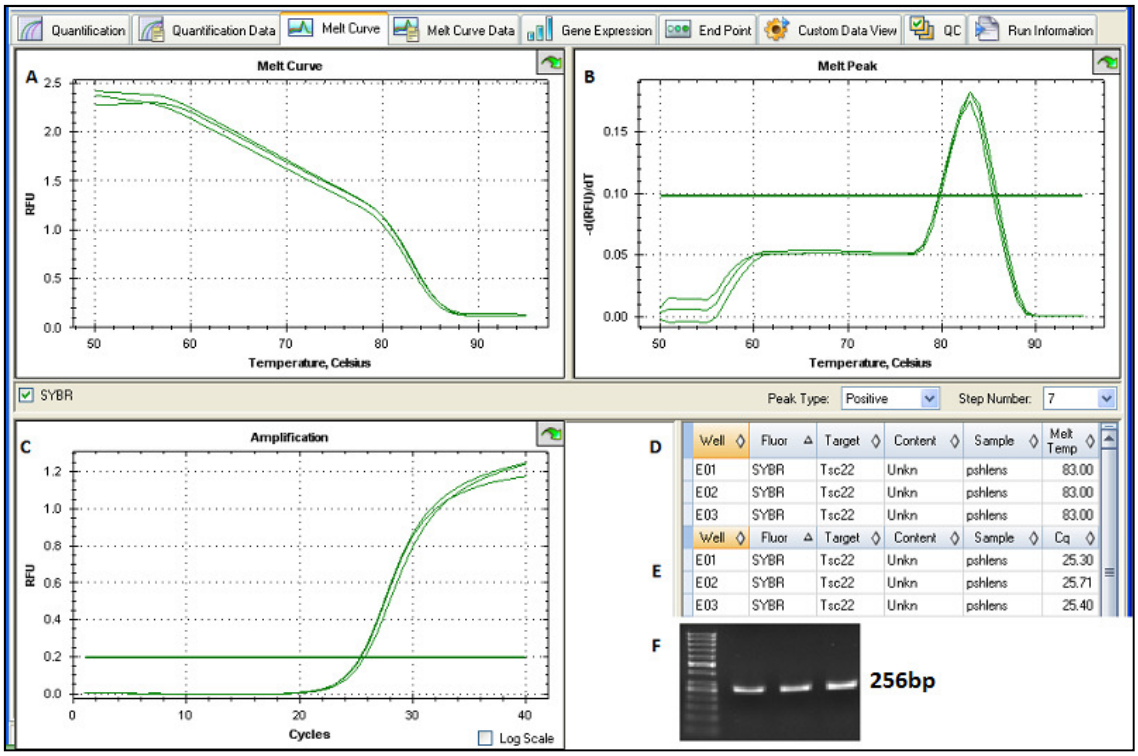

Figure 5.22: Melt curves, amplification curves and gel electrophoresis of qPCR product for *Tsc22* primer set. A) The melt curve B) Melt peak C) Amplification curves D) Melt temperature data E) Amplification data F) Gel electrophoresis of product.

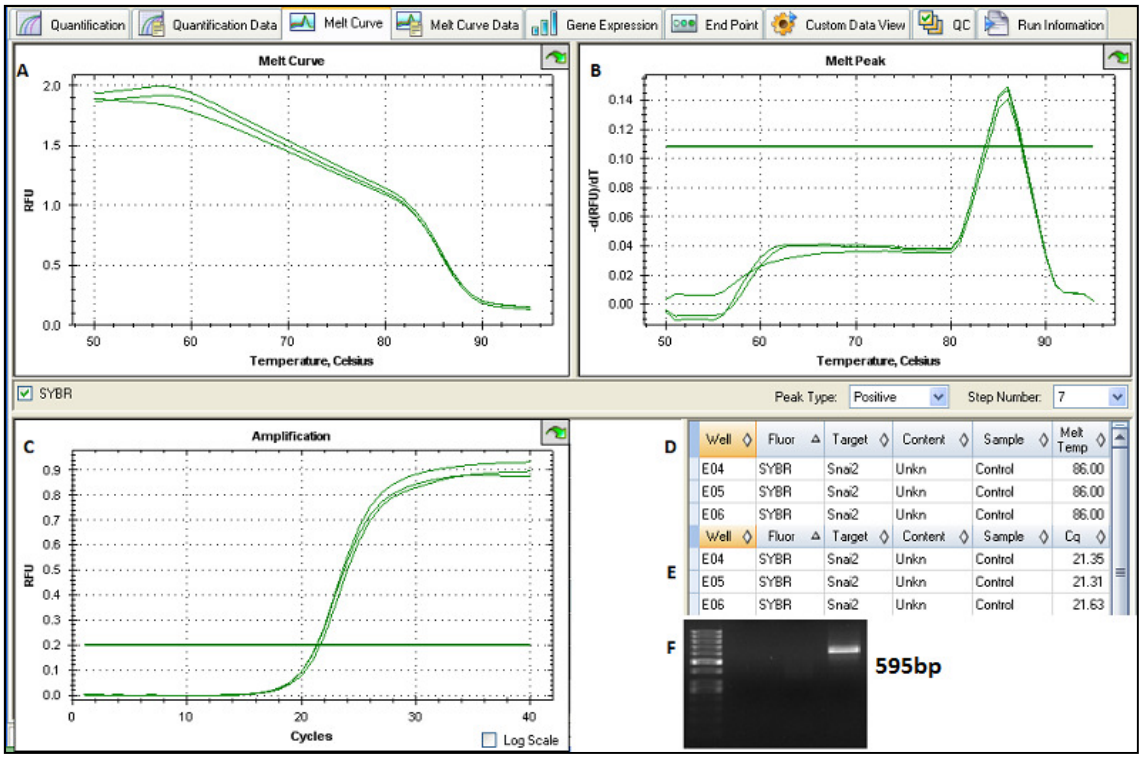

Figure 5.23: Melt curves, amplification curves and gel electrophoresis of qPCR product for *Slug/Snai2* primer set. A) The melt curve B) Melt peak C) Amplification curves D) Melt temperature data E) Amplification data F) Gel electrophoresis of product.

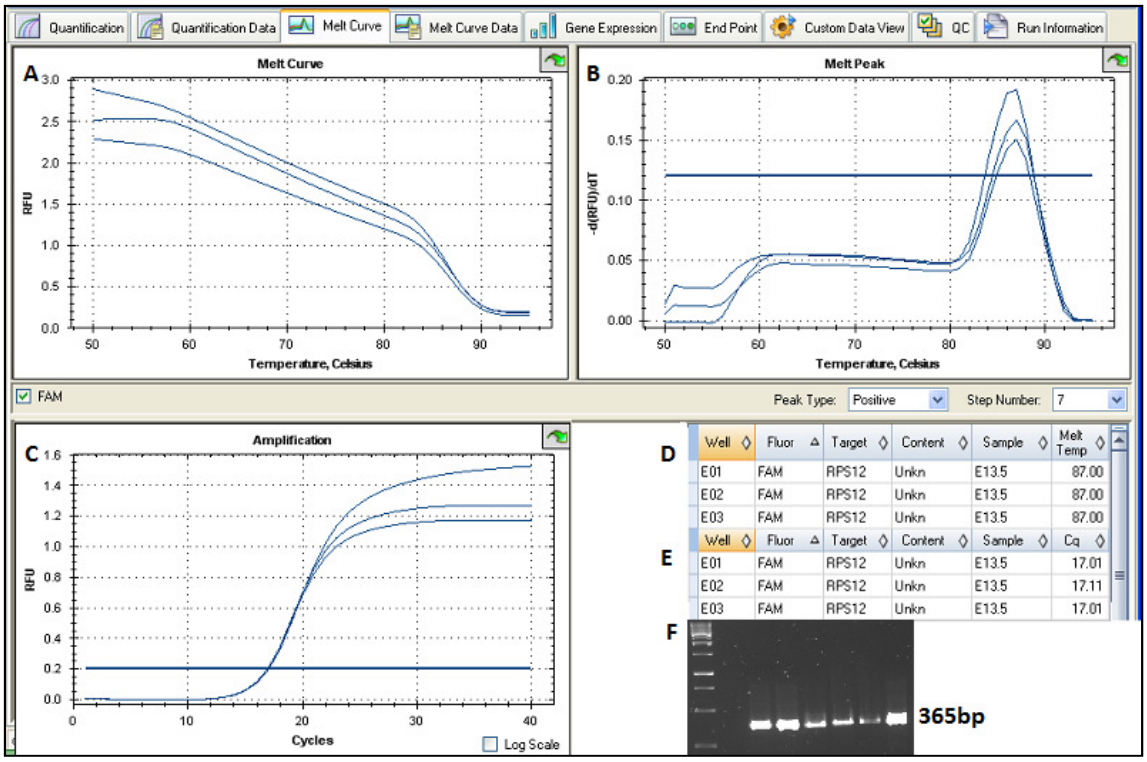

Figure 5.24: Melt curves, amplification curves and gel electrophoresis of qPCR product for *Rps12* primer set. A) The melt curve B) Melt peak C) Amplification curves D) Melt temperature data E) Amplification data F) Gel electrophoresis of product.

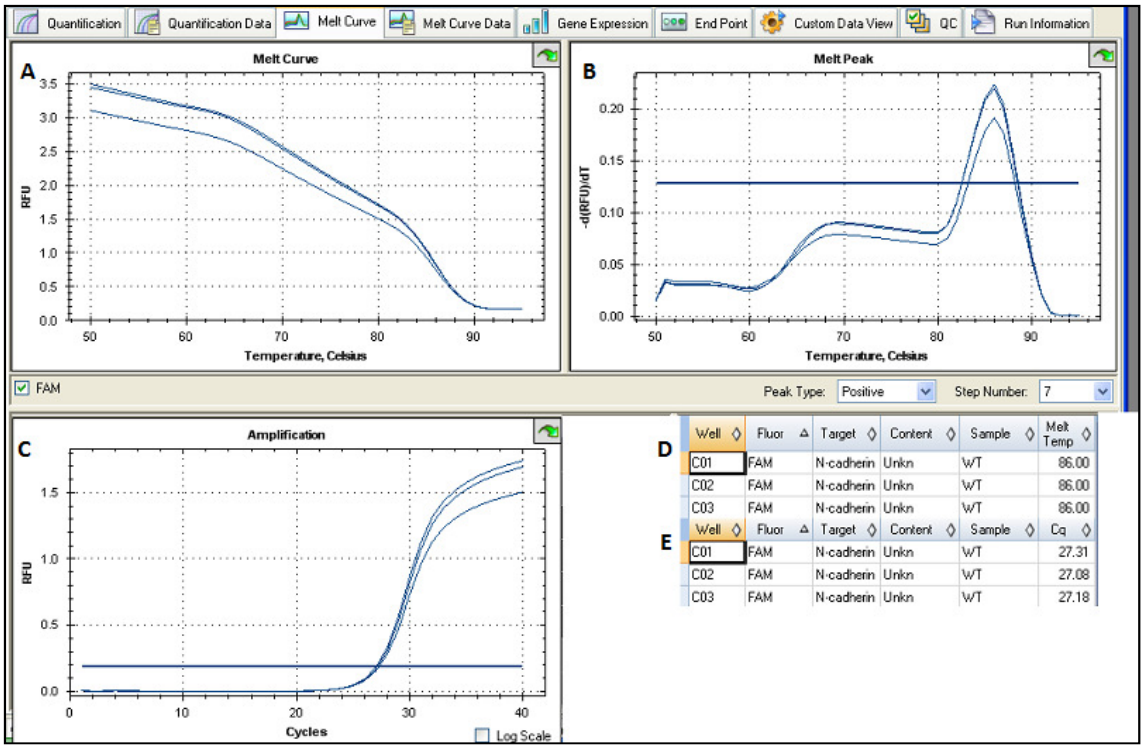

Figure 5.25: Melt curves and amplification curves for *N-cadherin* primer set. A) The melt curve B) Melt peak C) Amplification curves D) Melt temperature data E) Amplification data.

E.7.1. qPCR amplification efficiencies

Reaction efficiencies were calculated by plotting the Mean Cq value of serial dilutions of cDNA and obtaining the slope (m) which was plugged into the equation:

PCR efficiency = $10^{-1/slope}$ -1

At http://www.genomics.agilent.com/CalculatorPopupWindow.aspx?CalID=8

The figures below show A) screen shot of amplification of cDNA serial dilution and B) plot of mean C_q value against dilution for each primer set. Each dilution was run in triplicate but only one curve per dilution has been shown for clarity.

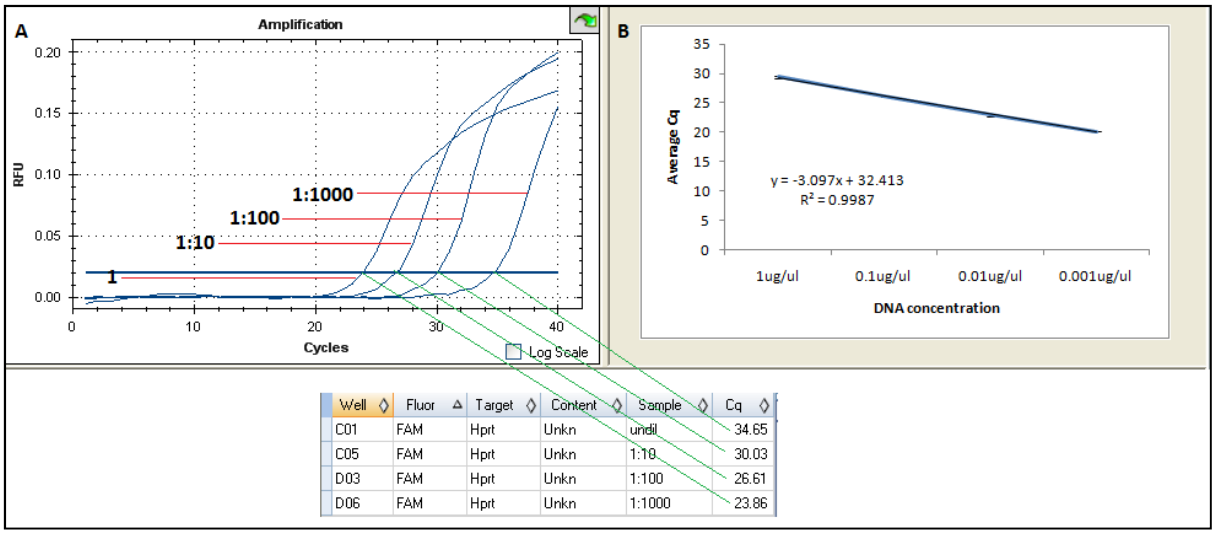

Figure 5.26: Amplification curves for the serial dilution of E12.5 cDNA and plot used to determine qPCR amplification efficiency for the *Hprt* primer set. A) *In silico* screen of amplification of cDNA serial dilution and B) Plot of mean C_q value against dilution. Red lines show the curve corresponding to the different dilutions and the green lines show the C_q values generated for each dilution. Reaction efficiency = 110.33%.

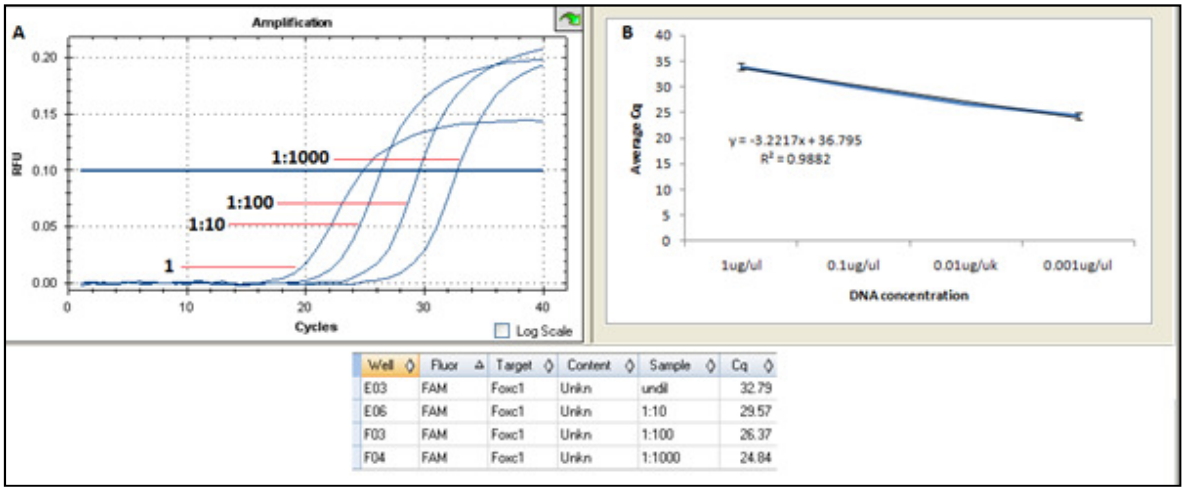

Figure 5.27: Amplification curves for the serial dilution of E12.5 cDNA and plot used to determine qPCR amplification efficiency for the *Foxc1* primer set. A) *In silico* screen of amplification of cDNA serial dilution and B) Plot of mean C_q value against dilution. Reaction efficiency = 104.36%.

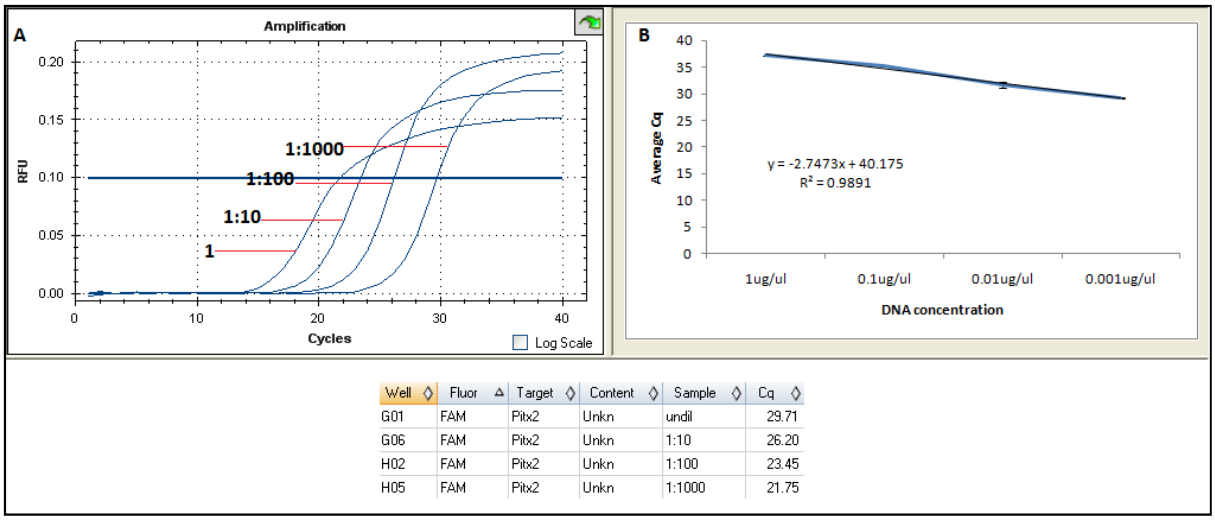

Well	Fluor	Target	Content	Sample	Cq
G01	FAM	Pitx2	Unkn	undil	29.71
G06	FAM	Pitx2	Unkn	1:10	26.20
H02	FAM	Pitx2	Unkn	1:100	23.45
H05	FAM	Pitx2	Unkn	1:1000	21.75

Figure 5.28: Amplification curves for the serial dilution of E12.5 cDNA and plot used to determine qPCR amplification efficiency for the *Pitx2* primer set. A) *In silico* screen of amplification of cDNA serial dilution and B) Plot of mean C_q value against dilution. Reaction efficiency = 131.20%.

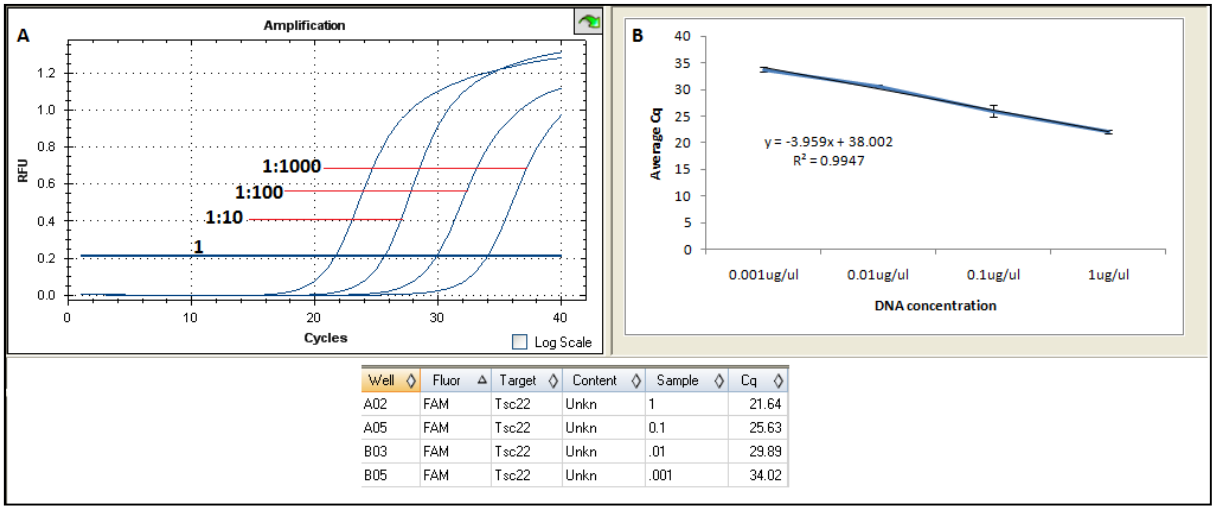

Well	Fluor	Target	Content	Sample	Cq
A02	FAM	Tsc22	Unkn	1	21.64
A05	FAM	Tsc22	Unkn	0.1	25.63
B03	FAM	Tsc22	Unkn	.01	29.89
B05	FAM	Tsc22	Unkn	.001	34.02

Figure 5.29: Amplification curves for the serial dilution of E12.5 cDNA and plot used to determine qPCR amplification efficiency for the *Tsc22* primer set. A) *In silico* screen of amplification of cDNA serial dilution and B) Plot of mean C_q value against dilution. Reaction efficiency = 78.89%.

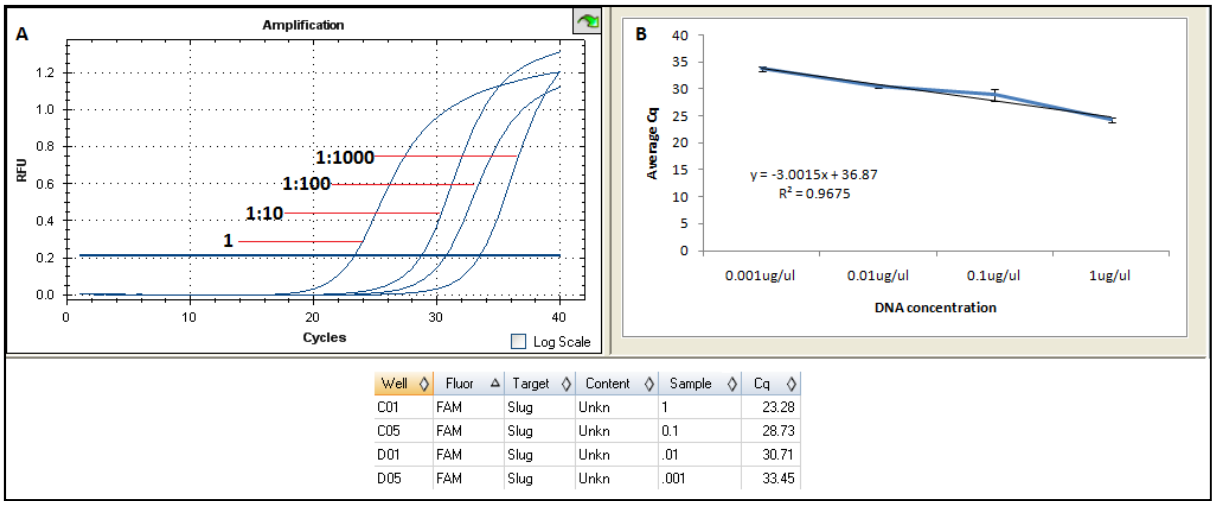

Well	Fluor	Target	Content	Sample	Cq
C01	FAM	Slug	Unkn	1	23.28
C05	FAM	Slug	Unkn	0.1	28.73
D01	FAM	Slug	Unkn	.01	30.71
D05	FAM	Slug	Unkn	.001	33.45

Figure 5.30: Amplification curves for the serial dilution of E12.5 cDNA and plot used to determine qPCR amplification efficiency for the *Slug* primer set. A) *In silico* screen of amplification of cDNA serial dilution and B) Plot of mean C_q value against dilution. Reaction efficiency = 138.59%.

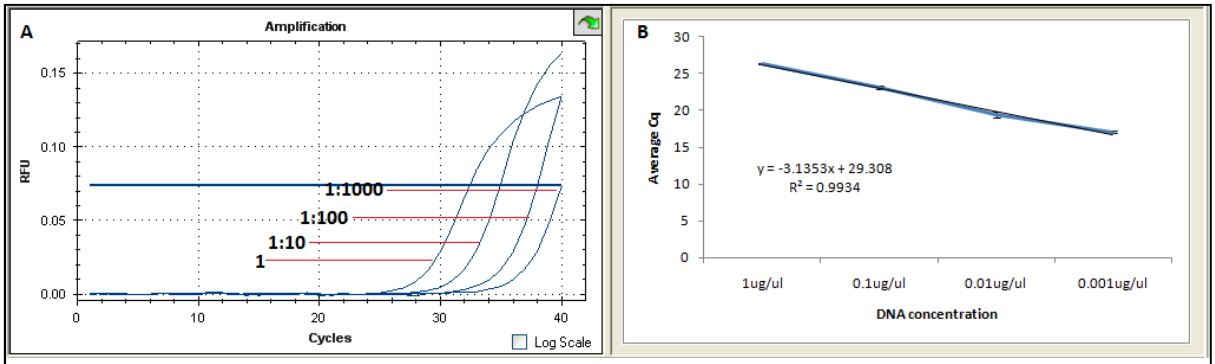

Well	Fluor	Target	Content	Sample	Cq
A02	FAM	Rps12	Unkn	undil	N/A
A05	FAM	Rps12	Unkn	1:10	38.02
B02	FAM	Rps12	Unkn	1:100	34.95
B04	FAM	Rps12	Unkn	1:1000	32.41

Figure 5.31: Amplification curves for the serial dilution of E12.5 cDNA and plot used to determine qPCR amplification efficiency for the *Rps12* primer set. A) *In silico* screen of amplification of cDNA serial dilution and B) Plot of mean C_q value against dilution. Reaction efficiency = 108.42%.

E.8. Data analysis

qPCR data was analysed by the CFX Manager software reading fluorescence at 0.2 RFU. Outlying C_q values were discarded. Experiments were carried out in triplicate per technical run and 3 technical runs were performed for each biological repeat. Analyses presented in this report are based on 3 data sets generated from 2 biological repeats. Only one reference gene was used due to the 48 well capacity of the thermal cycler. All experiments

were normalised against a reference gene (*Hprt* or *Rps12*) to generate a fold change in treatment relative to the control. Statistical significance of the fold changes were evaluated by one sample T-tests, Paired samples T-tests and One-way ANOVA of the fold changes using SPSS v21 (IBM). The output was used to plot bar graphs presented with the corresponding standard error of the mean (SEM).

E.9. No-template controls

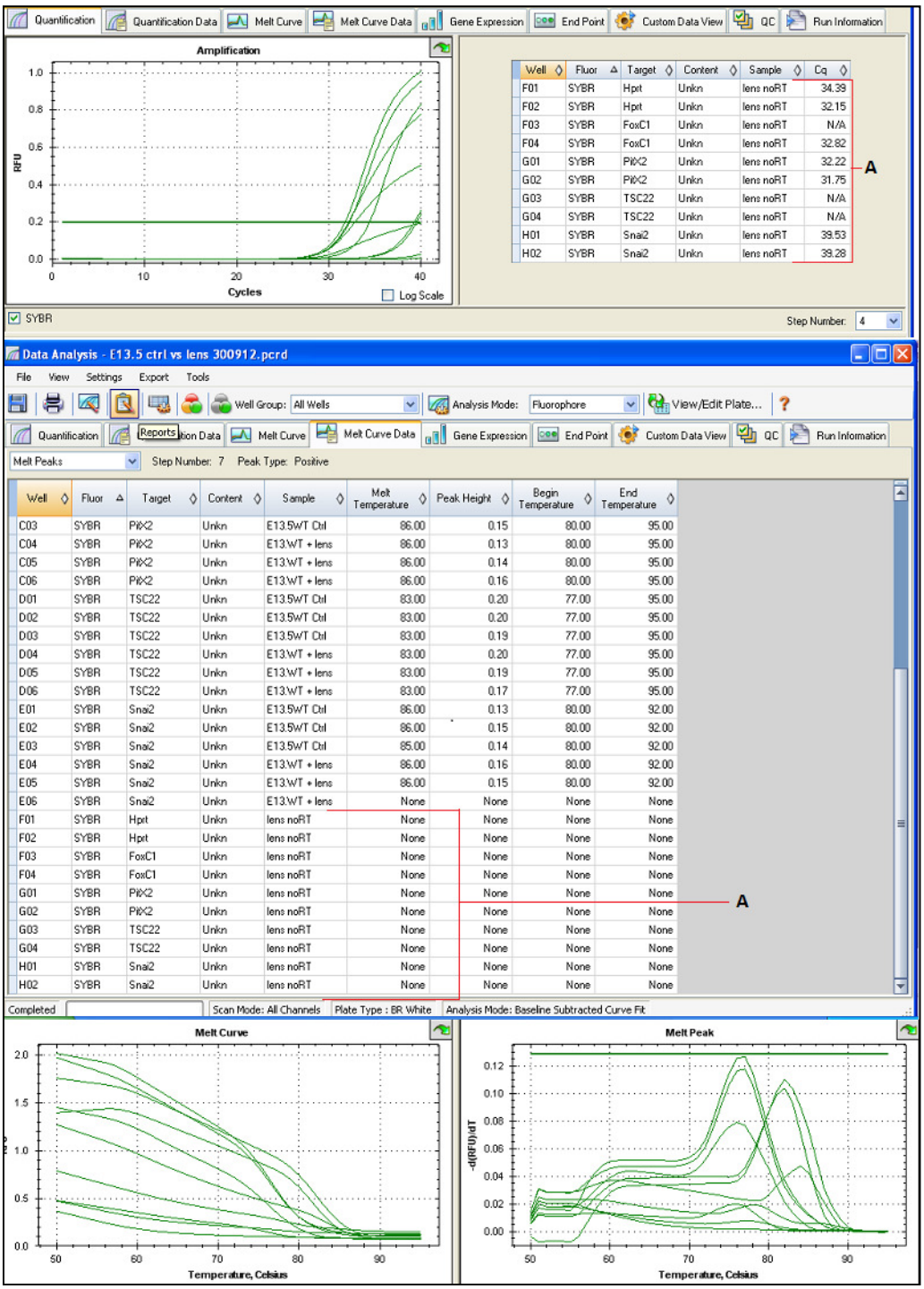

Well	Fluor	Target	Content	Sample	Cq
F01	SYBR	Hprt	Unkn	lens noRT	34.39
F02	SYBR	Hprt	Unkn	lens noRT	32.15
F03	SYBR	FoxC1	Unkn	lens noRT	N/A
F04	SYBR	FoxC1	Unkn	lens noRT	32.82
G01	SYBR	Pitx2	Unkn	lens noRT	32.22
G02	SYBR	Pitx2	Unkn	lens noRT	31.75
G03	SYBR	TSC22	Unkn	lens noRT	N/A
G04	SYBR	TSC22	Unkn	lens noRT	N/A
H01	SYBR	Snai2	Unkn	lens noRT	39.53
H02	SYBR	Snai2	Unkn	lens noRT	39.28

Well	Fluor	Target	Content	Sample	Melt Temperature	Peak Height	Begin Temperature	End Temperature
C03	SYBR	Pitx2	Unkn	E13.5WT Ctrl	86.00	0.15	80.00	95.00
C04	SYBR	Pitx2	Unkn	E13.WT + lens	86.00	0.13	80.00	95.00
C05	SYBR	Pitx2	Unkn	E13.WT + lens	86.00	0.14	80.00	95.00
C06	SYBR	Pitx2	Unkn	E13.WT + lens	86.00	0.16	80.00	95.00
D01	SYBR	TSC22	Unkn	E13.5WT Ctrl	83.00	0.20	77.00	95.00
D02	SYBR	TSC22	Unkn	E13.5WT Ctrl	83.00	0.20	77.00	95.00
D03	SYBR	TSC22	Unkn	E13.5WT Ctrl	83.00	0.19	77.00	95.00
D04	SYBR	TSC22	Unkn	E13.WT + lens	83.00	0.20	77.00	95.00
D05	SYBR	TSC22	Unkn	E13.WT + lens	83.00	0.19	77.00	95.00
D06	SYBR	TSC22	Unkn	E13.WT + lens	83.00	0.17	77.00	95.00
E01	SYBR	Snai2	Unkn	E13.5WT Ctrl	86.00	0.13	80.00	92.00
E02	SYBR	Snai2	Unkn	E13.5WT Ctrl	86.00	0.15	80.00	92.00
E03	SYBR	Snai2	Unkn	E13.5WT Ctrl	85.00	0.14	80.00	92.00
E04	SYBR	Snai2	Unkn	E13.WT + lens	86.00	0.16	80.00	92.00
E05	SYBR	Snai2	Unkn	E13.WT + lens	86.00	0.15	80.00	92.00
E06	SYBR	Snai2	Unkn	E13.WT + lens	None	None	None	None
F01	SYBR	Hprt	Unkn	lens noRT	None	None	None	None
F02	SYBR	Hprt	Unkn	lens noRT	None	None	None	None
F03	SYBR	FoxC1	Unkn	lens noRT	None	None	None	None
F04	SYBR	FoxC1	Unkn	lens noRT	None	None	None	None
G01	SYBR	Pitx2	Unkn	lens noRT	None	None	None	None
G02	SYBR	Pitx2	Unkn	lens noRT	None	None	None	None
G03	SYBR	TSC22	Unkn	lens noRT	None	None	None	None
G04	SYBR	TSC22	Unkn	lens noRT	None	None	None	None
H01	SYBR	Snai2	Unkn	lens noRT	None	None	None	None
H02	SYBR	Snai2	Unkn	lens noRT	None	None	None	None

Figure 5.32: No-template control quantitation for *Hprt*, *Pitx2*, *Foxc1*, *Tsc22* and *Slug*. Analysis of the products by agarose gel electrophoresis showed that the peaks corresponded to primer dimer. A) C_q values generated corresponding to B) Melt temperatures.

Appendix F: Immunostaining and confocal microscopy

To assess whether any bleed-through fluorescence was affecting the results, no-primary and no-secondary antibody controls were carried out. Figure 5.33 and 5.34 below show the results:

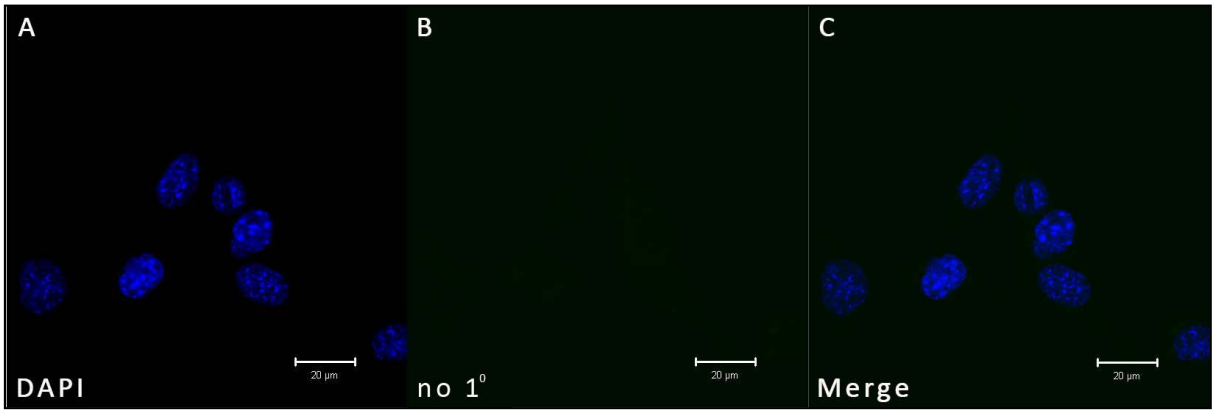

Figure 5.33: 63x confocal image of E12.5$^{+/+}$ no-primary antibody control. Scale bar is 20µm.

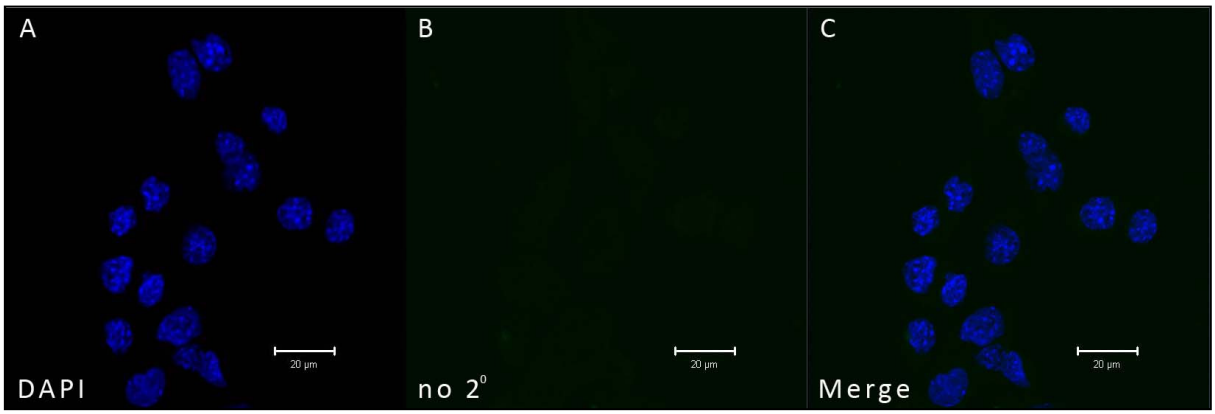

Figure 5.34: 63x confocal image of E12.5$^{+/+}$ monolayer no-secondary antibody control. Scale bar is 20µm.

No bleed-through was evident.

Appendix G: Kits

Kits used to manufacturer's specification:

QIAquick gel extraction kit

QIAprep Miniprep kit

QIAgen RNeasy Mini kit

DNeasy Blood and Tissue kit

Amended kit protocols:

QIAprep Midi/Maxi kit – An overnight elution step at 4°C was included.

REFERENCES

Acloque H, Adams MS, Fishwick K, Bronner-Fraser and Nieto MA, 2009. Epithelial-mesenchymal transitions: the importance of changing cell state in development and disease. Journal of Clincal Investigation 119:1438–49.

Adler R and Canto-Soler MV, 2007. Molecular mechanisms of optic vesicle development: complexities, ambiguities and controversies. Developmental Biology, 305: 1-13.

Ahuja D, Sáenz-Roble MT, and Pipas JM, 2005. SV40 large T antigen targets multiple cellular pathways to elicit cellular transformation. Oncogene, 24:7729-45.

Araki-Sasaki K, Aizawa S, Hiramoto M, Nakamura M, Iwase O, Nakata K, Sasaki Y, Mano T, Handa H, and Tano Y, 2000. Substance P-induced cadherin expression and its signal transduction in a cloned human corneal epithelial cell line. Journal of Cell Physiology, 182:189-95.

Barsted R, 2001. Geneome wide RNAi. Current Opinion in Chemical Biology, 5:63-6.

Baulmann DC, Ohlmann A, Flügel-Koch C, Goswami S, Cvekl A and Tamm ER, 2002. Pax6 heterozygous eyes show defects in chamber angle differentiation that are associated with a wide spectrum of other anterior eye segment abnormalities. Mechanisms of Development, 118:3-17.

Baum B, Settleman J and Quinlan MP, 2008. Transitions between epithelial and mesenchymal states in development and disease. Seminars in Cell and Developmental Biology, 19:294-308.

Beebe DC and Coats JM, 2000. The lens organizes the anterior segment: specification of neural crest cell differentiation in the avian eye. Developmental Biology, 220:424-31.

Berry FB, Lines MA, Oas JM, Footz T, Underhill DA, Gage PJ and Walter MA, 2006. Functional interactions between FOXC1 and PITX2 underlie the sensitivity to FOXC1 gene dose in Axenfeld-Rieger syndrome and anterior segment dysgenesis. Human Molecular Genetics, 15:905-19.

Bolós V, Peinado H, Pérez-Moreno MA, Fraga MF, Esteller M and Cano A, 2003. The transcription factor SLUG represses E-cadherin expression and induces epithelial to mesenchymal transitions: a comparison with SNAIL and E47 repressors. Journal of Cell Science, 116: 499–511.

Braga VM, Del Maschio A, Machesky L and Dejana E, 1999. Regulation of cadherin function by Rho and Rac: modulation by junction maturation and cellular context. Molecular Biology of the Cell, 10:9-22.

Bustin SA, Benes V, Garson JA, Hellemans J, Huggett J, Kubista M, Mueller R, Nolan T, Pfaffl MW, Shipley GL, Vandesompele J and Wittwer CT, 2009. The MIQE guidelines: minimum information for publication of quantitative real-time PCR experiments. Clinical Chemistry, 55:611-22.

Buxton PG, Kostakopoulou K, Brickell P, Thorogood P and Ferretti P, 1997. Expression of the transcription factor slug correlates with growth of the limb bud and is regulated by FGF-4 and retinoic acid. International Journal of Developmental Biology, 41:559-68.

Castanotto D, Li H, and Rossi JJ, 2002. Functional siRNA expression from transfected PCR products. RNA, 8:1454–60.

Chen H-C, Zhu Y-T, Chen S-Y and Tseng SCG , 2012. Selective Activation of p120^{ctn}-Kaiso Signaling to Unlock Contact Inhibition of ARPE-19 Cells without Epithelial-Mesenchymal Transition. PLoS ONE 7(5):e36864.

Choi SJ, Moon JH, Ahn YW, Ahn JH, Kim DU and Han TH, 2005. Tsc-22 enhances TGF-beta signaling by associating with Smad4 and induces erythroid cell differentiation. Molecular and Cellular Biochemistry, 271:23-8.

Coulombre AJ and Coulombre JL, 1964[1]. Lens Development. I. Role of the lens in eye growth. Journal of Experimental Zoology, 156:39-47.

Cubitt CL, Tang Q, Monteiro CA, Lausch RN and Oakes JE, 1993. IL-8 gene expression in cultures of human corneal epithelial cells and keratocytes. Investigative Ophthalmology and Visual Science, 34:3199–206.

1. Cited in Materials and Methods Section only.

Cvekl A and Duncan MK, 2007. Genetic and epigenetic mechanisms of gene regulation during lens development. Progress in Retinal and Eye Research, 26:555-97.

Cvekl A and Tamm ER, 2004. Anterior eye development and ocular mesenchyme: new insights from mouse models and human diseases. BioEssays, 26:374-86.

Davies A, Mirza G, Flinter F and Ragoussis J, 1999. An interstitial deletion of 6p24-p25 proximal to the FKHL7 locus and including AP-2a that affects anterior eye chamber development. Journal of Medical Genetics, 36:708–710.

Davis J, Duncan MK, Robison WG Jr and Piatigorsky J, 2003. Requirement for Pax6 in corneal morphogenesis: a role in adhesion. Journal of Cell Science, 116:2157-67.

del Barrio MG and Nieto MA, 2002. Overexpression of Snail family members highlights their ability to promote chick neural crest formation. Development, 129:1583-93.

Doherty P and Walsh FS, 1996. CAM-FGF receptor interactions: a model for axonal growth. Molecular and Cellular Neuroscience, 8:99-111.

Dohrmann CE, Belaoussoff M and Raftery LA, 1999. Dynamic expression of TSC-22 at sites of epithelial-mesenchymal interactions during mouse development. Mechanisms of Development, 84:147-51.

Donner AL, Lachke SA and Maas RL, 2006. Lens induction in vertebrates: variations on a conserved theme of signaling events. Seminars in Cell and Developmental Biology, 17:676-85.

Evans AL and Gage PJ, 2005. Expression of the homeobox gene Pitx2 in neural crest is required for optic stalk and ocular anterior segment development. Human Molecular Genetics, 14:3347-59.

Flügel-Koch C, Ohlmann A, Piatigorsky J and Tamm ER, 2002. Disruption of anterior segment development by TGF-beta1 overexpression in the eyes of transgenic mice. Developmental Dynamics, 225:111-25.

Gage P J and Zacharias AL, 2009. Signaling “cross-talk” is integrated by transcription factors in the development of the anterior segment in the eye. Developmental Dynamics, 238: 2149–2162.

Gage PJ, Rhoades W, Prucka SK and Hjalt T, 2005. Fate maps of neural crest and mesoderm in the mammalian eye. Investigative Opthalmology and Visual Science, 46:4200-8.

García-Castro MI, Vielmetter E and Bronner-Fraser M, 2002. N-Cadherin, a Cell Adhesion Molecule Involved in Establishment of Embryonic Left-Right Asymmetry. Science, 288:1047-51.

Genis-Galvez JM, 1966. Role of the lens in the morphogenesis of the iris and cornea. Nature, 210:209-10.

Gilbert S. F. (2006). Developmental Biology. 8th Edition. Sinauer Associates, Inc. Massachusetts. 139-150; 397-402.

Gould DB and John SWM, 2002. Anterior segment dysgenesis and developmental glaucomas are complex traits. Human molecular Genetics, 11:1185-93.

Gould DB, Smith RS and John SWM, 2004. Anterior segment development relevant to glaucoma. International Journal of Developmental Biology, 48:1-15.

Graw J, 1999. Cataract mutations and lens development. Progress in Retinal and Eye Research, 18:235-67.

Graw J, 2010. Eye development. Current Topics in developmental Biology, 90:343-86.

Grindley JC, Davidson DR and Hill RE, 1995. The role of Pax-6 in eye and nasal development. Developmet, 121:1433-42.

Gupta RA, Sarraf P, Mueller E, Brockman JA, Prusakiewicz JJ, Eng C, Willson TM and DuBois RN, 2003. Peroxisome proliferator-activated receptor gamma-mediated differentiation: a mutation in colon cancer cells reveals divergent and cell type-specific mechanisms. Journal of Biological Chemistry, 278:22669-77.

Hartsock A and Nelson WJ, 2007. Adherens and Tight Junctions: Structure, Function and Connections to the Actin Cytoskeleton. Biochimica et Biophysica Acta, 1778: 660–9.

Hashiguchi A, Okabayashi K and Asashima M, 2004. Role of TSC-22 during early embryogenesis in Xenopus laevis. Development, Growth and Differetiation, 46:535-44.

Hayashi H and Kume T, 2008. Forkhead transcription factors regulate expression of the chemokine receptor CXCR4 in endothelial cells and CXCL12-induced cell migration. Biochemical and Biophysical Research Communications, 367:584-9.

Hazan RB, Phillips GR, Qiao RF, Norton L and Aaronson S, 2000. Exogenous expression of N-Cadherin in Breats Cancer Migration, Invasion and Metastasis. Journal of Cell Biology, 148:779-90.

Hemavathy K, Ashraf SI and Ip YT, 2000. Snail/slug family of repressors: slowly going into the fast lane of development and cancer. Gene, 257:1-12.

Hjalt TA, Semina EV, Amendt BA and Murray JC, 2000. The Pitx2 protein in mouse development. Developmental Dynamics, 218:195-200.

http://hmg.oxfordjournals.org/content/16/7/798/F2.expansion accessed 09012013

http://marineyes.com/anterior-segment accessed 09012013

http://www.empowher.com/media/reference/corneal-abrasion accessed 11012013

http:www.aafp.org/afp/2004/0701/p123.html accessed 11012013

http:www.biographixmedia.com/humaneye-anatomy.html accessed 16012013

http:www.bionalogy.com/eye_and_ear.htm accessed 17012013

http:www.theodora.com/anatomy/the_organ_of_sight.html accessed 06122013

Huang L, Chi J, Berry FB, Footz TK, Sharp MW and Walter MA, 2008. Human p32 is a novel FOXC1-interacting protein that regulates FOXC1 transcriptional activity in ocular cells. Investigative Opthalomology and Visual Science, 49:5243-9.

Huang Y, Huang K, Boskovic G, Dementieva Y, Denvir J, Primerano DA and Zhu GZ, 2009. Proteomic and genomic analysis of PITX2 interacting and regulating networks. FEBS Letters, 583:638-42.

Hung CF, Lu KC, Cheng TL, Wu RH, Huang LY, Teng CF and Chang WT, 2006. A novel siRNA validation system for functional screening and identification of effective RNAi probes in mammalian cells. Biochemical and Biophysical Research Communications, 346:707-20.

Huser CA, Pringle MA, Heath VJ, Bell AK, Kendrick H, Smalley MJ, Crighton D, Ryan KM, Gusterson BA and Stein T, 2010. TSC-22D1 isoforms have opposing roles in mammary epithelial cell survival. Cell Death and Differentiation, 17:304-15.

Ittner M, Wurdak H, Shwerdtfeger K, Kunz T, Ille F, Leveen P, Hjalt TA, Suter U, Karlsson S, Hafezi F, Born W and Sommer L. 2005. Compound developmental eye disorders following inactivation of TGFβ signalling in neural-crest stem cells. Journal of Biology, 4:11.

Iwao K, Inatani M, Matsumoto Y, Ogata-Iwao M, Takihara Y, Irie F, Yamaguchi Y, Okinami S and Tanihara H, 2009. Heparan sulfate deficiency leads to Peters anomaly in mice by disturbing neural crest TGF-beta2 signaling. Journal of Clinical Investigation, 119:1997-2008.

Jiang R, Lan Y, Norton CR, Sundberg JP and Gridley T, 1998. The Slug gene is not essential for mesoderm or neural crest development in mice. Developmental Biology, 198:277-85.

Kester HA, Ward-van Oostwaard TM, Goumans MJ, van Rooijen MA, van Der Saag PT, van Der Burg B and Mummery CL, 2000. Expression of TGF-beta stimulated clone-22 (TSC-22) in mouse development and TGF-beta signalling. Developmental Dynamics, 218:563-72.

Kidson SH, Kume T, Deng K, Winfrey V and Hogan BLM, 1999. The Forkhead/Winged-Helix Gene, Mf1 Is Necessary for the Normal Development of the Cornea and Formation of the Anterior Chamber in the Mouse Eye. Developmental Biology, 211:306-322.

Kivelä T and Uusitalo M, 1998. Structure, development and function of cytoskeletal elements in non-neuronal cells of the Human Eye, Progress in Retinal and Eye Research, 17:385-428.

Kume T, Deng K and Hogan BL, 2000. Murine forkhead/winged helix genes *Foxc1* (Mf1) and *Foxc2* (Mfh1) are required for the early organogenesis of the kidney and urinary tract. Development 127:1387–95.

Kume T, Deng KY, Winfrey V, Gould DB, Walter MA and Hogan BL, 1998. The forkhead/winged helix gene Mf1 is disrupted in the pleiotropic mouse mutation congenital hydrocephalus. Cell, 93:985-96.

Le Douarin NM, Creuzet S, Couly G and Dupin E, 2000. Neural crest cell plasticity and its limits. Development, 131:4637-50.

Lehmann OJ, Tuft S, Brice G, Smith R, Blixt A, Bell R, Johansson B, Jordan T, Hitchings RA, Khaw PT, John SW, Carlsson P and Bhattacharya SS, 2003. Novel anterior segment phenotypes resulting from forkhead gene alterations: evidence for cross-species conservation of function. Investigative Opthalmology and Visual Science, 44:2627-33.

Livak KJ and Schmittgen TD, 2001. Analysis of relative gene expression data using real-time quantitative PCR and the 2(-Delta Delta C(T)) Method. Methods, 25:402-8.

Lovicu FJ, McAvoy JW, 2007. Growth factor regulation of lens development. Developmental Biology, 280:1-14.

Mani SA, Guo W, Liao MJ, Eaton EN, Ayyanan A, Zhou AY, Brooks M, Reinhard F, Zhang CC, Shipitsin M, Campbell LL, Polyak K, Brisken C, Yang J and Weinberg RA, 2008. The epithelial-mesenchymal transition generates cells with properties of stem cells. Cell, 133:704-15.

Mann I, 1964. The development of the human eye. 3rd Edition. Grune and Stralton, New York.

Martin DM, Skidmore JM, Philips ST, Vieira C, Gage PJ, Condie BG, Raphael Y, Martinez S and Camper SA, 2004. PITX2 is required for normal development of neurons in the mouse subthalamic nucleus and midbrain. Developmental Biology, 267:93-108.

Matsuo T, 1993. The genes involved in the morphogenesis of the eye. Japanese Journey of Opthalmology, 37:215-51.

Mattiske D, Kume T and Hogan BL, 2006(a). The mouse forkhead gene Foxc1 is required for primordial germ cell migration and antral follicle development. Developmental Biology, 290:447-58.

Mattiske D, Sommer P, Kidson SH and Hogan BL, 2006(b). The role of the forkhead transcription factor, Foxc1, in the development of the mouse lacrimal gland. Developmental Dynamics, 235:1074-80.

McAvoy JW and Chamberlain CG, 1989. Fibroblast growth factor (FGF) induces different responses in lens epithelial cells depending on its concentration. Development 107:221-8.

Mears AJ, Jordan T, Mirzayans F, Dubois S, Kume T, Parlee M, Ritch R, Koop B, Kuo WL, Collins C, Marshall J, Gould DB, Pearce W, Carlsson P, Enerback S, Morissette J, Bhattacharya S, Hogan B, Raymond V and Walter MA, 1998. Mutations of the forkhead/winged-helix gene, FKHL7, in patients with Axenfeld-Rieger anomaly. American Journal of Human Genetics, 63:1316–28.

Nakamura M and Tokura Y, 2011. Epithelial-mesenchymal transition in the skin. Journal of Dermatological Science, 61:7-13.

Napier HRL and Kidson SH, 2007. Molecular events in early development of the ciliary body: A question of folding. Experimental Eye Research, 84:615-625.

Nieman MT, Prudoff RS, Johnson KR and Wheelock MJ, 1999. N-cadherin promotes motility in human breast cancer cells regardless of their E-cadherin expression. Journal of Cell Biology, 147:631-44.

Nishimura DY, Searby CC, Alward WL, Walton D, Craig JE, Mackey DA, Kawase K, Kanis AB, Patil SR, Stone EM and Sheffield VC, 2001. A Spectrum of *FOXC1* Mutations Suggests Gene Dosage as a Mechanism for Developmental Defects of the Anterior Chamber of the Eye. American Journal of Human Genetics, 68:364–72.

O'Connor MD and McAvoy JW, 2007. In vitro generation of functional lens-like structures with relevance to age-related nuclear cataract. Investigative Opthalmology and Visual Science, 48:1245-52.

Pei YF and Rhodin JAG, 1970. The prenatal development of the mouse eye. Anatomical Record, 168:105-26.

Portt L, Norman G, Clapp C, Grrenwood M and Greenwood MT, 2011. Anti apoptosis and cell survival: A review. Biochemica et Biophysica Acta, 1813:238-59.

Prince S, Illing N and Kidson SH, 2001. SV-40 large T antigen reversibly inhibits expression of tyrosinase, TRP-1, TRP-2 and Mitf, but not Pax-3, in conditionally immortalized mouse melanocytes. Cell Biology International, 25:91-102.

Quinn JC, West JD and Hill RE, 1996. Multiple functions for Pax6 in mouse eye and nasal development. Genes and Development, 10:435-46.

Ray PS, Wang J, Qu Y, Sim MS, Shamonki J, Bagaria SP, Ye X, Liu B, Elashoff D, Hoon DS, Walter MA, Martens JW, Richardson AL, Giuliano AE and Cui X, 2010. FOXC1 is a potential prognostic biomarker with functional significance in basal-like breast cancer. Cancer Research, 70:3870-6.

Reneker LW, Silversides DW, Xu L and Overbeek PA, 2000. Formation of corneal endothelium is essential for anterior segment development - a transgenic mouse model of anterior segment dysgenesis. Development, 127:533-42.

Roelz R, Pilz IH, Mutschler M and Pahl HL, 2010. Of mice and men: human RNA polymerase III promoter U6 is more efficient than its murine homologue for shRNA expression from a lentiviral vector in both human and murine progenitor cells. Experimental Hematology, 38:792-7.

Ros MA, Sefton M and Nieto MA, 1997. Slug, a zinc finger gene previously implicated in the early patterning of the mesoderm and the neural crest, is also involved in chick limb development. Development, 124:1821-9.

Rubinek T, Yu R, Hadani M, Barkai G, Nass D, Melmed S and Shimon I, 2003. The cell adhesion molecules N-cadherin and neural cell adhesion molecule regulate human growth hormone: a novel mechanism for regulating pituitary hormone secretion. Journal of Clinical Endocrinology and Metabolism, 88:3724-30.

Saika S, Saika S, Liu CY, Azhar M, Sanford LP, Doetschman T, Gendron RL, Kao CW and Kao WW, 2001. TGFbeta2 in corneal morphogenesis during mouse embryonic development. Developmental Biology, 240:419-32.

Saika S, 2006. TGFβ pathobiology in the eye. Laboratory Investigation, 86:106-15.

Saleem RA, SBanerjee-Basu S, Berry FB, Baxevanis AD, and Walter MA, 2001. Analyses of the Effects That Disease-Causing Missense Mutations Have on the Structure and Function of the Winged-Helix Protein FOXC1. American Journal of Human Genetics, 68:627–41.

Scheef EA, Qiong Huang Q, Wang S, Sorenson CM, Sheibani N, 2007. Isolation and characterization of corneal endothelial cells from wild type and thrombospondin-1 deficient mice. Molecular Vision, 13:1483-95.

Shibanuma M, Kuroki T and Nose K, 1992. Isolation of a gene encoding a putative leucine zipper structure that is induced by transforming growth factor beta 1 and other growth factors. Journal of Biological chemistry, 267:10219-24.

Smith RS, Zabaleta A, Kume T, Savinova OV, Kidson SH, Martin JE, Nishimura DY, Alward WL, Hogan BL and John SW, 2000. Haploinsufficiency of the transcription factors FOXC1 and FOXC2 results in aberrant ocular development. Human Molecular Genetics 9:1021–32.

Strungaru MH, Dinu I, Walter MA, 2007. Genotype-Phenotype Correlations in Axenfeld-Rieger Malformations and Glaucoma Patients in Foxc1 and Pitx2 Mutations. Investigative Opthalmology and Visual Sciences, 48:228-37.

Sommer P, Napier HR, Hogan BL and Kidson SH, 2006. Identification of Tgfβ1i4 as a downstream target of Foxc1. Development Growth and Differentiation 48:297–308.

Sowden JC, 2007. Molecular and developmental mechanisms of anterior segment dysgenesis. Eye, 21:1310-8.

Suyama K, Shapiro I, Guttman M and Hazan RB, 2002. A signaling pathway leading to metastasis is controlled by N-cadherin and the FGF receptor. Cancer Cell, 2:301-14.

Tamimi Y, Skarie JM, Footz T, Berry FB, Link BA and Walter MA, 2006. FGF19 is a target for FOXC1 regulation in ciliary body-derived cells. Human Molecular Genetics, 15:3229-40.

Tamm, 2009. The trabecular meshwork outflow pathways: structural and functional aspects. Experimental Eye Research, 88:648-55.

Thiery JP, Acloque H, Huang RY and Nieto MA, 2009. Epithelial-mesenchymal transitions in development and disease. Cell, 139:871-90.

Thiery JP, 2003. Epithelial-mesenchymal transitions in development and pathologies. Current Opinion in Cell Biology, 15:740-6.

Tholozan FM and Quinlan RA, 2007. Lens cells: more than meets the eye. International Journal of Biochemistry and Cell Biology, 39:1754-9.

Thut CJ, Rountree RB, Hwa M and Kingsley DM, 2001. A large-scale in situ screen provides molecular evidence for the induction of eye anterior segment structures by the developing lens. Developmental Biology, 231:63-76.

Tortora and Grabowski, 2003. Principles of Anatomy and Physiology. 8th Edition. John Wiley and Sons, New York.

Tran NL, Nagle RB, Cress AE and Heimark RL, 1999. N-Cadherin Expression in Human Prostate Carcinoma Cell Lines: An Epithelial-Mesenchymal Transformation Mediating Adhesion with Stromal Cells. The American Journal of Pathology, 155:787-98.

Tripathi BJ, Tripathi RC, Livingstone AM and Borisruth NS, 1999. The role of growth factors in the embryogenesis and differentiation of the eye. American Journal of Anatomy, 192:442-71.

Van Roy and Berx G, 2008. The cell-cell adhesion molecule E-cadherin. Cellular and Molecular Life Sciences, 65:3756-88.

Vassilev VS, Mandai M, Yonemura S and Takeichi M, 2012. Loss of N-cadherin from the endothelium causes stromal edema and epithelial dysgenesis in the mouse cornea. Investigative Ophthalmology and Visual Science, 53:7183-93.

Wormstone IM, Collison DJ, Hansom SP and Duncan G, 2006. A focus on the human lens in vitro. Environmental Toxicology and Pharmacology, 21:215-21.

Wurm A, Sock E, Fuchshofer R, Wegner M and Tamm ER, 2008. Anterior segment dysgenesis in the eyes of mice deficient for the high-mobility-group transcription factor Sox11. Experimental eye Research, 86:895-907.

Yang G, Yuan L, Lu X, Lu Z and Yao L, 2012. A rational design of completely random shRNA library. Biochemical and Biophysical Research Communications, 430:987-92.

Yap AS, Crampton MS, Hardin, 2007. Making and breaking contacts: the cellular biology of cadherin regulation. Current Opinion in Cell Biology, 19:508-14.

Zacharias AL, Lewandoski M, Rudnicki MA and Gage PJ, 2011. Pitx2 is an upstream activator of extraocular myogenesis and survival. Developmental Biology, 349:395-405.

Zarbalis K, Siegenthaler, JA, Choe Y, May SR, Peterson AS, Pleasure SJ, 2007. Cortical dysplasia and skull defects in mice with a *Foxc1* allele reveal the role of meningeal differentiation in regulating cortical development. Proceedings of the National Academy of Sciences of the United States of America, 104:14002-7.

Zhou Y, Kato H, Asanoma K, Kondo H, Arima T, Kato K, Matsuda T and Wake N, 2002. Identification of FOXC1 as a TGF-beta1 responsive gene and its involvement in negative regulation of cell growth. Geneomics, 80:465-72.